

**ABIOTIC REDUCTION OF PERFLUOROALKYL ACIDS BY NIFE⁰-
ACTIVATED CARBON**

by

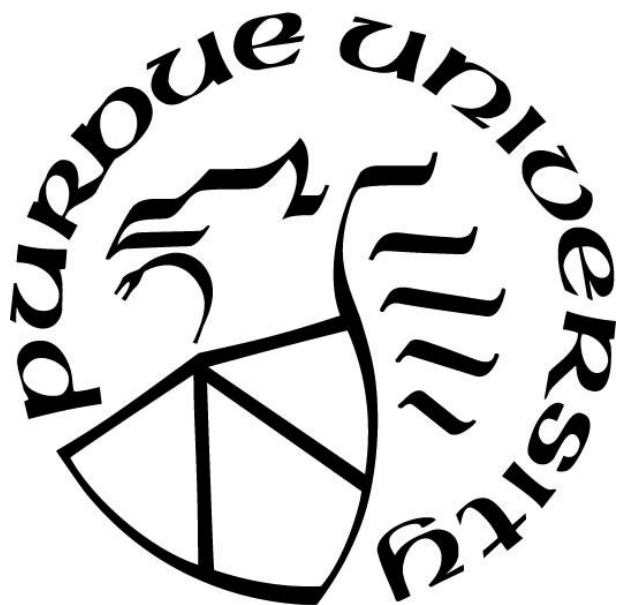
Jenny E. Zenobio

A Dissertation

Submitted to the Faculty of Purdue University

In Partial Fulfillment of the Requirements for the degree of

Doctor of Philosophy



Department of Agronomy

West Lafayette, Indiana

May 2019

**THE PURDUE UNIVERSITY GRADUATE SCHOOL
STATEMENT OF COMMITTEE APPROVAL**

Dr. Linda S. Lee, Chair

Department of Agronomy

Dr. Chad D. Vecitis

School of Engineering and Applied Sciences, Harvard University

Dr. Chad T. Jafvert

Lyles School of Civil Engineering

Dr. Loring F. Nies

Lyles School of Civil Engineering

Approved by:

Dr. Ronal F. Turco and Linda S. Lee

Head of the Graduate Program

A mi familia, especialmente a mi alma gemela Luis, por acompañarme y alentarme cada día y por los hijos maravillosos que me dio, Nicolas y Natalie.

ACKNOWLEDGMENTS

I would first like to deeply thank my advisor Prof. Linda S. Lee for her orientation, support, and motivation throughout my PhD program. Prof. Lee provided me the opportunity to join her research lab first as an intern and then as a PhD student. I profoundly appreciate her friendship. She is the best role model for a scientist, mentor, and mother.

I would like to acknowledge the Strategic Environmental Research and Development Program (SERDP/ER-2426) and FONDECYT-CONCYTEC (grant contract number 276-2015-FONDECYT) for facilitating this research.

Also, I would like to express my sincere gratitude to my advisor at Harvard University, Prof. Chad D. Vecitis for his continuous support. I am very grateful for having the privilege of working in a great multi-interdisciplinary team.

I would like to also extend my appreciation to the committee members, Prof. Chad Jafvert and Prof. Loring Nies for accepting to be on my committee and for their insightful comments and hard questions, which motivated me to analyze my research from various perspectives.

In addition, I would like to thank Prof. Scot Martin, Prof. Elsie Sunderland and Prof. Philip Kim from Harvard University for their comments, discussions, and technical support that helped me sort out my research work.

I thank my fellow labmates at Purdue and Harvard: Younjeong Choi, Rooney Kim, Saerom Park, Chloe de Perre, Aaron Zull, Carlo Amadei, Andrea Tokranov, Marielle Remillard, Gregory Silverberg, Paula Rivas, Bianca Chaves, Gustavo Cunha and Qiaoying Zhang,

for the stimulating discussions, showing me things with a different perspective, their advice during lab work and meetings, the sleepless nights we were working together and all the fun we have had over the last five years.

Last but not the least, I would like to thank my family in Peru for providing me with unfailing support and continuous encouragement throughout my years of study. My husband, my soulmate, for his unconditional support all these years and for the beautiful family he gave me. This accomplishment would not have been possible without them.

TABLE OF CONTENTS

LIST OF TABLES	ix
LIST OF FIGURES	xii
LIST OF ABBREVIATIONS.....	xv
ABSTRACT.....	xvi
CHAPTER 1. INTRODUCTION	1
1.1. Introduction.....	1
1.2. Research Objectives.....	4
1.3. Organization.....	6
CHAPTER 2. LITERATURE REVIEW	8
2.1. Physical and Chemical Properties of Per- and Polyfluoroalkyl Substances.....	8
2.2. Releases to the environment	13
2.3. Levels in the environment and regulatory responses.....	15
2.4. Chemical Treatments Tested for Perfluorooctane sulfonate.....	19
2.4.1. Ex-situ Oxidation	20
2.4.2. Ex-Situ Reduction.....	21
2.4.3. In-Situ Oxidation	25
2.4.4. In-Situ Reduction	25
CHAPTER 3. EVIDENCE OF REDUCTIVE TRANSFORMATION OF PERFLUOROCTANE SULFONATE BY NiFe ⁰ NANOPARTICLES SYNTHESIZED ONTO ACTIVATED CARBON	29
3.1. Abstract.....	29
3.2. Introduction.....	29
3.3. Materials and Methods.....	31
3.3.1. Chemicals.....	31
3.3.2. Particle Synthesis	32
3.3.3. Batch Reactions	32
3.3.4. Particle Extraction and PFOS Analysis	33
3.3.5. Extraction of F ⁻ and SO ₃ ²⁻ from nNiFe ⁰ -AC.....	34
3.3.6. Analytical Methods.....	34

3.3.6.1. HPLC/MS/MS for PFOS Quantification	34
3.3.6.2. uPLC-QToF MS for Organic Transformation Product Identification	35
3.3.6.3. Ion Chromatography	36
3.3.6.4. ICP-MS	37
3.3.7.4 Particle Characterization and Desorption Analysis	37
3.3.7. Organic Product Detection and Identification	38
3.4. Results and Discussion	39
3.4.1. Exploring Reactivity Potential with 1-h SST Particles in 5-d PFOS Reactions	40
3.4.2. Effect of SST on L- and Br-PFOS	41
3.4.3. pH Effect on Inorganic Anion Quantitation.....	42
3.4.4. Organic Products.....	43
CHAPTER 4. KINETICS AND MECHANISM OF REDUCTIVE TRANSFORMATION OF PERFLUOROCTANE SULFONATE BY NIFE ⁰ -AC PARTICLES.....	47
4.1. Abstract.....	47
4.2. Introduction.....	48
4.3. Materials and Methods.....	50
4.3.1. Standards and Reagents	50
4.3.2. Particle Synthesis	51
4.3.3. Batch Reactions and Particle Extractions	51
4.3.4. LC/MS Analysis.....	52
4.3.5. PFOS Isomer-Specific Analysis	52
4.3.6. Nontarget Screening for Organic Product Detection	54
4.3.7. Inorganic Products Extraction and Analysis.....	54
4.3.8. XPS Analysis	55
4.4. Results and Discussion	55
4.4.1. Total PFOS Transformation.....	55
4.4.2. PFOS transformation kinetics	58
4.4.3. Br-PFOS Isomers	59
4.4.4. PFOS Products over time.....	60
4.4.5. Degradation Pathways and Potential Mechanisms	66
4.5. Summary	69

CHAPTER 5. EFFECTS OF CARBON-CHAIN LENGTH, FUNCTIONAL GROUP, AND COMMON GROUNDWATER CONSTITUENTS ON PFAAS REDUCTION BY NIFE ⁰ -AC	70
5.1. Abstract.....	70
5.2. Introduction.....	71
5.3. Materials and Methods.....	73
5.3.1. Chemicals.....	73
5.3.2. Bimetals Synthesis.....	73
5.3.3. Batch Experiments.....	74
5.3.4. Extractions.....	75
5.3.5. Analytical Methods.....	75
5.3.6. LCMS.....	75
5.3.7. ICS.....	76
5.4. Results and Discussion.....	76
5.4.1. Transformation of PFCAs and PFSAAs in single solute DI water.....	76
5.4.1.1. PFCAs and PFSAAs inorganic byproducts.....	78
5.4.1.2. Organic transformation products from PFAA reduction.....	79
5.4.1.3. Proposed degradation pathways.....	84
5.4.2. Transformation of PFAAs in a PFAA-contaminated groundwater.....	87
CHAPTER 6. CONCLUSIONS AND FUTURE WORK.....	90
6.1. Conclusion.....	90
6.2. Future work.....	92
APPENDIX A. SUPPORTING INFORMATION: EVIDENCE OF REDUCTIVE TRANSFORMATION OF PERFLUOROOCTANE SULFONATE BY NIFE ⁰ NANOPARTICLES SYNTHESIZED ONTO ACTIVATED CARBON.....	95
APPENDIX B. SUPPORTING INFORMATION: KINETICS AND MECHANISM OF REDUCTIVE TRANSFORMATION OF PERFLUOROOCTANE SULFONATE BY NIFE ⁰ -AC PARTICLES.....	113
APPENDIX C. SUPPORTING INFORMATION: EFFECTS OF CARBON-CHAIN LENGTH, FUNCTIONAL GROUP, AND COMMON GROUNDWATER CONSTITUENTS ON PFAAS REDUCTION BY NIFE ⁰ -AC.....	125
REFERENCES.....	133

LIST OF TABLES

Table 2-1. Physical and chemical properties of perfluoroalkyl substances.....	11
Table 2-2 Groundwater concentrations (ng/L) of PFOA, PFHxA, PFBA, PFOS, PFHxS, and PFBS by source.....	18
Table 2-3. Summary of ex-situ oxidation and reduction treatments for PFAAs.....	24
Table 2-4. Summary of in-situ reduction treatments for PFAAs.....	27
Table 2-5. Energy need to degrade PFOS using different treatment.....	28
Table 3-1. Summary of the products identified in the solvent extracts. For reference, PFOS m/z is 498.9297 with a retention time of 8.8817 min. All products identified are from the loss/gain of F/H or the cleavage of SO ₃ ²⁻ (see Tables A6, A7 and A8).....	46
Table 4.1. Products detected in concentrated samples at four or more sampling times with one exception after 6 μM PFOS solution react with nNiFe ⁰ -AC at 60 °C. Degradation products were detected using QToF electrospray ionization (ESI) and atmospheric pressure chemical ionization (APCI), both in negative mode. The exception is m/z 431.96, which was observed only at 120 h. PFOS (C ₈ F ₁₇ SO ₃ ⁻ , m/z 498.9297 tr = 11.34 min). *Products detected only in the concentrated samples.....	62
Table 4-2. % F based on F content in initial PFOS (17 F/PFOS) calculated based on sum of F associated with PFOS remaining and measured fluoride (F ⁻).....	66
Table 5-1. Products detected after individual 6 μM solutions of PFBS and PFHxS reacted with nNiFe ⁰ -AC at 60 °C for 1 d or 5 d. Degradation products were detected using Q-ToF ESI . All samples were concentrated 3 times to increase product detection.....	81
Table 5-2. Products detected after individual 6 μM solutions of PFBA, PFHxA, PFOA reacted with nNiFe ⁰ -AC at 60 °C for 1 d or 5 d. Degradation products were detected using Q-ToF ESI. All samples were concentrated 3 times to increase product detection.....	82
Table 5-3. F and SO ₃ ²⁻ mass balance from 5-d reactions with PFCAs (PFBA, PFHxA, and PFOA) and PFSAAs (PFBS and PFHxS). All experiments were performed using DI water. *PFOS data reported in chapter 4 was used for comparison.....	83
Table 5-4. a) Initial PFAS concentration and b) ions measured in the groundwater sample. Ions data was provided from Barber et al. and Weber et al. (Barber <i>et al.</i> , 2017; Weber <i>et al.</i> , 2017).....	89

Table A1. Agilent 6460 Triple-Quad LC/MS source parameters for negative ion mode.....	98
Table A2. MS/MS conditions for PFOS and M8PFOS (internal standard) quantification using an Agilent 6460 Triple-Quad LC/MS.....	99
Table A3. Quadrupole time of flight (QToF) negative and positive electrospray ionization (ESI ⁻ and ESI ⁺ , respectively) source parameters.....	99
Table A4. SWATH parameters used for unknown identification.....	100
Table A5. Negative mode APCI (APCI ⁻) optimized parameters for negative mode of C ₈ F ₁₈ analysis.....	101
Table A6. Single bond defluorinated transformation products identified after nNiFe ⁰ -AC reacted with PFOS using accurate-mass identification. Precursor and daughter ions were identified by QToF. In column one, the number in parenthesis is the observed m/z of the precursor ions.....	102
Table A7. Double bond defluorinated transformation products identified after nNiFe ⁰ -AC reacted with PFOS using accurate-mass identification. Precursor and daughter ions were identified by QToF. In column one, the number in parenthesis is the observed m/z of the precursor ions.....	104
Table A8. Paraffin product identified after nNiFe ⁰ -AC reacted with PFOS using accurate-mass identification. Precursor and daughter ions were identified by QToF. In column one, the number in parenthesis is the observed m/z of the precursor ions.....	105
Table B1. Optimized LCMS parameters for quantification of PFCAs and PFOS (linear and branched).....	115
Table B2. Quadrupole time of flight (QToF) source parameters used for PFOS isomers separation.....	116
Table B3. Quadrupole time of flight (QToF) source parameters using electrospray ionization in negative mode (ESI ⁻) for identification of organic products.....	117
Table B4. Quadrupole time of flight (QToF) source parameters using atmospheric pressure chemical ionization (APCI) for identification of organic byproducts.....	117
Table B5. Gradient program of the mobile phase for separation of PFOS byproducts using QToF.....	118
Table B6. PFOS isomers retention time (min) separated using QToF-MS.....	119

Table B7. Limit of detection (LOD) and quantification (LOQ) of PFOS isomers using QToF-MS. The highest and lowest concentrations detected in the samples are reported in $\mu\text{g/L}$	120
Table B8. Limit of detection (LOD) and quantification (LOQ) of the perfluorocarboxylic acid products detected in the concentrated samples using LCMS. The highest and lowest product concentrations in ng/L were also reported.....	120
Table B9. Fragmentation of the transformation products identified for PFOS.....	121
Table C1. LCMS conditions for PFAAs quantification.....	126
Table C2. LCMS gradient conditions for PFAAs quantification.....	127
Table C3. IC gradient separation for F^- and SO_4^{2-} quantification. [A] = Water and [B] = 30 mM NaOH.....	127
Table C4. % Transformation of PFSAAs and PFCAs at 1-d and 5-d of reaction.....	128
Table C5. Final pH measured at 1 d or 5 d after reaction of PFAAs with $\text{nNiFe}^0\text{-AC}$	128
Table C6. Transformation products identified after $\text{nNiFe}^0\text{-AC}$ reacted with PFSAAs using accurate-mass identification. Precursor and daughter ions were identified by QToF. In column one, the number in parenthesis is the observed m/z of the precursor ions.....	129
Table C7. Transformation products identified after $\text{nNiFe}^0\text{-AC}$ reacted with PFCAs using accurate-mass identification. Precursor and daughter ions were identified by QToF. In column one, the number in parenthesis is the observed m/z of the precursor ions.....	130

LIST OF FIGURES

- Figure 2-1. Examples of PFAS' chemical structure (per- and poly) of some of the PFAS subclasses and their charged functional group head (anionic, cationic, and zwitterionic). $n = 2$ to 18.....9
- Figure 2-2. Chemical structures of perfluoroalkyl sulfonic acids (PFSA: PFOS, PFH_xS, and PFBS) and perfluorocarboxylic acids (PFCA: PFOA, PFH_xA, and PFBA) of long- and short-carbon chain.....13
- Figure 2-3. Composition of fluorosurfactants detected in groundwater at AFFF-impacted sites (U.S. military bases) (Backe *et al.*, 2013; Houtz *et al.*, 2013; Schultz *et al.*, 2004).....16
- Figure 3-1. Mole percentage of PFOS recovered in the aqueous phase and solvent extracts and mol SO₃²⁻ generated (measured in only the aqueous phase) relative to initial (t=0) moles of PFOS after a 5-d reaction with various particle types in unbuffered deionized water with no pH adjustments. The pH shown above the bars is final pH after the 5-day reaction. nNiFe⁰-AC particles were prepared with 1-h SST.....41
- Figure 3-2. Mole percentage of Br- and L-PFOS recovered relative to initial (t=0) moles of PFOS (a) after 1-d reaction with nNiFe⁰-AC particles prepared different synthesis stirring times (SST); and b) after a 5-d reaction along with mol percentage of F⁻ and SO₃²⁻ generated relative to initial (t=0) moles of PFOS for 1-h and 3-h SST prepared nNiFe⁰-AC particles. First bar in each graph represents the PFOS control (no particles); isomer ratios is approximately 68/32 L-/Br-PFOS. Reactions were in unbuffered deionized water with no pH adjustments. *Extraction of inorganic ions with 0.02 M NaOH was performed only for the 5-d reaction with 3-h SST particles in which no fluoride was observed (n=6).....42
- Figure 4-1. a) Mol % of total PFOS recovery and F⁻ and SO₃²⁻ generated relative to initial PFOS moles over time with nNiFe⁰-AC; 17 moles of F⁻ and one mole of SO₃²⁻ can be generated from one mole of PFOS, and b) pH and ORP (mV) measurements over time with the measurements for the matrix control being: pH = 6 and ORP = -556 meV and for the PFOS solution: pH = 5.6 and ORP = 266 meV. Particles were prepared with 3-h SST and in unbuffered deionized water with no pH adjustments. Seventeen moles of F⁻ and one mole of SO₃²⁻ can be generated from one mole of PFOS.....57

Figure 4-2. Linear regression of pseudo first-order reaction of L-PFOS and Br-PFOS isomers over time (1 h, 6 h, 12 h, 18 h, 24 h and 120 h).....	58
Figure 4-3. Natural logarithm of the ratio between the concentration of specific PFOS isomer at a given time relative to its concentration at t=0 versus reaction time. Points are an average of 3 replicates.....	60
Figure 4-4. Generation of single-bond products over time from PFOS reduction. Sequential a) F/H exchanges and generation of b) shorter carbon chain [C ₇ - C ₄] products. Peak areas of individual products were normalized by M8PFOS IS (188 µg/L) peak area. All products shown were detected using electrospray ionization in negative mode (ESI-)......	64
Figure 4-5. Generation over time during PFOS reduction of a) double-bond, b) PFCAs, and c) paraffin products. Peak areas of individual products were normalized by M8PFOS IS (188 µg/L) peak area. All products shown were detected using electrospray ionization in negative mode (ESI-) except for the paraffins, which required atmospheric pressure chemical ionization (APCI-). Data for PFCAs and paraffin are from concentrated (x3) samples.....	65
Figure 4-6. Reaction pathways proposed for PFOS reduction by nNiFe ⁰ -AC. Defluorination, desulfonation, and formation of single, double-bond, and paraffin products. Formulas colored with blue and red were confirmed with MS and MS/MS and only MS, respectively.....	68
Figure 5-1. Transformation of a) PFSAAs and b) PFCAs at 1-d and 5-d of reaction, and c) generation of inorganic products F ⁻ and/or SO ₃ ²⁻ (quantified as SO ₄ ²⁻) after 5-d. Average and standard deviation (bars) of three replicates.....	78
Figure 5-2. PFOA degradation pathway. Formulas colored with blue and red were confirmed with MS and MS/MS and only MS, respectively.....	86
Figure 5-3. PFHxS degradation pathway. Formulas colored with blue and red were confirmed with MS and MS/MS, and only MS, respectively.....	87
Figure 5-4. PFSAAs and PFCAs degradation using contaminated groundwater sampled from a former fire training area in Massachusetts. Reaction time: 5-d. *% mol removed in controlled studies with single solute in Milli-Q water for comparison.....	89
Figure A1. HPLC/MS/MS chromatogram of linear PFOS (the peak on the right) and branched PFOS (the peaks on the left) with intensity on the y-axis and retention time.....	106

- Figure A2. XPS spectra of (a-b) PFOS powder, (c-d) PFOS-reacted nNiFe⁰-AC; and (e-f) PFOS-reacted nNiFe⁰-AC after solvent extraction showing F 1s (675-695 eV) in the left column of graphs and S 2p_{3/2} (158-178 eV) in the right column of graphs. Reaction was for 5-d at 60 °C with PFOS and nNiFe⁰-AC that were synthesized with a 1-h stirring time.....107
- Figure A3. TEM images of 1-h SST nNiFe⁰-AC NPs after a 5-d reaction with PFOS at 60 °C. The gray sheets are AC, and the black NPs are nNiFe⁰.....108
- Figure A4. SEM images of the morphology and associated size distribution histograms determined of AC-supported nNiFe⁰ synthesized with different stirring time (SST) after a 5-d reaction period with PFOS (~ 6 μM) in unbuffered and unadjusted pH solutions at 60 °C: a) 1-h SST; b) 2-h SST; and c) 3-h SST.....109
- Figure A5. Ion chromatograms for solutions associated with nNiFe⁰-AC (Ni = 2 wt% of Fe⁰) particles prepared with different synthesis stirring time (SST): a) 1-h SST nNiFe⁰-AC and b) 3-h SST nNiFe⁰-AC. Upper two graphs are chromatograms after a 5-d reaction at 60 °C in unbuffered solutions containing PFOS (~ 6 μM, ~ 3 mg/L) with and without a fluoride (F⁻) standard addition, respectively. Red dashed line represents where the F peak should be located in the chromatogram. In Fig A5b, fluoride concentration was estimated to be 170 μg/L from the F⁻ standard curve. Based on the standard addition, F⁻ concentration after the 5-day PFOS reaction with 3-h SST nNiFe⁰-AC was estimated by Gaussian fitting using OriginPro 2016 software.....110
- Figure A6. Identification process for PFOS transformation products using QToF/MS.....111
- Figure A7. MS-MS spectrum of m/z 435 precursor ion in the a) sample and in the b) 23 ppm perfluorooctane (C₈F₁₈) standard solution injected in flow injection mode. The sample was injected directly in the syringe in APCI negative mode.....112
- Figure B1. L- and Br-PFOS present in the technical PFOS used to perform batch experiments.....122
- Figure B2. PFOS isomers and specific product ion used for isomers identification.....123
- Figure B3. Fe 2p_{3/2} XPS spectra of nNiFe⁰-AC nanoparticles at different reaction times (1 h, 6 h, 18 h, 24 h, and 120 h) and matrix control (NPs and water mixed for 120 h).....124

LIST OF ABBREVIATIONS

AFFF = Aqueous film-forming foam
PFAS = Per- and polyfluoroalkyl substance
PFAA = Perfluoroalkyl acid
PFSA = Perfluoroalkyl sulfonic acid
PFCA = Perfluoroalkyl carboxylic acid
PFOS = Perfluorooctanesulfonate
PFHpS = Perfluoroheptanesulfonate
PFHxS = Perfluorohexanesulfonate
PFPeS = Perfluoropentanesulfonate
PFBS = Perfluorobutanesulfonate
PFNA = Perfluorononanoic acid
PFOA = Perfluorooctanoic acid
PFHpA = Perfluoroheptanoic acid
PFHxA = Perfluorohexanoic acid
PFPeA = Perfluoropentanoic acid
PFBA = Perfluorobutyric acid
6:2 FtS = 6:2 fluorotelomer sulfonate
8:2 FtS = 8:2 fluorotelomer sulfonate
HPLC = High performance liquid chromatography
QToF = Quadrupole time-of-flight
ESI = Electrospray ionization
APCI = Atmospheric pressure chemical ionization
MS = Mass spectrometry
IC = Ion chromatography
AC = Activated carbon
CMC = Critical micelle concentration
ECF = Electrochemical fluorination
TM = Telomerization
L-PFOS = Linear PFOS
Br-PFOS = Branched PFOS
ZVM = Zero valent metals
ZVI = Zero valent iron
SST = Synthesis stirring time

ABSTRACT

Author: Zenobio, Jenny, E. PhD

Institution: Purdue University

Degree Received: May 2019

Title: Abiotic Reduction of Perfluoroalkyl Acids by NiFe⁰-Activated Carbon

Committee Chair: Dr. Linda S. Lee

In recent years, the presence of per- and polyfluoroalkyl substances (PFAS) in aquatic systems has led to research on their fate, effects and treatability. PFAS have been found in various environmental matrices including wastewater effluents, surface, ground, and drinking water. Perfluoroalkyl acids (PFAAs) are the class of PFAS most commonly tested due to their ability to migrate rapidly through groundwater and include perfluoroalkyl sulfonic acids (PFSAs) and perfluoroalkyl carboxylic acids (PFCAs). Of the globally distributed and persistent PFAAs, PFSAs are the most resistant to biological and oxidative chemical attack. This doctoral study focused on a reductive treatment approach with zero valent metals/bimetals nanoparticles (NPs) synthesized onto a carbon material to reduce NP aggregation. Initial work focused on exploring reactivity of different combinations of nano (n) Ni, nFe⁰ and activated carbon (AC) at 22 °C to 60 °C for transforming perfluorooctanesulfonate (PFOS) from which nNiFe⁰-AC at 60 °C led to transformation of both linear (L-) and branched (Br-) PFOS isomers. The remaining research focused on work with nNiFe⁰-AC at 60 °C in batch reactors including optimizing nNiFe⁰-AC preparation, quantifying PFOS transformation kinetics and evaluating the effects of PFAA chain length (C4, C6 and C8) and polar head group (PFSA versus PFCA) as well a groundwater matrix on transformation magnitude. Optimization of analytical methods to provide multiple lines of evidence of transformation including fluoride, sulfite and organic product generation was an ongoing throughout the research.

nNiFe⁰-AC prepared with a 3-h synthesis stirring time led to the highest PFOS transformation of $51.1 \pm 2.1\%$ with generation of ~ 1 mole of sulfite (measured as sulfate) and 12 moles of fluoride. Several poly/per-fluorinated intermediates with single and double bonds were identified using quadrupole time-of-flight mass spectrometry (QToF-MS) in negative electrospray ionization (ESI-) mode with MS/MS fragmentation confirmation as well as one and later two desulfonated products with QToF negative atmospheric pressure chemical ionization (APCI-). All organic transformation products were found in only particle extracts as well as most of the sulfite generated. PFOS transformation kinetics showed that generated fluoride concentrations increased for the first day whereas sulfate concentrations continued to increase during the 5-d reaction. The transformation products identified showed defluorination of single- and double-bond structures, formation of C8 to C4 PFCAs and paraffins from cleavage of the C-S bond.

The length of the perfluoroalkyl chain affected the length of time to achieve peak removal, but overall magnitude of transformation when reactions appeared complete were similar for both PFSAs and PFCAs. Like PFOS, PFOA transformation maxed in 1 d whereas shorter chains required more time to reach their peak removal, which is hypothesized to be due to lower sorption of the shorter chain PFAAs to the reactive surfaces. Measured F mass balance was higher for PFOS and PFOA (>90% F) compared to shorter chain PFAAs (~50-70% F). The Perfluorohexanesulfonate (PFHxS) and perfluorobutanesulfonate (PFBS) degradation products include single bond polyfluoroalkyl sulfonates and shorter-chain perfluoroalkyl carboxylates. For example, PFHxS transformation resulted in perfluorohexane carboxylic acid (PFHxA) and perfluorobutane carboxylic acid (PFBA). PFCA transformation products included per- & polyfluoroalkyl carboxylates with single bonds and alcohols with single and double bonds. The

effect of inorganic matrix on transformation with nNiFe⁰-AC at 60 °C was explored using a contaminated groundwater collected at a former fire-training area in Massachusetts.

Transformation appeared ‘generally’ lower than in the single-solute clean water systems, which may have been due to the presence of PFAS precursors that degraded to PFAAs and competitive adsorption between anionic PFAAs and inorganic ions onto the NP surface.

The research presented here demonstrates that nNiFe⁰-AC at 60 °C can mineralize PFAAs even in a typical groundwater matrix. Additional lab and pilot scale studies are needed to clarify the mechanisms leading to transformation as well as why transformation reactions plateau prior to all the parent compounds being transformed. The latter may be due to a poisoning phenomenon that can occur in closed systems, which may not occur in a flowing system more characteristic of an environmental scenario, as well as surface area and reactive site constraints or particle passivation.

CHAPTER 1. INTRODUCTION

1.1. Introduction

Perfluoroalkyl acids (PFAAs) are highly fluorinated aliphatic chemicals having a perfluoroalkyl moiety (C_nF_{2n+1}) with different polar heads (e.g. $-SO_3^-$ or $-CO_2$). PFAAs are used in a wide range of commercial and industrial products due to their unique hydro- and oleophobic properties. They have been used in surface coating products; oil and stains; manufacture of fluoropolymers and plastics; etc. Major PFAAs applications include textiles, leather products, cookware, food packaging, carpets, surfactants, cosmetics, lubricants, and firefighting foams (Park *et al.*, 2011; Yamamoto *et al.*, 2007; Zhuo *et al.*, 2011). Fluorinated Class B aqueous film-forming foams (AFFFs) are effective in extinguishing hydrocarbon-fueled fires. They have been used for fire training and suppression at military installations, refineries, airports and chemical manufacturing plants (Hu *et al.*, 2016). AFFF have three types of products containing fluorosurfactants: legacy PFOS AFFF (containing perfluorooctane sulfonic acid (PFOS) and its precursors), legacy fluorotelomer AFFF (containing mainly long-chain PFAAs), and modern fluorotelomer AFFF (containing exclusively short-chain PFAAs). Fluorosurfactants, the active ingredient in AFFF's, had been manufacturing by electrochemical fluorination (ECF) and telomerization (TM). The main differences of these two processes is the resulting isomeric PFAA products generated. The ECF process produces even and odd numbered of ~70% linear (L-) and 30% branched (Br) chains, while TM produces only even numbered of straight carbon chain isomers (3M, 2000). 3M company was the first producer of perfluorooctane sulfonyl fluoride (POSF), the main raw material for the synthesis of PFOS and other perfluorooctane sulfonyl substances. 3M was the world's largest PFOS producer from 1949 to 2002. Their largest

production was between 1970 and 2002, producing a total of approximately 96,000 tons of POSF and generating about 26,500 tons of wastes (Paul *et al.*, 2009). They terminated the production of eight-carbon PFOS-related compounds in 2002 and start to produce four-carbon PFAAs based on perfluorobutanesulfonate (PFBS) (OECD, 2002). Other manufacturing producers such as DuPont, Daikin, Asahi, Clariant, Atofina, and Glass use the TM process to manufacture PFAAs. Hence, the straight-chain isomer is the dominant isomer in commercial mixtures and therefore in environmental samples.

AFFF has been identified as a major source of PFAA contamination in groundwater (Houtz *et al.*, 2016). Multiple releases of PFAAs into the environment over a long period of time have resulted in loads to both soil and groundwater above the health advisory levels of 70 ng/L established by the United States Environmental Protection Agency (USEPA) for perfluorooctanoic acid (PFOA) and PFOS (individual or combined) for drinking water (Cousins *et al.*, 2016; Gottschall *et al.*, 2010; Hu *et al.*, 2016; Oliaei *et al.*, 2013; Pistocchi & Loos, 2009; Sharma *et al.*, 2016; Wang *et al.*, 2010; Xiao *et al.*, 2015). PFOS is commonly detected at AFFF release sites at concentrations up to 2.3 mg/L, well above the USEPA provisional health advisory values.

Of the PFAAs known to exist at AFFF impacted sites, PFOS (C₈F₁₇SO₃), has received the greatest attention due to its toxicity, mobility, persistence and bioaccumulative potential (Damjanovic *et al.*, 2011; Ericson *et al.*, 2009; Fei *et al.*, 2008; Park *et al.*, 2009; Park *et al.*, 2011; Park *et al.*, 2016; Yang *et al.*, 2013). PFOS have not been shown to be biodegradable to date, in fact they can be formed by environmental microbial degradation or by metabolism in large organisms from PFAAs precursors (Dasu *et al.*, 2013; Royer *et al.*, 2015), thus abiotic chemical treatments must be the focus of any management strategy.

Currently, only sorptive technologies like granular activated carbon (GAC) are used as a remedial to treat PFAS-contaminated water (Appleman *et al.*, 2014). However, GAC is only effective for the removal of long-chain PFAAs but does not perform well on short-chain PFAAs or PFAAs precursors (Appleman *et al.*, 2014). Also, matrix effects can lead to much earlier breath through of even PFOA and PFOS, thus requiring several GAC reactors in series. Sorption technologies do not destroy PFAAs, in fact additional ex-situ treatments are required to destroy the PFAA-containing GAC, thus increasing treatment costs. Destructive technologies are the preferred approach for removing PFAAs. Conventional water treatment processes are not effective for PFAAs degradation. Although some ex- and in-situ oxidative techniques have shown success for perfluoroalkyl carboxylates (PFCAs) (Park *et al.*, 2016). PFOS cannot be decomposed by advance oxidation technologies that utilize the hydroxyl radicals for oxidation. Currently, there are few ex-situ and only two in-situ treatments (elemental iron and Vitamin B12) that have shown success for PFOS decomposition with evidence of transformation. The in-situ technologies able to transform PFOS have some limitation. For example, elemental iron is capable to mineralize PFOS, but the conditions used are extreme for in-situ applications (350°C and 20 MPa). While, Vitamin B12 requires elevated temperature (e.g., 70 °C), an alkaline pH, and it is only able to degrade the branched isomers, but not L-PFOS, which is the dominant isomer.

The use of zero-valent metals are attractive due to their low cost and use in passive treatment methods such as permeable reactive barriers (PRBs) (Cheng & Wu, 2000; Kim *et al.*, 2004; Roberts *et al.*, 1996; Tratnyek *et al.*, 1997). Under anaerobic conditions, $n\text{Fe}^0$ is oxidized by H_2O or H^+ producing Fe^{2+} and H_2 . Thus, three major reductants will be present in the reaction system (Fe^0 , Fe^{2+} and H_2). These reductants may react with the organic contaminant by electron

transfer from $n\text{Fe}^0$ to form Fe^{2+} and Fe^{2+} to form Fe^{3+} or from H_2 if a catalyst is present. PFOS was shown to be degraded rapidly by Fe^0 in sub- or supercritical water at 350 °C, (Hori *et al.*, 2006) but this approach is not conducive for in-situ application. Both decreasing particle size, e.g., Fe^0 nanoparticles (NP) as well as adding a catalyst, e.g., Ni, Pt, Cu, or Pd, to Fe^0 can enhance reactivity as observed with dehalogenation of halo-organic contaminants.(Bokare *et al.*, 2008; Chen *et al.*, 2011; Cho & Choi, 2010) For example, Pd^0 added to $n\text{Fe}^0$ effectively transformed a wide range of contaminants (Cho & Choi, 2010; Wang *et al.*, 2013); however, not PFOS (Saerom Park *et al.*, 2017). Ni has the potential to be a more reactive catalyst with its wide range of stable oxidation states ($\text{Ni}^0/\text{Ni}^{+1}/\text{Ni}^{+2}/\text{Ni}^{+3}$) (Ananikov, 2015) and is less expensive. NiFe^0 particles have also been shown to have enhanced stability relative to some other bimetal particles (Han & Yan, 2014). Ni also can catalyze C-C bond cleavage forming short chains (Schrack *et al.*, 2002). Therefore, addition of Ni as a catalyst to Fe^0 nanoparticles may enable PFOS degradation without the need for high temperatures and supercritical water conditions. One other factor that has to be addressed when considering NPs is their increased tendency to aggregate, which may reduce accessibility to reaction sites (Zhang, 2014). Various approaches have been used to facilitate NP dispersion (Hotze *et al.*, 2010; Serp & Machado, 2015; Zhang, 2014). One approach to minimizing aggregation is to support the NPs on activated carbon (AC), which aligns with common materials used in water treatment. AC may also reduce PFAA mobility through sorptive processes and increase PFAA proximity to the reactive metals further facilitating reductive transformation.

1.2. Research Objectives

The ineffectiveness of traditional technologies and oxidation to degrade both PFSAAs and PFCAs, especially in situ, leads to the need for exploring reductive technologies. This

dissertation research evaluates the potential for nano NiFe⁰ particles supported on AC (nNiFe⁰-AC) to transform both linear and branch PFOS isomers as well as other PFAAs under conditions amenable for potential use as part of an in-situ treatment strategy following the aims listed below. In conducting the research described under each of the aims, considerable effort was given to collect evidence that PFAA removal was not just due to adsorption but transformation with evidence of fluoride and sulfite generation as well as organic transformation products.

Aim 1. Evaluate if nNiFe⁰-AC degrades PFOS with evidence of inorganic and organic product generation. Anaerobic batch reactors and fixed reaction times were used (1) to test the hypotheses that under anaerobic conditions a reductive treatment using bimetal nanoparticles will transform total PFOS to less fluorinated compounds, (2) to confirm transformation includes L-PFOS, the isomer most resistant to even attack, and (3) that fluoride and sulfate generation is observed as main degradation products.

Aim 2. Quantify the anaerobic transformation kinetics of PFOS by nNiFe⁰-AC at 60 °C and characterize transformation pathways. Kinetic studies were used to test the hypothesis that (1) PFOS transformation could be fit to a pseudo first-order reaction, because the concentration of the nanoparticles are in excess and the rate of the reaction will depend only on PFOS concentration (2) fluoride and sulfate concentrations will increase associated to PFOS decrease over time, (3) organic degradation products will be generated and further reduced over time, and (4) more than one pathway is followed as PFOS is transformed.

Aim 3. Evaluate the effect of carbon chain length and polar head functional group on

PFAA transformation. Batch studies using single solute in deionized water to investigate the hypothesis that (1) PFAA transformation will decrease with decreasing is alkyl chain length, and (2) PFCAs will degrade faster than their PFSA homologues (same alkyl carbon chain length) due to their lower thermal activation energy.

Aim 4. Evaluate the effect of groundwater constituents on PFAA transformation.

Effectiveness of nNiFe⁰-AC at 60 °C to transform PFAAs in a PFAA-contaminated groundwater compared to single solute transformation in deionized water was investigated to test the hypothesis that PFAA degradation may be reduced in the presence of high inorganic ion concentration compared to the orders of magnitude lower PFAA concentrations due to competition for surface sites.

1.3. Organization

This work consists of 6 chapters including the introduction already presented, a literature review on PFAS treatment approaches, 3 chapters addressing Aims 1, 2 and then 3 and 4 together, and a closing summary chapter.

Chapter 2. A literature review of including some background on PFAS, physical and chemical properties particularly for the PFAAs, PFAS release and PFAA concentrations in the environment, and a summary of oxidation and reduction techniques used to degrade PFAAs highlighting the treatments most amenable for in-situ applications.

Chapter 3. This chapter focuses on the exploration of various approaches for enhancing reactivity of zero valent iron to avoid extreme conditions such as high temperature and pressure conditions. Particle reactivity was evaluated at room temperature and at an elevated but not extreme temperature of 60 °C and with addition of Ni as a catalyst, activated carbon as a support to decrease aggregation and increase surface area, and prolonged mechanical stirring during particle synthesis. Transformation of L- and Br-PFOS was quantified to evaluate if transformation was isomer specific with and individual L-PFOS experiments as a confirmation that L-PFOS was transformed.

Chapter 4. This chapter focus on the transformation kinetic of PFOS with nNiFe⁰-AC under anaerobic conditions. Transformation rates of L- and Br-PFOS were quantified in batch experiments over time to assess whether the L- and Br-PFOS transformation rates exhibited the same degradation rates. The formation and subsequent reduction over time of the organic intermediates were assessed to aid in constructing transformation pathways.

Chapter 5. This chapter focuses on the effects of carbon-chain length, functional group, and mixtures in a groundwater matrix on PFAA transformation. Single solute experiments using deionized water were performed using C4, C6 and C8 PFCAs and the PFSA homologues and transformation trends compared. Mixture and matrix effects on PFAA chemical reduction was explored using groundwater from a former fire-training in Massachusetts.

Chapter 6. The most important finding from these investigations are summarized along with future work needed.

CHAPTER 2. LITERATURE REVIEW

2.1. Physical and Chemical Properties of Per- and Polyfluoroalkyl Substances

Per- and polyfluoroalkyl substances (PFAS) are a large group (>6,000) of highly fluorinated aliphatic chemicals that have been synthesized for over 60 years (Wang *et al.*, 2017). These synthetic chemicals have a fluorinated hydrophobic linear carbon chain and a hydrophilic functional group. The alkyl chain consists of 2 to 16 carbon atoms completely saturated with fluorine (perfluoroalkyl) or partially fluorinated containing few C-H bonds (polyfluoroalkyl). Their hydrophilic moiety has a neutral (i.e. $-\text{CH}_2\text{CH}_2\text{OH}$ and $-\text{SO}_3\text{NH}_2$), anionic ($-\text{COO}^-$, $-\text{SO}_3^-$, $-\text{OPO}_3^-$), cationic (attached to another moiety such as a quaternary ammonium group) or zwitterionic (containing both cationic and anionic functional groups) group. Examples of PFAS' molecular structure and their ionic functional group are presented in Figure 2-1. Perfluoroalkyl acids (PFAAs), one of the group of the PFAS family, are the terminal degradation product (daughter products) of several polyfluoroalkyl substances, called precursors (Benskin *et al.*, 2012; Buck *et al.*, 2011; Eriksson *et al.*, 2017; Liu & Avendano, 2013). Their chemical structure can be represented by $\text{C}_n\text{F}_{2n+1}\text{-R}$, where $\text{C}_n\text{F}_{2n+1}$ defines the length of the perfluoroalkyl chain and R represents the attached functional group head. The functional group could be a sulfonic acid, carboxylic acid, phosphonic acid, sulfinic acid or other substituents (Buck *et al.*, 2011). Examples shown in Figure 2-1. The perfluoroalkyl moiety ($\text{C}_n\text{F}_{2n+1}$) is the responsible of their hydrophobic and lipophobic properties, while the polar functional group provides their surfactant properties. PFAAs are chemically and thermally stable and do not breakdown into the environment (Surma & Zielinski, 2015). The stability of PFAAs against degradation is attributed to the strength of the C-F bonds and the absence of reactive sites in the PFOS molecule because

the carbon chain is hidden by fluorine atoms (Kissa, 2001) . PFAAs are divided into two major groups: perfluoroalkyl sulfonic acids (PFSAs, $C_nF_{2n+1}SO_3H$) and perfluoroalkyl carboxylic acids (PFCAs, $C_nF_{2n+1}COOH$).

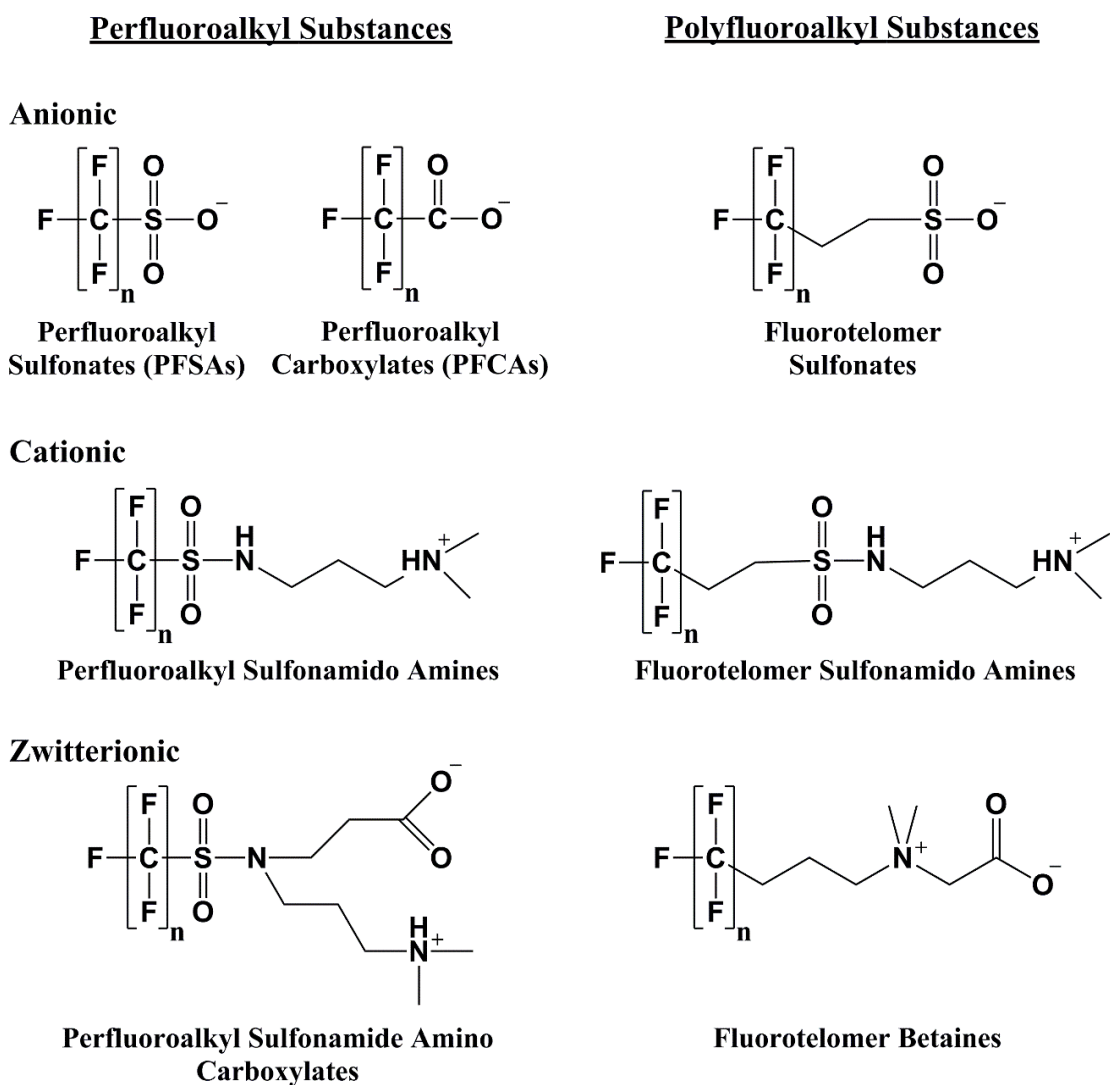


Figure 2-1 Examples of PFAS' chemical structure (per- and poly) of some of the PFAS subclasses and their charged functional group head (anionic, cationic, and zwitterionic). n = 2 to 18.

Physical and chemical properties of PFAAs are summarized in Table 2-1 and example structures are shown in Figure 2-2. This information includes chemical formulas, molecular weight, monoisotopic mass, boiling and melting points, etc. Their surfactant's properties determine their potential for partitioning, persistence and accumulation in the environment and biota. Due to their low pK_a values (Table 1), PFAAs exist primarily as anions in the environment and biotic media. Their relative high solubility and low vapor pressure help to reinforce this statement. Accurate measurements of their octanol-water partition coefficients (K_{ow}) are not experimentally feasible due to their amphiphilic properties; therefore, only estimations are presented in Table 1. PFAAs are less volatile than several other water contaminants and only the acid forms of PFAAs are able to partition into air from aqueous solutions at very low pH (Kaiser, 2010). PFAAs are expected to have low mobility if released to soil, based on their K_{oc} values. At higher concentrations, PFAAs form aggregates where their hydrophilic part interacts with water and their hydrophobic moiety interact each other. The critical micelle concentration (CMC) varies with chain length, functional groups, and counterions. Chain length has the largest and most consistent effect with CMC decreasing with increasing chain length (Table 2-1).

Table 2-1. Physical and chemical properties of perfluoroalkyl substances.

Property	PFCAs			PFSAs		
	PFOA	PFHxA	PFBA	PFOS	PFHxS	PFBS
Chemical Formula	C ₈ HF ₁₅ O ₂	C ₆ HF ₁₁ O ₂	C ₄ HF ₇ O ₂	C ₈ HF ₁₇ O ₃ S	C ₆ HF ₁₃ O ₃ S	C ₄ HF ₉ O ₃ S
Chemical Abstract Service (CAS) number	335-67-1	307-24-4	375-22-4	1763-23-1	355-46-4	375-73-5
Physical state	Solid	Liquid	Liquid	Solid	Solid	Liquid
Molecular Weight (g/mol)	414.07	314.05	214.04	500.13	400.11	300.10
Monoisotopic Mass (g/mol)	413.97	313.98	213.99	499.94	399.94	299.95
Chain Length	Long	Short	Short	Long	Long	Short
Boiling Point (°C)	189 – 192 ^a	168 ^k	121	No data	452 ⁿ	447 ⁿ
Melting Point (°C)	45 – 50 ^a	No data	-17.5 ^k	>400 ^a	190 ⁿ	188 ⁿ
Vapor Pressure at 25 °C (Pa)	1.21 x 10 ^p	1.21 x 10 ^{2p}	8.99 x 10 ^{2p}	3.2 x 10 ^{-1p}	1.08 x 10 ⁻⁶ⁿ	1.49 x 10 ⁻⁶ⁿ
Henry's Law Constant at 20 °C (Pa·m ³ /mol)	0.362 ^j	No data	1.24 ^j	4.34 x 10 ^{-7q}	No data	No data
Log K _{oc} (mL/g)	1.89 – 3.5 ^b	1.31 – 2.1 ^b	1.88 ^b	2.6 – 3.8 ^b	2.05 – 3.7 ^b	1.22 – 1.79 ^b
Log K _{ow}	5.30 – 6.26 ^{c,d}	4.06 – 4.50 ^{c,d}	2.82 – 2.91 ^{c,d}	4.67 – 7.66 ^{c,d}	0.97 – 5.17 ^{c,e}	3.90 ^c
Water solubility at 25 °C (mg/L)	3400 – 4340 ^e	15700 – 21700 ^{c,g}	563 ^c	570 ^{e,g}	1400 ^g	510 – 46200 ^{e,g}
pK _a	-0.21 ^{f,g}	-0.17 – -0.16 ^{f,g}	0.05 ^{f,g}	-3.27 – 0.14 ^{f,g}	0.14 ^{f,g}	0.14 ^{f,g}
Critical micelle concentration (CMC, mM, sodium or potassium salts)	8.7, 9, 9.1, 10.5 ^h	51, 82 ^h	710, 740, 750 ^h	8 ^h	No data	No data

^a(Larsen & Giovalle, 2015), ^b(Pereira *et al.*, 2018), ^c(Wang *et al.*, 2011), ^d(Rayne & Forest, 2009), ^e(Rahman *et al.*, 2014), ^f(Ahrens *et al.*, 2012), ^g(Du *et al.*, 2014), ^h(Kissa, 2005), ⁱ(Kaiser *et al.*, 2005), ^j(Kwan, 2001), ^k(Lide, 2005), ^l(Kauck & Diesslin, 1951), ^m(3M, 2008), ⁿ(EPA., 2015), ^p(Ding & Peijnenburg, 2013), ^q(OECD, 2002).

Properties, transport, degradation, and toxicity of PFAAs are related to their carbon-chain length and functional group. Long-chain PFAAs, which are defined as $n \geq 6$ for PFSA and $n \geq 7$ for PFCAs, are recognized as persistent, bioaccumulative and toxic chemicals (Armitage *et al.*, 2009). The difference in what is considered long and short between the PFSA and the PFCAs is a function of the perfluorinated carbons ($n+1$) in the alkyl chain, i.e., $\text{CF}_3(\text{CF})_n$, with the carboxylate carbon in the PFCAs not having any C-F bonds. Of the known 'long-chain' PFAAs, perfluorooctane sulfonate (PFOS, $\text{C}_8\text{F}_{17}\text{SO}_3^-$) and perfluorooctanoic acid (PFOA, $\text{C}_7\text{F}_{15}\text{COO}^-$) were the most extensively produced and are the most widely studied in the United States. They are solid at room temperature with a low vapor pressure and high stability. Short-chain PFAAs are being introduced as alternatives to C8-PFAAs (PFOS and PFOA), because they are deemed less bioaccumulative. However, these shorter chain PFAAs are equally persistent and more water soluble and sorb less to particles, thus with a higher potential for long-range transport than their long-chain analogues (Brendel *et al.*, 2018). Short-chain PFAAs have been detected in remote areas (Kirchgeorg *et al.*, 2016; Llorca *et al.*, 2012) likely as result of the degradation of their volatile precursors.

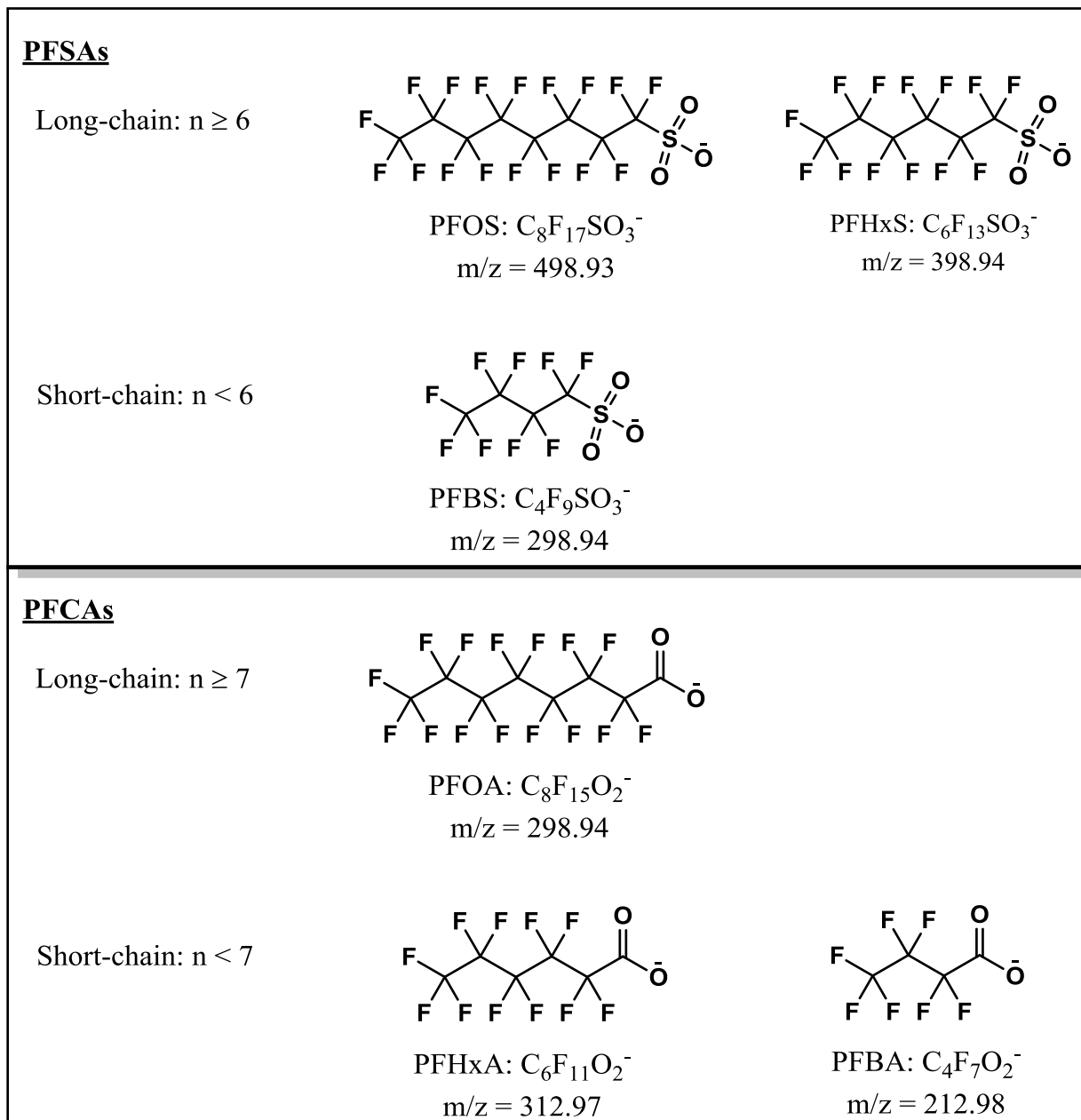


Figure 2-2. Chemical structures of perfluoroalkyl sulfonic acids (PFSAs: PFOS, PFHxS, and PFBS) and perfluorocarboxylic acids (PFCAs: PFOA, PFHxA, and PFBA) of long- and short-carbon chain.

2.2. Releases to the environment

PFAAs have been detected as mixtures in various environmental matrices including soil, sediments, wastewater effluents, surface, ground, and drinking water (Hu *et al.*, 2016; Oliaei *et*

al., 2013; Ullah *et al.*, 2011; Xiao *et al.*, 2015). PFAAs can enter to the environment from four major sources: industrial sites; fire training and response sites; landfills; and wastewater plants/biosolids. According to Hu *et al.* (Hu *et al.*, 2016), industrial emissions are significantly higher than domestic sources, being the main responsible for PFAS contamination in the environment. Industrial sources include manufacturing facilities that produce PFAS and facilities that use PFAS to produce goods (such as textile processors, paper mills, industrial surfactants, etc.). PFAS can be released from manufacturing facilities via wastewater discharges, waste disposal, incidental releases (leaks and spills), and stack emissions. Firefighting foams containing fluorosurfactants are commonly used in military and civilian airports to extinguish fire. These foams contain a mixture of PFAS, with significant amount of PFAAs. Common release mechanisms from fire training sites include release during storage or equipment testing and calibration, and fire training activities. Wastewater treatment plants (WWTP) have been demonstrated as a point of PFAS contamination to the environment (Dauchy *et al.*, 2019). PFAS enter to the wastewater stream from industrial and domestic inputs. However, wastewater treatment processes provide negligible removal of these chemicals (Appleman *et al.*, 2014). PFAS entering the WWTP are either going to end up either in the effluent or the sludge that is transformed to biosolids that are land-applied. During biological treatment within the WWTP (activated sludge process), two things happen: degradation or sorption to the sludge. Degradation processes only convert degradable PFAS into PFAAs, thus referred to as PFAA-precursors. Some potential PFAA-precursors include perfluoro sulfonamido carboxylates, perfluoro sulphonamides, perfluoro sulfonamido amines, perfluoro sulfonamidoethanol, perfluoro sulfonamide amine oxides, perfluoro thioamido sulfonates, fluorotelomers, etc. (CONCAWE, 2017).

Biosolids are organic materials derived from wastewater treatment processes. Several long and short-chain PFAS have been detected in municipal wastewater and biosolids (Chu & Letcher, 2017; Navarro *et al.*, 2016). Thus, the application of biosolids to agriculture lands can result in a transfer of PFAS to soil and PFAS leaching to groundwater. A new requirement to the composting facilities to test for PFOS, PFOA, and PFBS was established in Maine in March 2019, after a farm was contaminated with PFAS from municipal sludge applications.

Another root of PFAAs in the environment is through environmental biodegradation of PFAA precursors. Fluorotelomer alcohols (e.g. 6:2 FTOH) are commonly found in AFFF-impacted groundwater up to 220 µg/L (Backe *et al.*, 2013). Biodegradation of 6:2 FTOH and 8:2 FTOH by *P.chrysosporium*, a fungus commonly found in soil reveal generation of PFCAs as metabolites (Tseng, 2012).

2.3. Levels in the environment and regulatory responses

PFAAs are widely detected in air, soil, water, and wildlife species at different trophic levels (Bao *et al.*, 2019; Chu & Letcher, 2017; Ghisi *et al.*, 2019; Houtz *et al.*, 2013; Hu *et al.*, 2016; Liu *et al.*, 2016; Oliaei *et al.*, 2013; Paul *et al.*, 2009; Rahman *et al.*, 2014; Szabo *et al.*, 2018). PFAAs are extremely stable and do not breakdown in the environment. In fact, they accumulate increasing their concentration over time causing concern for their long-term exposure (Buck *et al.*, 2011; Sunderland *et al.*, 2019). Groundwater redox condition might produce biological oxidation of PFAA-precursors transforming them to persistent PFAAs: PFCAs and PFSAAs (Houtz & Sedlak, 2012). PFAAs and their precursors are routinely found at elevated concentrations in groundwater near to military and firefighter training areas (Figure 2-3 and Table 2-2). Backe *et al.* (Backe *et al.*, 2013; Houtz *et al.*, 2013; Schultz *et al.*, 2004) found that <85%-92%> of the fluorosurfactants detected in groundwater at AFFF-impacted sites (1940s

to 1990s) were PFCAs and PFSAs, and <8%-15%> PFAA-precursors. While Schultz *et al.* (Schultz *et al.*, 2004) reported that 82% of PFAS detected near to an air force base in Florida (1980s to 1990s) was PFAA-precursors, 16% PFSAs, and only 2% PFCAs.

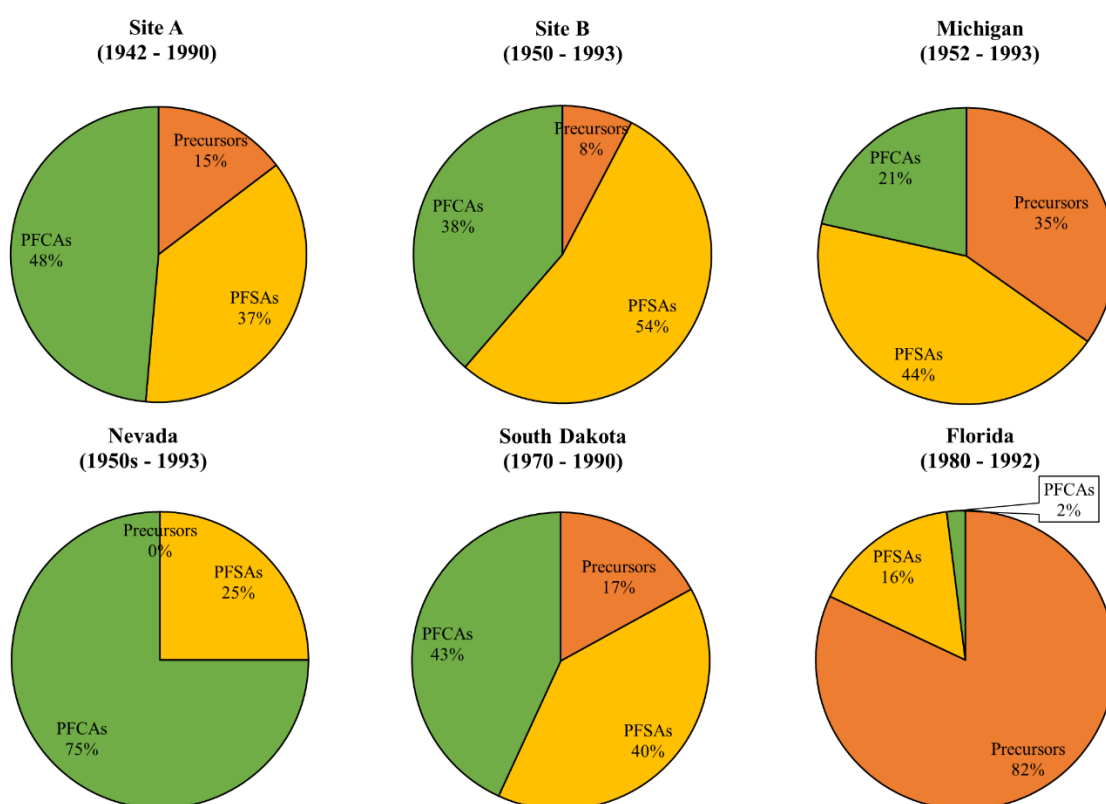


Figure 2-3. Composition of fluorosurfactants detected in groundwater at AFFF-impacted sites (U.S. military bases) (Backe *et al.*, 2013; Houtz *et al.*, 2013; Schultz *et al.*, 2004).

Of the precursors detected in groundwater, the most commonly measured were fluorotelomer sulfonates (FtS): 4:2 FtS, 6:2 FtS, and 8:2 FtS. Among these precursors, 6:2 FtS was the dominant fluorotelomer detected at high concentrations. PFAAs-precursors transformation and PFAAs migration can occur simultaneously, thus increasing total PFAA concentration in the environment. Table 2-2 report levels typically found in PFAA-impacted groundwater. PFOA has the greatest maximum concentration of ~6.6 mg/L with the widest range of <n.d. - 6,6 mg/L>,

followed by PFOS (n.d. – 2.3 mg/L), PFHxS (n.d. – 0.92 mg/L), PFHxA (n.d. – 0.37 mg/L), PFBS (n.d. – 0.21 mg/L), and PFBA (n.d. – 0.087 mg/L). Concentration of PFAAs near manufacturing sites, wastewater treatment plants and biosolids impacted fields are usually in the ng/L range, much lower than at military sites.

PFAS have been in the environment for more than 60 years, but not until the past few years did health concerns lead authorities to start establishing regulatory values. While the United States Environmental Protection Agency (USEPA) has not established maximum contaminant levels for PFAS, in 2016 EPA did established a lifetime health advisory of 70 ng/L for both PFOS and PFOA in drinking water. Multiple releases of PFAAs into the environment over a long period of time, such as those described above specific to military operations, have led to PFOA and PFOS concentrations in groundwater above EPA recommended guidance levels in many cases. IN addition, a study published in 2016 (Hu et al.) revealed that approximately six million U.S. residents have drinking water contaminated with PFOS and/or PFOA (combined) above the USEPA’s lifetime health advisory (70 ng/L). In response, several states are acting to reduce PFAS exposure. For example, California, Colorado, Iowa, Kentucky, Maine, Massachusetts, and Connecticut are prohibiting the use of PFAS in firefighting foam, food packaging, and cosmetics. Other states like Florida are requiring entities who discharge PFAS to report their discharge to EPA, additional to a continuous monitoring of PFAS concentration in rivers, lakes, wells, and fish. Some states are establishing their own health screening limits, for example Michigan sets health screening level for drinking water for 5 PFAAs: PFOA (9 ng/L), PFOS (8 ng/L), PFNA (9 ng/L), PFHxS (84 ng/L), and PFBS (1000 ng/L).

Table 2-2 Groundwater concentrations (ng/L) of PFOA, PFHxA, PFBA, PFOS, PFHxS, and PFBS by source.

Type of area	Sampling location	PFCAs				PFSA		References
		PFOA	PFHxA	PFBA	PFOS	PFHxS	PFBS	
AFFF-impacted sites	Site A (1942 - 1990)	12,000 - 220,000	19,000 - 350,000	3,400 - 57,000	15,000 - 78,000	36,000 - 360,000	7,100 - 150,000	(Backe <i>et al.</i> , 2013)
	Site B (1950 - 1993)	8.6 - 57,000	<4.7 - 99,000	8.5 - 13,000	88 - 65,000	81 - 170,000	12 - 24,000	(Backe <i>et al.</i> , 2013)
	Michigan, USA (1952 - 1993)	n.d. - 105,000	n.d. - 5,000	-	4,000 - 110,000	5,000 - 120,000	-	(Schultz <i>et al.</i> , 2004)
	Florida, USA (1980 - 1992)	n.d. - 116,000	n.d. - 144,000	-	147,000 - 2,300,000	107,000 - 920,000	10,000 - 144,000	(Schultz <i>et al.</i> , 2004)
	Nevada, USA (1950s - 1993)	n.d. - 6,570,000	n.d. - 372,000	-	n.d. - 380,000	n.d. - 876,000	n.d. - 210,000	(Schultz <i>et al.</i> , 2004)
Manufacture facilities (Fluoropolymer plant perimeter)	South Dakota, USA (1970 - 1990)	n.d. - 190,000	n.d. - 320,000	n.d. - 87,000	n.d. - 100,000	n.d. - 530,000	n.d. - 140,000	(Houtz <i>et al.</i> , 2013)
	Shandong, China	0.52 - 239,644	0.07 - 8,878	0.05 - 24,178	0.02 - 37.8	0.12 - 4.62	0.12 - 43	(Liu <i>et al.</i> , 2016)
	Changshu, China	1.8 - 475.0	<0.2 - 286.3	<0.1 - 41.1	<0.5 - 37.0	<0.5	<0.5 - 7.4	(Lu <i>et al.</i> , 2018)
WWTP	Wuhu, China	81.7 - 4,151	1175	352 - 3,613	0.15 - 1.05	-	22.4 - 865	(Wang <i>et al.</i> , 2016)
	Melbourne, Australia	<0.09 - 6.9	<0.03 - 27.2	<0.1 - 13	<0.03 - 34	<0.03 - 18	<0.09 - 2.9	(Szabo <i>et al.</i> , 2018)
Biosolids impacted fields	France, Europe	<4 - 12	<4 - 28	<4 - 8	<4 - 50	<4 - 32	<4 - 6	(Boiteux <i>et al.</i> , 2012)
	Sweden, Europe	<0.4 - 436	<0.09 - 1890	<0.25 - 409	<0.21 - 29	<0.15 - 80	<0.22 - 22	(Ahrens <i>et al.</i> , 2016)
	Alabama, USA	149.2 - 6,410	9.7 - 3970	10.4 - 1260	12.0 - 150.6	12.7 - 87.5	10.1 - 76.6	(Lindstrom <i>et al.</i> , 2011)

2.4. Chemical Treatments Tested for Perfluorooctane sulfonate

Perfluoroalkyl acids (PFAAs) are stable and not biodegrade or breakdown in the environment. In fact, they can be generated from microbial degradation of PFAA-precursors (Dasu *et al.*, 2013; Royer *et al.*, 2015) or after oxidative treatments from conventional water treatment process (Eriksson *et al.*, 2017). Thus, abiotic treatments must be the focus of any management strategy for reducing PFAA loads in the environment.

Ex-situ chemical treatments are easier to contain, monitor, and control, however they require pumping of groundwater, treated, and re-injected, leading to increased costs. In-situ chemical process have been demonstrated to be promising alternatives to conventional pump-and-treat practice for contaminated groundwater. It is useful for addressing source areas contaminated by nonaqueous phase liquids (NAPLs) and for intercepting plumes to remove mobile organic contaminants. Despite the fact that in-situ chemical technologies offer substantial benefits over conventional pump-and-treat technology, there is still concerns about their delivery or implementation, fate over time and potential environmental effects of washing reagents in some cases.

Reduction/oxidation chemical treatment methods are chosen to convert hazardous contaminants to less toxic compounds. Oxidation processes are used to oxidize organic contaminants with a wide range of chemical structures. These processes involve the production of very reactive radicals including hydroxyl ($\bullet\text{OH}$), hydroperoxyl ($\text{HO}_2\bullet$), superoxide ($\text{O}_2\bullet$), sulfate, ($\text{SO}_4\bullet$), and carbonate ($\text{CO}_3\bullet$) as oxidizing agents. The $\bullet\text{OH}$ has a high standard reduction potential (2.80V) and has been able to oxidize a large number of organic compounds (Benitez *et al.*, 2001; Pandiyan *et al.*, 2002), but the process is pH-dependent. However, PFAAs generally tend to be resistant to oxidative processes with only PFCAs showing vulnerability to

oxidation treatments. Reduction processes are rarely used, and they have very specific applications. Thus, while oxidation processes use oxidizing radicals, reduction treatments decompose organic contaminants by producing highly reactive reducing radicals like aqueous, or also known as aquated, electrons (e_{aq}^-) or H-atoms (H^\bullet). However, H-atoms are mostly ineffective to treat PFAAs.

Currently, there are no feasible in situ treatment method available to transform the range of PFAS congeners common to military sites. Here literature available on in-situ and ex-situ treatments for PFAAs degradation will be explored with a focus on PFOS as it has been shown to be the most resistant to breakdown.

2.4.1. Ex-situ Oxidation

Of the several ex-situ abiotic treatments investigated for PFAAs only 3 oxidation treatments (UV/ Fe^{3+}), sonochemical oxidation and electrochemical) were able to transform PFOS with evidence of degradation products (Table 2-3). The first technique shown to decompose PFOS was sonochemistry in an argon atmosphere. Sonochemistry is a chemical reaction caused by acoustic cavitation. Acoustic cavitation is the formation and collapse of bubbles in solution irradiated by intense ultrasound. According to Vecitis (Vecitis, 2009), PFOS degradation occurs at the bubble-water interface where 60% of PFOS was mineralized to F^- and SO_4^{2-} ions. In 2014, Jin (Jin *et al.*, 2014) explore photo-Fenton reactions to transform PFOS. Photo-Fenton processes are facilitated by UV light irradiation of aqueous ferric ions under 365 nm wavelength generating Fe^{2+} . Jin observed PFOS decomposition in the presence of ferric ion (Fe^{3+}) under UV irradiation. He claimed that Fe^{3+} enhanced PFOS decomposition by complexing PFOS with Fe^{3+} followed by desulfonation of the PFOS radical to form a perfluoroalkyl radical.

The perfluoroalkyl radical formed will react with oxygen or HO• to form C2-C8 PFCAs with the release of F⁻ ions.

Another ex-situ oxidation treatment investigated was electrochemical oxidation (EO). EO is an oxidation process that takes place at the interface of an electrode (solid metal or semiconductor) and an ionic conductor (electrolyte, e.g., NaClO₄, Na₂SO₄). EO can oxidize organic contaminants through direct or indirect oxidation processes. Direct oxidation reactions occur at the anode by electron transfer, when the target pollutant is adsorbed in the anode surface. While indirect oxidation reactions take place in solution through oxidation of strong oxidants produced during the electrolysis. Boron-doped diamond (BDD) electrodes are extensively used for PFAAs degradation by direct electron transfer. For example, destruction of PFOS [400 μM] was achieved in a reactor at current density of 20 mA/cm², at 22 °C, and with 10 mM NaClO₄ electrolyte solution (Carter & Farrell, 2008). The reaction products generated in an electrochemical oxidation consisted of F⁻, SO₄²⁻, CO₂, and < 3% trifluoroacetic acid (TFA). BDD electrodes performance was also tested with real groundwater samples in batch mode (Schaefer *et al.*, 2017; Schaefer *et al.*, 2018; Trautmann *et al.*, 2015).

2.4.2. Ex-Situ Reduction

Similar to oxidation treatments, effective reductive methods were limited (Table 2.3) and only three were able to decompose PFOS (UV/KI, alkaline 2-propanol photolysis, and discharge plasma).

Iodide photolysis under UV irradiation is an effective method to produce e_{aq}⁻. Iodide ions (I⁻) are photolabile to release e_{aq}⁻ via charge-transfer-to-solvent (CTTS). Hydrated electrons are the most reactive reducing species (E_{aq}⁰ = -2.9 V) that have been used for reductive decomposition of recalcitrant organic contaminants (Gu *et al.*, 2017; Liu *et al.*, 2015; Park *et al.*,

2011; Tian & Gu, 2018). Park (Park *et al.*, 2011) explored indirect photoreduction of PFOS by e_{aq}^- using UV/iodide under anoxic conditions (Park *et al.*, 2011). He found several desulfonated products ($C_xF_{2x+1}I$) in the headspace such as $C_8F_{17}I$, suggesting that the C-S bond was the first bond broken. The total F (inorganic and gaseous intermediates) quantified account for 76% of F contained in PFOS.

Another technique studied to treat PFOS was UV irradiation in alkaline 2-propanol solution. Most PFAS congeners do not absorb strongly above 300 nm thus their direct photolysis is very low. Alkaline alcohols have been used as photocatalyst for the production of isopropyl radicals, a strong reductant ($(CH_3)_2CO^-$, $E^0 = -2.1$ V). Yamamoto (Yamamoto *et al.*, 2007) observed PFOS (40 μ M) decomposition after 10 days of irradiation using a low-pressure mercury lamp (254 nm, 32 W) in water (68%) and alkaline 2-propanol solution (92%). The generation of F^- and SO_4^{2-} confirmed that the C-F and C-S bonds have been dissociated. The molar ratio of SO_4^{2-} to PFOS degraded was ~ 0.9 , thus sulfur-containing byproducts are not expected. Of the F contained in the PFOS that was degraded, 71% was converted to fluoride. The short-chain byproducts identified include alcohols (e.g. $C_8F_{17}OH$), PFCAs (e.g., PFOA) and paraffins (e.g., C_8HF_{17}).

Additionally, DC plasma is an electrical process where the discharge in and in contact with liquids can dissociate water molecule forming $\bullet OH$, H atoms and free electrons. OH and Hydrogen radicals are very reactive agents having a reduction potential of 2.8V and -2.3V, respectively, but their generation is pH-dependent. DC plasma was used effectively for the degradation of PFAAs (Hayashi *et al.*, 2015; Tachibana *et al.*, 2014; Yasuoka *et al.*, 2011). Tachibana studied the decomposition of PFOS by DC plasma generated in argon gas bubbles. In a 600 min reaction, 98% of PFOS was degraded and several organic byproducts generated in the

aqueous phase including polyfluoroalkyl sulfonic acids of shorter carbon-chain ($C_mHF_{2m}SO_3H$, $m = [2-8]$), polyfluoroalkyl carboxylic acids ($C_nHF_{2n}COOH$, $n = 2-7$) and PFOA. Volatile byproducts were also detected in the gas phase such as CHF_3 , C_2HF_5 and C_2F_6 . Inorganic anions produced immediately in the thermal decomposition of PFOS by heat from the plasma (1600 K) consisted of CO_2 , CO , F^- , and SO_4^{2-} . According to Tachibana *et al.* (2014), PFOS molecules adsorbed onto the plasma-liquid interface and pyrolyze to C1 fluoro-radicals and SO_3 , which then react with water vapor, H atoms, and OH radicals forming CO_2 , CO , and HF.

Table 2-3. Summary of ex-situ oxidation and reduction treatments for PFAAs.

Treatment	Conditions	PFAA decomposed (%)	Products	References
Ex-Situ Oxidation				
Photo-Fenton oxidation	254 nm [Fe(III)] ₀ = 100 μM pH = 3.6 [PFOS] ₀ = 8 μmol RT = 72 h Temp = 25 °C	[PFOS] _f = 8 μmol (100%)	57.5% F ⁻ SO ₄ ²⁻ Short-chain PFCAs: C _n F _{2n+1} COOH, n = [1-6]	(Jin <i>et al.</i> , 2014)
Electrochemical oxidation (EO)	BDD 20 mA/cm ² [NaClO ₄] = 10 mM [PFOS] ₀ = 400 μM RT = 0.5 h Temp = 22 °C Frequency = 358 kHz Power density = 250	[PFOS] _f = 396 μM (99%)	11% F ⁻ SO ₄ ²⁻ CO ₂ < 3% TFA	(Carter & Farrell, 2008)
Sonolysis	W/L [PFOS] ₀ = 20 μM Temp = 10 °C RT = 3 h	[PFOS] _f = 20 μM (100%)	95% F ⁻ 100% SO ₄ ²⁻	(Vecitis <i>et al.</i> , 2009)
Ex-Situ Reduction				
UV/KI photolysis	254 nm light [KI] = 10 mM [PFOS] ₀ = 20 μM RT = 10 d Temp = 50 °C	[PFOS] _f = 10 μM (50%)	50 % F ⁻ Gaseous fluorocarbon: C _n F _{2n+1} I	(Park <i>et al.</i> , 2011)
Alkaline 2-propanol photolysis	254 nm light [C ₃ H ₈ O] = 68 mmol [PFOS] ₀ = 40 μM RT = 10 d Temp = 50 °C	[PFOS] _f = 36.8 μM (92%)	71 % F ⁻ 91% SO ₄ ²⁻ Several fluorinated compounds: C _n F _{2n+1} H, C _n F _{2n+1} OH, C _{n-1} F _{2n-1} COOH n = [3-7]	(Yamamoto <i>et al.</i> , 2007)
Discharge Plasma	Current = 10mA Flow rate Ar = 100 sccm [PFOS] ₀ = 56 μM RT = 10 h Temp = 1600 K	[PFOS] _f = 55 μM (98%)	50 % F ⁻ CO CO ₂ Short-chain PFSAs and PFCAs: C _m HF _{2m} SO ₃ H, m = [2-8] C _n HF _{2n} COOH, n = [1-7] Gaseous fluorocarbon: CHF ₃ , C ₂ HF ₅ , and C ₂ F ₆	(Tachibana <i>et al.</i> , 2014)

2.4.3. In-Situ Oxidation

In-situ chemical oxidation (ISCO) treatments such as permanganate, persulfate, or hydrogen peroxide are not effective to transform PFOS. Treatability of PFAAs using ISCO is mostly limited to PFCAs.

2.4.4. In-Situ Reduction

Contrary to oxidation treatments, reduction of PFOS was obtained using zero valent metals (ZVM) and vitamin B12 (Table 2-4).

Nano zero valent iron ($n\text{Fe}^0$) has been successfully used for abiotic dehalogenation of chlorinated compounds (Kim *et al.*, 2010; Kim & Carraway, 2000; Kim *et al.*, 2004; Roberts *et al.*, 1996). Their small size and large surface area provide excellent adsorption properties, reducing capability, and activity. Under anaerobic conditions, $n\text{Fe}^0$ is oxidized by H_2O or H^+ producing Fe^{2+} and H_2 . Thus, three major reductants will be present in the reaction system (Fe^0 , Fe^{2+} and H_2). These reductants may react with the organic contaminant by electron transfer from $n\text{Fe}^0$ to form Fe^{2+} and Fe^{2+} to form Fe^{3+} or from H_2 if a catalyst is present. Subcritical water is liquid water under pressure and temperature between 100 °C to 374 °C. It has been used as a catalyst, reactant, and effective solvent for both polar and non-polar compounds. As the temperature increase the polarity, surface tension and viscosity dramatically decrease.

Reductive decomposition of PFOS using ZVMs in subcritical water at 350°C and 20 MPa for 6 h has been observed (Hori *et al.*, 2006). Fe^0 led to the greatest PFOS decomposition with ~98% PFOS lost (3.72 μmol), 51.4% mole conversion to fluoride, and a very small amount of CHF_3 (yield of 0.7%). According to Hori, the sorption interaction between PFOS and the metal

surface is the main driving force in the degradation of PFOS. Surface reactions require adsorption of the organic contaminant to the particle surface to be effective.

Another reduction technique tested was Vitamin B₁₂ as the electron mediator. Vitamin B₁₂ is an organometallic molecule used as a catalyst for reduction reactions. Vitamin B₁₂ have been used as electron-transfer shuttles in reductive process. Some common electron donors applied in these reactions include titanium citrate (Ochoa-Herrera *et al.*, 2008) and metals (S. Park *et al.*, 2017). The degradation process start with the reduction of Co³⁺ in the vitamin B₁₂ to Co²⁺ (vitamin B_{12r}) and Co¹⁺ (vitamin B_{12s}) by reductants such as Ti(III) (Duenas Fadic, 2013; Shimakoshi & Hisaeda, 2017). Then, the reduced Co¹⁺ will facilitate the electron transfer to the organic contaminant.

PFOS (54 μM) defluorination has been observed using vitamin B₁₂ (260 μM) and Ti(III)-citrate (36 mM) at 70 °C under alkaline (pH=9) conditions (Ochoa-Herrera *et al.*, 2008). However, only branched PFOS isomers (71%) were transformed and fluoride generation was observed (12 moles of fluoride per mol of PFOS lost). Similarly, Park et al. (S. Park *et al.*, 2017) confirmed degradation of only branched PFOS using vitamin B₁₂ and metals as the source of electrons (nZn⁰). The vitamin B₁₂/metal system was able to degrade 95% branched PFOS at 90 °C and 5 days. Of all PFOS isomers, 6-PFOS has the highest degradation followed by 5-PFOS and 3&4-PFOS. The higher reactivity of 6-PFOS in this system was attributed to its accessible LUMO orbital (Duenas Fadic, 2013; Torres *et al.*, 2009).

Table 2-4. Summary of in-situ reduction treatments for PFAAs.

Treatment	Conditions	PFAA decomposed (%)	Products	References
Sub-critical elemental iron	[nFe ⁰] = 960 mM pH = 10.4 [PFOS] ₀ = 372 μM RT = 6 h Temp = 350 °C	[PFOS] _f = <2 μM (>99%)	51.4 % F ⁻ [CHF ₃] = 21 μM	(Hori <i>et al.</i> , 2006)
Vitamin B12 electron mediator	[VB12] = 0.26 mM [Ti(III)-citrate] = 36 mM pH = 9 [Br-PFOS] ₀ = 54 μM RT = 5 d Temp = 70 °C & 90 °C	[Br-PFOS] _f = 38 μM (71%)	71 % F ⁻	(Ochoa-Herrera <i>et al.</i> , 2008)
	[VB12] = 0.4 mM [nZn ⁰] = 0.2 g pH = 10.4 [Br-PFSAs] ₀ = 2.6 μM RT = 5 d Temp = 70 °C & 90 °C	[Br-PFOS] _f = 2.47 μM (95%) [Br-PFHxS] _f = 1.43 μM (55%)	100% F ⁻ C ₈ HF ₁₆ SO ₃ ⁻ Polyfluorinated sulfonic acids: (C ₈ H _n F _{15-n} SO ₃ H, n = [2-9])	(S. Park <i>et al.</i> , 2017)

Table 2-5 summarizes the energy required for treatment of PFOS by ex-situ or in-situ chemical oxidation and reduction methods. In general, in-situ treatments were more energy efficient than ex-situ methods, but with some limitations. For example, vitamin B₁₂ technologies have lower energy requirements than many approaches, but are unable to transform L-PFOS. Sub-critical elemental iron is the most energy efficient treatment and capable of transforming both linear and branched PFOS, but required high temperature and pressure to drive the reaction, which are not amenable for in situ application. Nanosizing the particles to enhance reactivity and adding a catalyst to lower the activation energy may result in a treatment suitable for in situ remediation. Therefore, this dissertation research explored a reductive remediation approach

using nanoscale zero valent iron with Ni as a catalyst supported on activated carbon to minimize nanoparticle aggregation and with additional heat to enhance the reaction rates.

Table 2-5. Energy need to degrade PFOS using different treatment.

Treatment	Power (W)	Volume (L)	Rate (d⁻¹)	t_{1/2} (min)	[PFOS] μM	Energy (kJ/μmol)
Ex-Situ Oxidation						
Photo-Fenton oxidation	23.0	0.40	1.7	597.6	20	206.2
Electrochemical oxidation	62.5	0.25	83.2	12.0	20	18.0
Sonolysis	150.0	0.60	15.8	63.0	20	94.5
Ex-Situ Reduction						
UV/KI photolysis	1.5	0.03	2.88	346.50	20	103.95
Alkaline 2-propanol photolysis	32	0.75	0.93	1073.03	40	137.35
Discharge Plasma	332.3	0.05	33.3	30.00	111	215.53
In-Situ Reduction						
Sub-critical elemental iron	7.76	0.01	18.72	53.31	370	13.42
Vitamin B12 electron mediator	0.40	0.04	0.48	2079.0	54	49.78

Note: For sub-critical iron and vitamin B₁₂ the energy required was considered as the energy needed to heat the system.

CHAPTER 3. EVIDENCE OF REDUCTIVE TRANSFORMATION OF PERFLUOROOCTANE SULFONATE BY NiFe⁰ NANOPARTICLES SYNTHESIZED ONTO ACTIVATED CARBON

3.1. Abstract

Perfluorooctanesulfonate (PFOS) is one of the most recalcitrant of the environmentally persistent perfluoroalkyl acids. Here we present evidence that NiFe⁰ nano (n) particles (NPs) synthesized onto activated carbon (AC) transform both linear (L-PFOS) and branched PFOS (Br-PFOS) isomers at 60 °C with generation of sulfite, fluoride and defluorinated and desulfonated products. Initially, particle reactivity was explored for various nFe⁰, nNi⁰ and AC combinations in 5-d reactions at 22 °C and 60 °C, which revealed that both elevated temperatures and nFe in conjunction with Ni or AC were required for PFOS reduction to occur. nNiFe⁰-AC particles performed the best, which led to additional work with these particles including effect of synthesis stirring time (SST). nNiFe⁰-AC synthesized with a 3-h SST (versus a 1-h or 2-h SST) resulted in the highest PFOS removal at 51.1 ± 2.1% with nearly one mole of sulfite and 12 moles of fluoride generated per mole PFOS not recovered. Organic defluorohydrogenation products with a loss of up to 10 fluorine atoms were identified in particle extracts using quadrupole time of flight (QToF) negative electrospray ionization (ESI) with MS² fragmentation confirmation. One C8 desulfonation product was also identified using QToF atmospheric pressure negative ionization.

3.2. Introduction

Management of diffuse perfluoroalkyl acid (PFAA) plumes above EPA recommended drinking water guidance levels at a large number of sites such as military bases, refineries,

airports, and chemical plants calls for remediation technologies with in-situ potential (Cousins *et al.*, 2016; Gottschall *et al.*, 2010; Hu *et al.*, 2016; Oliaei *et al.*, 2013; Pistocchi & Loos, 2009; Sharma *et al.*, 2016; Wang *et al.*, 2010; Xiao *et al.*, 2015). PFAAs have not been shown to biodegrade, and in fact, are generated from microbial degradation of precursor poly- and perfluoroalkyl substances (PFAS) (Dasu *et al.*, 2013; Royer *et al.*, 2015), thus management strategies must focus on abiotic processes. Currently, primarily adsorption technologies (e.g., granulated activated carbon, GAC) are used to remediate PFAA-contaminated water. However, early PFAA breakthrough often occurs, and GAC regeneration is problematic. Oxidative technologies amenable for *in-situ* remediation have generally proven unsuccessful particularly for the perfluoroalkyl sulfonates such as perfluorooctane sulfonate (PFOS, C₈F₁₇SO₃) (Park *et al.*, 2016). Mineralization of perfluorocarboxylates (PFCAs) by heat-activated persulfate has been demonstrated (Liu *et al.*, 2012; Park *et al.*, 2016), but PFOS was not altered (Park *et al.*, 2016). Vitamin B12-based or cobalt-catalyzed technologies can defluorinate the branched (Br-) PFAS isomers, but not linear (L-) PFAS (Liu *et al.*, 2018; Ochoa-Herrera *et al.*, 2008; S. Park *et al.*, 2017); electrochemical production of PFOS yields about ~70% as L-PFOS (Alsmeyer *et al.*, 1994).

The use of zero-valent metals are attractive due to their low cost and use in passive treatment methods such as permeable reactive barriers (PRBs) (Cheng & Wu, 2000; Kim *et al.*, 2004; Roberts *et al.*, 1996; Tratnyek *et al.*, 1997). PFOS degrades rapidly by Fe⁰ in sub- or supercritical water at 350 °C (Hori *et al.*, 2006), but this approach is not conducive for *in-situ* application. Both decreasing particle size, e.g., Fe⁰ nanoparticles (NP) as well as adding a catalyst, e.g., Ni, Pt, Cu, or Pd, to Fe⁰ can enhance reactivity as observed with dehalogenation of halo-organic contaminants (Bokare *et al.*, 2008; Chen *et al.*, 2011; Cho & Choi, 2010). For

example, Pd⁰ added to nFe⁰ effectively transformed a wide range of contaminants (Cho & Choi, 2010; Wang *et al.*, 2013); however, not PFOS (Saerom Park *et al.*, 2017). Ni has the potential to be a more reactive catalyst with its wide range of stable oxidation states (Ni⁰/Ni⁺¹/Ni⁺²/Ni⁺³) (Ananikov, 2015) and is less expensive. NiFe⁰ particles have also been shown to have enhanced stability relative to some other bimetal particles (Han & Yan, 2014). Therefore, we chose to investigate reactivity of nNiFe⁰ to reduce PFOS. Given the tendency for NPs to aggregate, which may reduce accessibility to reaction sites (Zhang, 2014), we also chose to synthesize nNiFe⁰ onto activated carbon (AC) to minimize aggregation, thus optimizing reactivity. AC, a frequently used low-cost heterogeneous catalyst, has a high surface area, catalytic activity, and thermal stability (Ramirez *et al.*, 2007; Uemichi *et al.*, 1989; Zhang *et al.*, 2007). AC may also reduce PFAA mobility through sorptive processes and increase PFAA proximity to the reactive metals further facilitating reductive transformation. Here we explore if nNiFe⁰ supported on AC (nNiFe⁰-AC) can transform PFOS with multiple lines of evidence: generation of sulfite, fluoride, and both defluorination and desulfonation products.

3.3. Materials and Methods

3.3.1. Chemicals

Iron (II) chloride tetrahydrate (FeCl₂·4H₂O, 98%), sodium borohydride (NaBH₄, 99%), nickel chloride hexahydrate (NiCl₂·6H₂O, 98%), sodium fluoride (NaF, 99%), sodium sulfate (Na₂SO₄, 99%), sodium sulfite (Na₂SO₃, 98-100%), heptadecafluorooctanesulfonic acid potassium salt (PFOSK, C₈F₁₇SO₃K, 98%, 68.1% L-PFOS), and 1-bromoheptadecafluorooctane (C₈F₁₇Br, 99%) were purchased from Sigma-Aldrich (St. Louis, MO, USA). Perfluorooctane (C₈F₁₈, 98%) was obtained from Oakwood Chemical (West Columbia, SC, USA). Powdered AC

was supplied by Strem Chemicals (Newburyport, MA, USA). Sodium perfluoro- $^{13}\text{C}_8$ octane sulfonate (M8PFOS) was obtained from Wellington Laboratories (Lenexa, KS, USA). Ammonium acetate, formic acid, and methanol were HPLC grade and purchased from Fisher Scientific (Pittsburgh, PA, USA).

3.3.2. Particle Synthesis

nNiFe^0 -AC was synthesized for evaluating PFOS reduction as well as particles of nFe^0 , nFe^0 -AC, nNi^0 -AC and nNiFe^0 for comparison in the initial exploration. All particles were synthesized immediately before use in batch reactions. nFe^0 and nNiFe^0 NPs were synthesized similar to the procedure described elsewhere (Li *et al.*, 2006; Schrick *et al.*, 2002; Wang & Zhang, 1997), except in an N_2 -filled anaerobic chamber. Briefly, $\text{FeCl}_2 \cdot 4\text{H}_2\text{O}$ was reduced with NaBH_4 to form nFe^0 and washed with deoxygenated distilled water. Ni was plated onto nFe^0 by stirring aqueous $\text{NiCl}_2 \cdot 6\text{H}_2\text{O}$ (2 wt% Ni) with nFe^0 at 600 rpm for 1, 2, or 3 h (hereafter referred to as synthesis stirring time, SST) followed by sonication and washing. Transmission electron microscopy (TEM) coupled with energy dispersive X-ray (EDX) analysis confirmed Ni at ~2 wt. % relative to Fe with a diameter of ~42 nm. For AC-supported NPs, AC was mixed with $\text{FeCl}_2 \cdot 4\text{H}_2\text{O}$ or $\text{NiCl}_2 \cdot 6\text{H}_2\text{O}$ before reducing metals at a ratio to result in AC being ~15 wt% of the final composite.

3.3.3. Batch Reactions

Batch reactions using 60-mL high-density polyethylene bottles with rubber crimp caps were carried out in a N_2 -filled anaerobic chamber. PFOS (10-mL ~6 μM prepared in distilled water) was mixed with 0.2 g particles. Bottles were rotated (120 rpm) at 22 ± 2 °C or 60 °C. A PFOS control (no particles) and a matrix control (particles but no PFOS) were included for each

reaction set. Reactivity was probed in triplicate in 5-d reactions at 60 °C with each type of 1-h SST particle along with AC controls, which consisted of 0.03 g AC powder (same mass used to support the NPs) treated with NaBH₄ at the 1-h SST. Based on total PFOS loss in the reactions with particles prepared with a 1-h SST, additional studies were conducted with nNiFe⁰-AC to evaluate if SST altered reactivity to PFOS and if reactivity was isomer-specific (L- versus Br-PFOS). The effect of 1-h, 2-h and 3-h SST on nNiFe⁰-AC was evaluated in 1-d reactions with PFOS. To evaluate PFOS reaction time with nNiFe⁰-AC, L- and Br-PFOS transformation in 1-d versus 5-d reactions were evaluated using 1-h and 3-h SST particles. To probe which products may come from L- versus Br-PFOS, a Wellington L-PFOS standard was reacted for 5 d at 60 °C in duplicate with nNiFe⁰-AC (3-h SST). All reactions were stopped by immersing bottles in an ice slurry followed by particle separation and extraction.

3.3.4. Particle Extraction and PFOS Analysis

Samples were centrifuged, supernatant decanted into polypropylene tubes, and the remaining particles extracted 5 times with 10 mL 10:90 v/v water (1% acetic acid)/methanol. Aqueous supernatants and extracts were analyzed for PFOS with a subset screened for organic products. C-S cleavage leading to potentially volatile polyfluoroalkanes was expected, thus headspace was captured on C₁₈ cartridges, extracted with methanol, and screened for products (see Appendix A for details). Inorganic products were measured in the aqueous solutions only, except for a replicated (n=6) 5-d reaction with 3-h SST nNiFe⁰-AC in which particles were extracted with 0.02 M NaOH (see SI for details). H₂ generation was confirmed with a flame test and evaluated qualitatively in a subset of samples using a graduated glass syringe and recording how much the plunger moved upon entering the sealed reaction vessel.

3.3.5. Extraction of F⁻ and SO₃²⁻ from nNiFe⁰-AC

F⁻ and SO₃²⁻ adsorption to and extraction from nNiFe⁰-AC were evaluated using 60-mL HDPE bottles with rubber crimp caps as used in the PFOS reactions with particles. For the adsorption tests, 10 mL of an aqueous solution containing 316 µg F⁻/L (16.63 µM F⁻) and 487 µg SO₃²⁻/L (6.08 µM SO₃²⁻) was added to 0.2 g nNiFe⁰-AC particles and equilibrated for 5 days at 60 °C. Concentrations were selected based on the levels expected to be generated from PFOS (~ 6 µM) in 5-d reactions at 60 °C with 3-h SST nNiFe⁰-AC particles. After a 5-d equilibration, samples were then centrifuged for 15 min at 4500 rpm, supernatant removed, and particles extracted sequentially 4 times with 10 mL of 0.02 M NaOH. Anion concentrations in water and NaOH extracts were quantified by ion chromatography as already described. Solution pH was ~ 5.8 after 5-d reactions of particles with added F⁻ and SO₃²⁻.

From controlled adsorption/extraction experiments with nNiFe⁰-AC, 23.2 ± 3.4% F⁻ was quantified in the aqueous phase and 65.8 ± 8.9% F⁻ was detected in 0.02 M NaOH extracts. For sulfite (quantified as sulfate), 97.5% ± 3.4% was extracted with sulfite < LOQ or not detected after the 2nd extract. Using the same extraction method for a 5-d PFOS reaction at 60 °C with nNiFe⁰-AC prepared with 3-h SST, 36.3 ± 4.8 moles % F⁻ and a total of 54.5 ± 3.6 moles % SO₃²⁻ as SO₄²⁻ per moles of initial PFOS was quantified in the aqueous phase and particle extracts, respectively (Figure 3-2b).

3.3.6. Analytical Methods

3.3.6.1. HPLC/MS/MS for PFOS Quantification

L-PFOS (single peak) and Br-PFOS (single broad peak integrated) concentrations were quantified using an Agilent 6460 Triple-Quad with online SPE with a 2.7 µm reversed phase

poroshell 120 EC-C18 (3.0 mm x 50 mm) column (exemplified in Figure A1). Polypropylene bottles and sample dilution of 1:1 with MeOH were used to avoid PFAS adsorption and matrix effects. For analysis, a standard calibration curve was constructed and M8PFOS was added to each sample as internal standard. The mobile phases consisted of 2mM ammonium acetate in water and 2 mM ammonium acetate in methanol at 0.5 mL/min. The gradient conditions were: 3% B for 0.85 min, 60% B for 4 min, and 100% by 14 min. The mobile phases for the online SPE are 0.1% formic acid in water and 100% methanol. The injection volume was 300 μ L and the column temperature was maintained at 55°C. LC/MS parameters for PFOS and M8PFOS quantification conditions are described in Table A1 and A2.

3.3.6.2. uPLC-QToF MS for Organic Transformation Product Identification

Samples for organic products detection and identification were analyzed using a Shimadzu ultra high performance reverse-phase liquid chromatography (uPLC) system coupled to a Sciex 5600+ Triple Quadrupole Time-of-Flight (QToF) MS. The Q-ToF was equipped with a DualSpray source allowing either electrospray ionization (ESI, via the TurboIonSpray probe) or atmospheric pressure chemical ionization (APCI) ionization. PFOS quantitation was done with negative electrospray ionization (ESI-using a Kinetex EVO C18 (2x.1 x 100 mm, 5 μ m, 100 Å) column equipped with a Phenomenex AF0-8497 filter. The column temperature was maintained at 40 °C and 50 μ L of sample were injected. Mobile phases A and B were water with 0.15% acetic acid and 20 mM ammonium acetate in methanol, respectively. The gradient started with 3% of solvent B until 2.5 min and then ramped to 25% B over 3.5 min, increased to 45% at 4.5 min and kept it at 55% B for another 1.5 min with a flow rate of 0.5 ml/min. At 7 min, the flow rate decreased to 0.4 ml/min and solvent B was ramped to 60%, 80% at 15 min, 85% at 20 min, 90% at 23 min, 95% at 24 min, and 100% at 25 min. The starting flow rate of 0.5 ml/min

was restored at 25 min and kept it for 7 min and finally re-equilibrated at 3% until 46 min. Samples were injected in ToF-MS can mode (ESI+, ESI-, and APCI-) and a mass defect filtering (mass defect ~ 0.9 are common for perfluorinated compounds) was used to identify novel decomposition products by triggering MS/MS spectra of m/z of interest and studying the fragmentation patterns (Myers *et al.*, 2014). The mass calibration was carried out every 5 samples with calibration solutions injected via the automated calibration device system (CDS) in negative or positive mode, the polarity matching the polarity of the sample analysis. All MS and QToF parameters are summarized in Table A3. A sequential window acquisition of all theoretical fragment ion spectra (SWATH) acquisition mode was also used to detect low-levels of products in our complex matrix. In total, 17 product ion experiments were performed with a mass range from 100 to 1200 m/z and with an overlap of 1 m/z (Table A4). The accumulation time was 50 ms with a total cycle time of 950 ms. Data acquisition and processing were performed using the Analyst 1.7 and PeakView 2.2 software, respectively.

3.3.6.3. Ion Chromatography

Inorganic products (fluoride and sulfate) were quantified using an Ion chromatography (ICS-3000, Dionex) with an IonPac AS11-HC column (4.0 x 250 mm), IonPac AG11-HC guard column (4.0 x 50 mm) and sodium hydroxide (NaOH) in water as a mobile phase. The column was allowed to equilibrate for 30 min before each batch. An optimum gradient separation method with a flow rate of 1.5 mL/min, a column temperature of 30 °C and an injection volume of 50 μ L was employed for each anion. The optimal gradient for maximizing quantitation of fluoride and sulfate were different. For fluoride, the eluent concentration was kept at 3 mM for the first 7 min then ramped to 30 mM for 15 min to elute the excess of chloride ions and back to 3 mM for at least 10 min. Sulfate peaks became diffuse with the latter gradient. For sulfate, 15

mM sodium hydroxide was maintained for 10 min to separate sulfate and sulfite anions, and then increased to 30 mM for 5 min and finally to 15 mM for another 10 min. For estimating F^- concentration in the presence of partially co-eluting interfering peaks, F^- was estimated from F^- standard additions and Gaussian fitting of peaks using OriginPro 2016 software (Figure A5b).

3.3.6.4. ICP-MS

Trace metal analysis was performed on a Thermo iCAP Inductively Coupled Plasma Mass Spectrometry (ICP-MS). Combustion was used to identify trace metals in the AC powder. AC powder was put in an alumina crucible and oxidized overnight at 600 °C in a muffle furnace. Metals remaining in the crucible were washed out with nitric acid followed by ICP-MS analysis. A blank was included for comparison. Several elements were observed to be present in the AC powder including sodium (Na), magnesium (Mg), aluminum (Al), silicon (Si), phosphorus (P), iron (Fe), barium (Ba), copper (Cu), nickel (Ni), strontium (Sr), and cerium (Ce). Na, Ca, Si and Al were detected previously by the TEM-EDX analysis. The metals with the highest signal (cps) were $Fe > Ba > Sr > Ce$; there was no attempt to quantify metals in the AC.

3.3.7.4 Particle Characterization and Desorption Analysis

Transmission electron microscopy (TEM) with an energy dispersive X-ray (EDX) attached and scanning electron microscope (SEM) were used to characterize nNiFe⁰-AC. Micrographs were obtained using a FEI Tecnai G2 20 TEM. A droplet of aqueous sample containing the nanoparticles was placed on a carbon-coated Cu grid, the excess aqueous volume removed with a filter paper and the grid air-dried for 2 min. TEM images were analyzed using a Digital Micrograph software (Version 3.5.2, Gatan Company) to measure particle size. SEM images were obtained using an electron microscope ULTRA 55 (Zeiss). Samples were mounted

on an adhesive double-sided carbon tape of 0.5 cm by 0.5 cm before observation. Average NP diameter and particle size distribution were determined using Image J software of the SEM images. Desorption analysis was performed using an X-ray photoelectron spectrometer (XPS). XPS spectra were taken using a Thermo Scientific K-Alpha XPS instrument with a monochromatic Al K α X-ray source. Individual element scan was completed for F 1s (675-695 eV). After the 1-d or 5-d reactions, particles were dried overnight at 90 °C and mounted on a small carbon tape of 0.5 cm by 0.5 cm prior to XPS analysis.

3.3.7. Organic Product Detection and Identification

Products from PFOS reactions with nNiFe⁰-AC at 60 °C were identified using accurate mass and spectral accuracy approaches with an average mass error tolerance of less than 15 ppm, a signal-to-noise ratio of 10, and an isotope distribution error < 1%. Full scan spectra were compared to PFOS stock and the corresponding matrix control to identify defluorinated and/or desulfonated transformation products. The accurate mass was obtained on a QToF MS (-/+ mode) which gives an accuracy within 2 ppm with external mass calibration. Confident product identification was obtained by considering mass error, retention time, isotope pattern, and MS/MS fragmentation score as described in the workflow in Figure A6. First, an exhaustive screening for non-target compounds was performed using the Peakview software 2.2. Each sample was compared with the two controls (PFOS stock and matrix only) and the peaks detected only in the samples were further investigated. With the detected accurate masses of the selected candidates, a possible chemical formula that matches the exact mass was determined. Mass error of each candidate was calculated and reported in Table 1 (main) using Eq. 1. If the error was smaller than 15 ppm, the masses were supposed to be the same.

$$\text{Mass error (ppm)} = \frac{(\text{theoretical mass} - \text{measured mass})}{\text{theoretical mass}} \times 10^6 \quad \text{Eq. (1)}$$

The theoretical mass is the exact mass calculated from the formula and the measured mass is the experimentally measured mass value. In addition to mass accuracy, a spectral accuracy approach (isotope pattern) was also used for product confirmation. Thus, the observed isotope peaks intensities (M+1, M+2, M+3, etc.) relative to the molecular ion peak M (assumed to be 100) was compared to their theoretical value using an isotope distribution calculator from Scientific Instrument Services, INC. A relative spectral error of less than 1% was accepted to differentiate candidate formulas. Furthermore, the mass accuracy of fragmentation ions was used to confirm the identity of parent potential products; a mass error lower than 15 ppm compared to theoretical m/z of expected daughter ions was considered acceptable.

Retention times were also used to confirm the identity of the molecules detected by LC-Q-ToF-MS. For products that maintained the sulfonate group, retention times were expected to be less than PFOS and parallel the series of shorter retention times observed for the defluorination products.

3.4. Results and Discussion

Depending on particle reactivity, PFOS may be strongly sorbed or transformed. For reductive transformation, both C-S and C-F cleavage may occur with each mole of PFOS transformed generating up to one mole sulfite (SO_3^{2-}) and 17 moles fluoride (F^-) along with associated organic products. Therefore, PFOS loss coupled to generation of F^- , SO_3^{2-} or organic products serves to confirm PFOS transformation.

3.4.1. Exploring Reactivity Potential with 1-h SST Particles in 5-d PFOS Reactions

For all AC-supported particles, no PFOS was detected in the aqueous phase (Figure 3-1). In AC controls (pH = 6.5), PFOS recovery was limited to $29 \pm 7\%$; however, after depositing $n\text{Fe}^0$ or $n\text{NiFe}^0$ onto AC, PFOS recovery increased to 88-90% PFOS in the absence of PFOS degradation (e.g., no SO_3^{2-} generation) as shown for all reactions at $T = 22\text{ }^\circ\text{C}$ and $n\text{Ni}^0$ -AC at $60\text{ }^\circ\text{C}$ (Figure 3-1). This ability to extract more PFOS after the addition of the metal NPs (Fe, Ni) suggests that the NPs may be blocking the AC micropores from PFOS sorption within the pores, where they would be more difficult to extract. PFOS transformation was evident by SO_3^{2-} generation only at elevated temperatures and when $n\text{Fe}^0$ was present in conjunction with Ni or AC (Figure 3-1). Interestingly, although PFOS reactions with $n\text{Fe}^0$ -AC did yield a small amount of sulfite concomitant with PFOS loss, nothing was observed with $n\text{Ni}^0$ -AC for which there was also no H_2 generation, which may be due to Ni's higher standard reduction potential compared to Fe (Shih *et al.*, 2011) Only Fe^0 -containing particles caused H_2 generation (confirmed with a flame test), which ranged between 30-60 mL at the higher reaction temperature. $n\text{NiFe}^0$ -AC resulted in the highest PFOS loss ($35 \pm 7\%$) with $29 \pm 11\text{ mol}\%$ SO_3^{2-} generated per mole of initial PFOS. XPS spectra of the reacted $n\text{NiFe}^0$ -AC particles before and after extraction shows the disappearance of the F 1s peak for PFOS after extraction (Figure A2) indicating that the majority of PFOS remaining was extracted. Quantifying F^- to further support PFOS degradation was problematic for the 1-h SST particles as will be discussed.

The AC support enhanced PFOS transformation with both $n\text{Fe}^0$ and $n\text{NiFe}^0$ as evidenced by increased sulfite generation compared to the metal(s) alone (Figure 3-1). AC minimized NP aggregation (Figure A3), thus keeping surface area high allowing more PFOS to interact with the NP surface and increasing transformation potential. AC may have also increased reactivity due to

metals in the AC that could be reduced during particle synthesis. ICP-MS analysis of the AC revealed the presence of Ce, Cu, Fe, and Sr. In addition, quinone present in AC has been hypothesized to facilitate electron shuttling, e.g., azo dye reduction by sulfide (Van der Zee *et al.*, 2003).

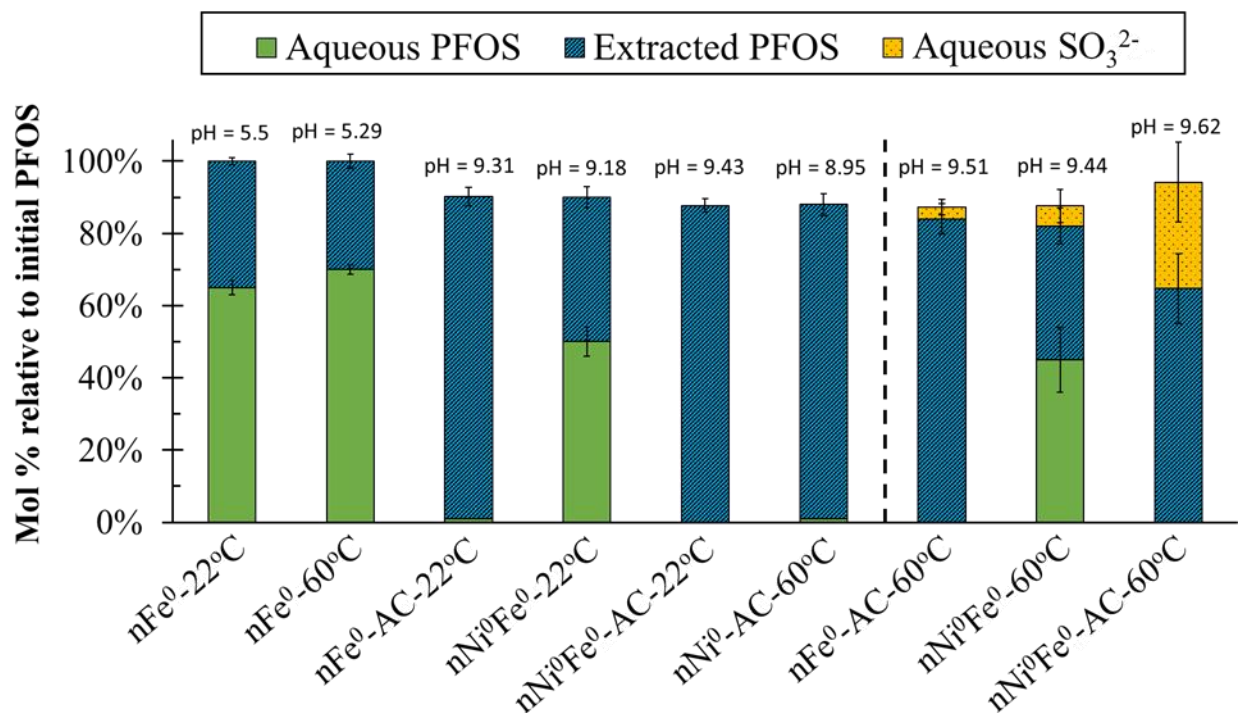


Figure 3-1. Mole percentage of PFOS recovered in the aqueous phase and solvent extracts and mol SO₃²⁻ generated (measured in only the aqueous phase) relative to initial (t=0) moles of PFOS after a 5-d reaction with various particle types in unbuffered deionized water with no pH adjustments. The pH shown above the bars is final pH after the 5-day reaction. nNiFe⁰-AC particles were prepared with 1-h SST.

3.4.2. Effect of SST on L- and Br-PFOS

Both L- and Br-PFOS loss occurred in 1-d reactions at 60 °C with nNiFe⁰-AC prepared with all three SST used to plate Ni onto nFe⁰-AC (Figure 3-2a) with more loss for the longer SST. For a given SST, longer reaction times with PFOS (1 d versus 5 d) increased removal of total PFOS (Figure 3-2a versus 3-2b) especially for the 1-h SST particles. The 3-h SST nNiFe⁰-

AC yielded the highest PFOS loss of 51.1 ± 2.1 % in 5 d with 54.5 ± 3.6 mol % SO_3^{2-} (aqueous plus extracted) and 36.3 ± 4.8 % F^- generated relative to the initial PFOS concentration.

Increasing SST in particle preparation changed the nNiFe^0 shape from cubic (crystalline) to spherical (amorphous), but NP size did not change significantly (all ~ 20 to 70 nm) (Figure A4).

Longer SST may have improved Ni distribution onto nFe^0 .

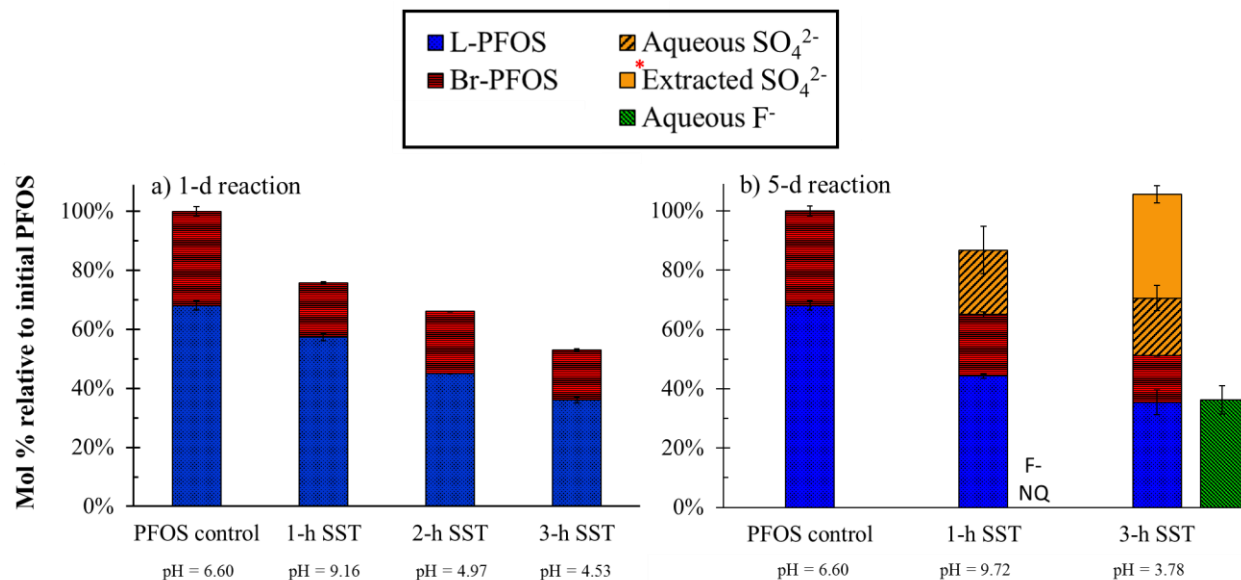


Figure 3-2. Mole percentage of Br- and L-PFOS recovered relative to initial ($t=0$) moles of PFOS (a) after 1-d reaction with nNiFe^0 -AC particles prepared different synthesis stirring times (SST); and b) after a 5-d reaction along with mol percentage of F^- and SO_3^{2-} generated relative to initial ($t=0$) moles of PFOS for 1-h and 3-h SST prepared nNiFe^0 -AC particles. First bar in each graph represents the PFOS control (no particles); isomer ratios is approximately 68/32 L-/Br-PFOS. Reactions were in unbuffered deionized water with no pH adjustments. *Extraction of inorganic ions with 0.02 M NaOH was performed only for the 5-d reaction with 3-h SST particles in which no fluoride was observed ($n=6$).

3.4.3. pH Effect on Inorganic Anion Quantitation

Final pH after reacting PFOS with nNiFe^0 -AC decreased for particles with longer SST. In the reactions with 1-h SST particles, concomitant with final pH values > 9 were peaks that co-eluted with fluoride such that using standard addition to estimate F^- concentrations was not

possible (Figure A5a). However, when pH dropped below 4.5, peak interferences were substantially reduced allowing reasonable estimations of F^- concentrations (Figure A5b). Interestingly, interfering peaks were only observed in PFOS reactions with the particles and not in matrix controls. Attempts to identify the interfering peaks led to only ruling out acetate and formate.

Sulfite quantitation was not hindered by interferences; however, under more acidic conditions, the NPs surface become positively charged (zero point of charge for iron oxides/hydroxides being in the 6 to 8 range) (Milonjic *et al.*, 1983; Parks, 1965), thus increasing sorption of anionic ligands (Hingston *et al.*, 1972; Mansour *et al.*, 2010).

Based on only the aqueous phase analysis, more SO_3^{2-} appeared to be generated in the 5-d reactions with the 1-h SST nNiFe⁰-AC particles (final pH 9.72 ± 0.15) compared to the 3-h SST nNiFe⁰-AC PFOS reactions (final pH 3.78 ± 0.53) (slashed orange bars in Figure 3-2b).

Assuming this was due to significant sorption of SO_3^{2-} at the lower pH, we repeated the 5-d PFOS reactions with 3-SST nNiFe⁰-AC and extracted the particles with 0.02 M NaOH (Figure 3-2b, see SI for details). Particle extracts contained almost two times more SO_3^{2-} than found in the aqueous phase resulting in total SO_3^{2-} generation being substantially greater with nNiFe⁰-AC prepared with a 3-h SST compared to a 1-h SST. No F^- was detected in the 0.02 N NaOH extracts. Control study for anion extraction is detailed in the SI.

3.4.4. Organic Products

Products from PFOS reactions with nNiFe⁰-AC at 60 °C included several C6-C8 single bond and C8 double bond polyfluoroalkyl sulfonates with up to 10 out of 17 fluorine atoms removed were identified (Table 3-1) with MS/MS fragmentation confirmation (Tables A6 and A7). These products are similar to those observed by Tachibana *et al.* (Tachibana *et al.*, 2014)

using DC plasma in an argon atmosphere. For reactions with the L-PFOS standard, only the single bond (C-C) products were identified indicating that products with double bonds (C=C) are formed only from Br-PFOS isomers. No products were observed in the aqueous phase indicating reactions occur with sorbed molecules consistent with previous Fe-mediated reductive reactions (Matheson & Tratnyek, 1994). For headspace samples, several peaks were observed in reacted samples that were not present in the stock or matrix controls, particularly in positive ESI mode, but they were not identifiable and did not appear to be reflective of F-containing compounds.

With SO_3^{2-} generation as evidence of the C-S bond breaking (C-S bond has the lowest energy, 259 kJ/mol, of all bonds in PFOS) (Cottrell, 1958), desulfonation products were expected; however, perfluoroalkanes do not ionize by ESI and only weakly ionize by APCI (Schutz *et al.*, 2015). During the instrumental development stage, we noticed an artifact of perfluoroalkane analysis using APCI ionization (detailed in SI). We first injected perfluorooctane (C_8F_{18}) and 1-bromo-perfluorooctane ($\text{C}_8\text{F}_{17}\text{Br}$) into the QToF-APCI to observe the MS/MS fragmentation and optimize detector response (detailed in the SI). The highest peak detected in APCI mode with the standards was 434.9707 for which the exact mass (434.9683, 5.5 ppm error) and MS/MS fragmentation correspond to $\text{C}_8\text{F}_{17}\text{O}^-$ (Figure A7 and Table A8). The halogen attached to the terminal carbon (CF_3^- or CF_2Br^-) swaps out with an oxygen in the APCI source, *i.e.*, O for F and O for Br, respectively, as observed by others for perfluoroalkanes (Marotta *et al.*, 2004; Schutz *et al.*, 2015). In samples, $\text{C}_8\text{F}_{17}\text{O}^-$ (434.9707) (Table 3-1) was detected. However, we suspect that the transformation product is actually $\text{C}_8\text{F}_{17}\text{H}$ resulting from cleavage of the sulfonate group of PFOS, but in the APCI source there was an H/O swap (C-H bond has lower energy than the C-F bond). Furthermore, the m/z 431.9633 (431.9643, 2.3 ppm error) was also detected corresponding to the $[\text{C}_8\text{F}_{16}\text{O}_2]^-$ molecule, which we propose was $\text{C}_8\text{F}_{16}\text{H}_2$ from

SO_3^{2-} cleavage of the defluorination product $\text{C}_8\text{HF}_{16}\text{SO}_3$ (Table 3-1). Headspace samples have not been explored yet with APCI. Although 14 defluorination products were observed in particle extracts reacted with technical PFOS, their peak intensities (assuming an intensity/concentration response similar to PFOS) suggest they represent only a few percent of the PFOS not recovered. With a high % sulfite generation, we suspect that defluorination products can undergo further desulfonation reaction to produce defluorinated/desulfonated products, but product identification is limited by detector sensitivity and lack of available standards.

The ability of $\text{nNiFe}^0\text{-AC}$ to reductively transform L- and Br-PFOS was evident by generation of fluoride, sulfite and defluorinated and desulfonated products. Results from exploring other Fe, Ni and AC combinations gave opportunity to glean a few insights on potential reaction mechanisms. Elevated temperatures were required indicating an activation energy that had to be met, which we hypothesize may be associated with contorting PFOS molecule to a less stable state (transition state). Only with nFe present in conjunction with Ni or AC did PFOS reduction occur which indicates Ni and AC serve a catalytic role. For Ni-AC no PFOS transformation or H_2 generation were evident, thus supporting that a key role of nFe is H_2 generation. Also Ni, and possibly the trace metals in the AC, may adsorb hydrogen and form metal hydride complexes, which may serve as a direct reductant for adsorbed PFOS (Song *et al.*, 2013; Tian *et al.*, 2016). AC also serves to increase PFOS concentrations near the bimetal through adsorption, keep the NPs from agglomerating, and may also channel electrons (Van der Zee *et al.*, 2003) to sorbed PFOS molecules. The formation of shorter carbon-chain products may be specific to Ni's ability to catalyze the breaking of C-C bonds (Schrack *et al.*, 2002). Future studies on PFOS reaction kinetics and transformation pathways, reduction of other PFAAs, reactions in groundwater type matrices, and particle longevity/regeneration will provide

additional details into mechanisms and potential application of nNiFe⁰-AC for subsurface remediation.

Table 3-1. Summary of the products identified in the solvent extracts. For reference, PFOS m/z is 498.9297 with a retention time of 8.8817 min. All products identified are from the loss/gain of F/H or the cleavage of SO₃²⁻ (see Tables A6, A7 and A8).

Theoretical m/z	Observed m/z	Difference Error (ppm) ^a	Formula	t _r ^b
Defluorination				
C-C Single bonds				
480.9391	480.9388	0.5164	C ₈ HF ₁₆ SO ₃ ⁻	8.5625
462.9485	462.9471	3.0341	C ₈ H ₂ F ₁₅ SO ₃ ⁻	8.4606
426.9674	426.9672	0.3604	C ₈ H ₄ F ₁₃ SO ₃ ⁻	8.4185
390.9862	390.9856	1.444	C ₈ H ₆ F ₁₁ SO ₃ ⁻	7.8339
355.005	355.005	0.1727	C ₈ H ₈ F ₉ SO ₃ ⁻	7.7603
319.0239	319.024	0.266	C ₈ H ₁₀ F ₇ SO ₃ ⁻	7.6786
430.9423	430.9418	1.0303	C ₇ HF ₁₄ SO ₃ ⁻	8.0800
380.9455	380.9455	0.0473	C ₆ HF ₁₂ SO ₃ ⁻	7.6740
C-C Double bond				
424.952	424.9517	0.7634	C ₈ H ₂ F ₁₃ SO ₃ ⁻	8.1151
406.9611	406.9611	0.0108	C ₈ H ₃ F ₁₂ SO ₃ ⁻	8.0383
370.98	370.9786	3.5899	C ₈ H ₅ F ₁₀ SO ₃ ⁻	7.7286
352.989	352.9893	0.8149	C ₈ H ₆ F ₉ SO ₃ ⁻	7.7110
334.9988	334.9989	0.1041	C ₈ H ₇ F ₈ SO ₃ ⁻	7.6708
317.0082	317.0081	0.3186	C ₈ H ₈ F ₇ SO ₃ ⁻	7.6039
Desulfonation - SO₃⁻ cleavage				
434.9678	434.9661	3.8302	C ₈ F ₁₇ O ^{-c}	
431.9643	431.9633	2.3150	C ₈ F ₁₆ O ₂ ^{-c}	

^a (Difference between theoretical mass and experimentally measured mass/theoretical mass) x 10⁶; ^b Retention time. ^c Actual transformation product proposed to be C₈F₁₇H and C₈F₁₆H₂ prior to hydrogen atom swapping out for one or two oxygen atoms in the APCI source (Marotta *et al.*, 2004; Schutz *et al.*, 2015), which was confirmed with a 1-bromo-perfluorooctane (C₈F₁₇Br) and perfluorooctane (C₈F₁₈) standards.

CHAPTER 4. KINETICS AND MECHANISM OF REDUCTIVE TRANSFORMATION OF PERFLUOROOCTANE SULFONATE BY nNiFe^0 -AC PARTICLES

4.1. Abstract

Per- and polyfluoroalkyl acids (PFAAs) are resistant to biological degradation and, in many cases, oxidative chemical attack especially the perfluoroalkyl sulfonic acids (PFSAAs). Previously, we demonstrated reductive degradation of both L- and Br-PFOS using nNiFe^0 particles supported on activated carbon (AC) at 60°C in batch systems for 1-d and 5-d reaction times. Here, isomer-specific PFOS degradation rates with nNiFe^0 -AC at 60°C are quantified along with generation of fluoride and sulfite at reaction times from 1 h to 120 h. Changes in pH and ORP were also monitored over time as well as organic transformation products at the different reaction. Using nontarget screening with time-of-flight (ToF) mass spectrometry (MS), several organic products were identified over the reaction time including single-bonded C8-C4 and several double-bonded C8 polyfluoroalkyl sulfonic acids (F_{15} to F_7), C4-, C6-, C7- and C8-perfluorocarboxylic acids (PFCAs) and two paraffins, which led to several proposed degradation pathways. Organic products were only detected in particle extracts, nothing in the aqueous solution. The latter coupled to the observed transformation products indicated defluorination and desulfonation reactions are happening in the surface layer of the nNiFe^0 -AC particles by direct electron transfer. The broad area of the nanomaterial provided numerous sites to capture PFOS, with the sorbed PFOS being in close proximity to the electrons as they were generated, thus enhancing and accelerating the electron transfer from nNiFe^0 to PFOS.

4.2. Introduction

Perfluoroalkyl acids (PFAAs) can be released directly into the environment from fire training areas, refineries, airports, chemical plants, military facilities and/or from microbial degradation of precursor (Becker *et al.*, 2008; Becker *et al.*, 2010; Oliaei *et al.*, 2013; Paul *et al.*, 2009; Pistocchi & Loos, 2009; Wang *et al.*, 2010). Of the globally distributed and persistent PFAAs, the perfluoroalkyl sulfonic acids (PFSAs) are the most resistant to biological and oxidative chemical attack. PFSAs are typically found at AFFF-impacted sites at elevated concentrations (Backe *et al.*, 2013). The elevated levels of PFSAs found at AFFF-impacted groundwater and the inefficiency of sorptive materials for ex-situ treatment calls for in-situ technologies. Conventional water treatment processes are not effective for PFSAs degradation. Although some oxidative techniques have shown success for perfluoroalkyl carboxylates (PFCAs) such as PFOA (Park *et al.*, 2016). PFOS cannot be decomposed by advance oxidation process which utilize the hydroxyl radicals ($\bullet\text{OH}$) for oxidation. There are only two techniques that have shown success for PFOS decomposition for in-situ application. Both were reductive treatments using metals or vitamin B12 as the electron mediator. The first technique to show reductive decomposition of PFOS was using ZVMs in subcritical water at 350 °C and 20 MPa (Hori *et al.*, 2006). Of the different ZVMs (Al, Cu, Zn, and Fe) tested, Fe led to the greatest PFOS decomposition of both L- and Br-PFOS, with ~98% PFOS lost, 50% mole conversion to fluoride, and small amounts of trifluoromethane (CHF_3 : 0.7%) in the headspace. No perfluorocarboxylic acids were reported. Zero valent metals (ZVMs) have the potential to be used in passive treatment modes such as permeable reactive barriers (PRBs) due to their low cost and toxicity. However, the conditions used in the previous studies are not feasible for field applications. Another reductive treatment evaluated to destroy PFOS was vitamin B12 in

combination with titanium (III) citrate. Defluorination reactions using vitamin B12 (260 μM) and Ti(III)-citrate (36 mM) at 70 $^{\circ}\text{C}$ under alkaline conditions were investigated by Ochoa et al. (Ochoa-Herrera *et al.*, 2008). PFOS was mineralized to fluoride (3 moles of fluoride per mol of PFOS lost) and CO_2 (14.7% of total carbon in the PFOS molecule) as the main degradation products. Additionally, small amounts of volatile fluorinated compounds were detected but counting for less than 0.1% of the PFOS transformed. However, only 71% of Br-PFOS, which constitute only 30% of the total PFOS, were transformed.

From the previous observations, zero valent iron will be the focus of this study with the purpose to enhance iron reactivity with potential for in-situ applications through PRBs. As explained in the previous chapter, Fe^0 is a reducing agent that can serve as an electron donor to reduce recalcitrant chemicals. Addition of a second metal, such as Ni, as a catalyst to metal particles has resulted in increased activity and selectivity combined with enhanced degradation. The exceptional characteristic of high surface area, high catalytic activity, and high thermal stability (Ghaedi *et al.*, 2012; Li *et al.*, 2016) of activated carbon (AC) will be used to immobilize or reduce PFOS mobility attracting it to the surface of the bimetal nanoparticles (NPs).

In our previous study (dissertation chapter 3) nanosized (n) NiFe^0 supported on AC ($\text{nNiFe}^0\text{-AC}$) was found to transform both L- and Br- PFOS at 60 $^{\circ}\text{C}$ up to 51 % generating fluoride, sulfite and several less fluorinated single bonded and double bonded products in 120 h reaction. Reactions with a pure L-PFOS standard revealed that formation of double-bond byproducts were from the transformation of only Br-PFOS isomers. Here, we quantify reaction kinetics for L-PFOS and Br-PFOS isomers transformation in batch reactors with $\text{nNiFe}^0\text{-AC}$ at 60 $^{\circ}\text{C}$. Loss of specific isomers, generation of fluoride, sulfite, organic products and changes in

pH and ORP were monitored over time from 1 h to 120 h. Results were used to propose potential pathways and clarify reaction mechanism.

4.3. Materials and Methods

4.3.1. Standards and Reagents

Iron (II) chloride tetrahydrate ($\text{FeCl}_2 \cdot 4\text{H}_2\text{O}$, 98%), nickel chloride hexahydrate ($\text{NiCl}_2 \cdot 6\text{H}_2\text{O}$, 98%), sodium borohydride (NaBH_4 , 99%), sodium fluoride (NaF , 99%), sodium sulfate (Na_2SO_4 , 99%), sodium sulfite (Na_2SO_3 , 98-100%), heptadecafluorooctanesulfonic acid potassium salt (PFOSK, $\text{C}_8\text{F}_{17}\text{SO}_3\text{K}$, 98%), Perfluorobutanoic acid (PFBA, $\text{C}_3\text{F}_7\text{COOH}$, 98%), perfluoropentanoic acid (PFPeA, $\text{C}_4\text{F}_9\text{COOH}$, 98%), perfluorohexanoic acid (PFHxA, $\text{C}_5\text{F}_{11}\text{COOH}$, 98%), perfluoroheptanoic acid (PFHpA, $\text{C}_6\text{F}_{13}\text{COOH}$, 98%), and perfluorooctanoic acid (PFOA, $\text{C}_7\text{F}_{15}\text{COOH}$, 98%) were purchased from Sigma-Aldrich (St. Louis, MO). Powder activated carbon was supplied by Strem Chemicals (Newburyport, MA). Sodium perfluoro-[13C8]octanesulfonate (M8PFOS), mass-labelled PFCA/PFSA solution/mixture (MPFAC-MXA), sodium perfluoro-1-octanesulfonate (L-PFOS), perfluoro-1-methylheptane sulfonate (1-PFOS), perfluoro-3-methylheptane sulfonate (3-PFOS), perfluoro-4-methylheptane sulfonate (4-PFOS), perfluoro-5-methylheptane sulfonate (5-PFOS), perfluoro-6-methylheptane sulfonate (6-PFOS) were obtained from Wellington Laboratories (Lenexa, KS). Formic acid, ammonium acetate, acetic acid, sodium hydroxide, and methanol were analytical grade from Fisher Scientific (Pittsburgh, PA). The N_2 gas of high purity grade (99.99%) used for the synthesis of the bimetallic nanoparticles was obtained from Airgas (Independence, OH).

4.3.2. Particle Synthesis

nNiFe⁰-AC particles preparation was performed under anaerobic conditions as described previously (dissertation chapter 3). Briefly, FeCl₂·4H₂O and AC were mixed for 10 min under mechanical stirring (600 rpm) and then NaBH₄ were added dropwise for another 10 min to precipitate Fe⁰ onto the AC surface. After Fe⁰ precipitated, samples were washed three times with deoxygenated water (18.2 MΩ cm), centrifuged at 4,500 rpm (2604 g) and supernatant was discarded. Finally, an aqueous solution of NiCl₂·6H₂O was added to the wet Fe⁰ with strong stirring (600 rpm) for 3 hours and then sonicated for an additional of 30 min. Again, the resulting nanocomposite was washed, and the supernatant was removed. Ni content over Fe⁰ was ~2 wt%. A total of ~0.2 g of nNiFe⁰-AC was synthesized immediately before use. The deionized water used in nanocomposite synthesis was deoxygenated by N₂ purging for 2 h. Only mechanical stirring was used to mix the solutions; magnetic stirring can cause magnetically induced aggregation of the NPs being produced.

4.3.3. Batch Reactions and Particle Extractions

Batch experiments were carried out under a N₂ atmosphere using 60-mL high-density polyethylene (HDPE) bottles with rubber crimp caps. To each bottle, 10 mL of ~6 μM PFOS solution was mixed with the nNiFe⁰-AC (2% Ni/Fe⁰ wt/wt) in a temperature-controlled chamber at 60 °C and 150 rpm. Samples were reacted for 1-h, 6-h, 12-h, 18-h, 24-h and 120-h. At each reaction time, three bottles were sacrificed for organic compound analysis and three for inorganic product analysis. Two controls, including a 10 mL PFOS solution and a matrix control (nNiFe⁰-AC and 10 ml deoxygenated water) were kept under the same conditions for each reaction period. pH and oxidation-reduction potential (ORP) were also monitored during the

experiments inside the glovebox using a stirring hot plate to heat and mix the particles during reaction. Measurements of pH and ORP were performed using a pH and ORP wireless sensors from Vernier (Beaverton, OR). All reactions were conducted in unbuffered solutions with no pH adjustments. After a reaction, all water (~10 mL) from each vial was transferred to a 15 mL polypropylene tube and particles were extracted 5 times with 10 mL of acidified methanol (1% acetic acid in water: methanol 10:90 v/v). The solvent-particle slurries were vortexed and rotated for 24 h in a circular tube rotator at 140 rpm and room temperature. Then, samples were centrifugated for 15 min at 4500 rpm (2604 g) and the supernatants transferred to a new 15-mL polypropylene tubes for analysis.

4.3.4. LC/MS Analysis

Quantification of PFCAs and PFOS as two single peaks (linear and branches) were achieved using an Agilent 6460 Triple-Quad mass spectrometer (MS) (Table B1) with online SPE and couple with a reversed phase poroshell 120 EC-C18 (3.0 mm x 50 mm) column as described elsewhere (Tokranov *et al.*, 2019; Weber *et al.*, 2017). Briefly, the mobile phase was a combination of 2 mM ammonium acetate (solvent A) in water and 2 mM ammonium acetate in methanol (solvent B). While the mobile phases for the online SPE were 0.1% formic acid in water and 100% methanol. The following gradient was applied at a flow rate of 0.5 mL/min: 0 to 0.85 min, 3% B; 0.85 to 3.50 min, 54% B; 3.50 to 16.0 min, 85% B; 16.0 to 16.5 min, 100% B; 16.5 to 17.5 min, 100% B. The injection volume was 300 μ L and the column temperature 55 $^{\circ}$ C.

4.3.5. PFOS Isomer-Specific Analysis

L- and Br-PFOS isomers were separated and identified using a Sciex5600 Triple Quadrupole Time-of-Flight (QToF) and a Shimadzu ultra-HPLC system equipped with a

SelexIon unit (Table B2). Samples were injected onto an Ascentis Express F5 PFP column (2.1 x 100 mm, 2.7 μm , 90 \AA) at a temperature of 30 $^{\circ}\text{C}$ and injection volume of 20 μl . The mobile phase consisted of 100% MeOH and 0.15% acetic acid at 250 $\mu\text{L}/\text{min}$. The gradient conditions were: 10% B for 0.50 min, 55% B for 3 min, 88% B for 14 min, 100% by 14.5 min, and 10% by 21 min. Samples were diluted with a final composition of 50:50 MeOH/water, transferred to a 1.5 mL polypropylene vials, and spiked with M8PFOS as internal standard. Identification of PFOS isomers was confirmed using individual isomers standards from Wellington Laboratories. Isomer-specific quantification was done by internal standard (M8PFOS) calculation using nine-points individual isomer-specific calibration curves detected in the m/z 499/99 transition. PFOS isomers were separated and quantified individually. Of the 11 known PFOS isomers (Figure B2) present in PFOS powder from Sigma-Aldrich (used in this study), six individual standards (L-PFOS, 6-PFOS, 5-PFOS, 4-PFOS, 3-PFOS, and 1-PFOS) with the higher contribution to PFOS composition (S. Park *et al.*, 2017) were acquired for peak identification. 2-PFOS was not commercially available and the dimethyl branched isomers (dm-PFOS) were not acquired due to their low contribution to the total PFOS composition. PFOS isomers were identified using isomer-specific product ions for a complete separation, and their retention time is reported in Table B6. L-PFOS and the major PFOS isomers (5- and 6-PFOS) were completely separated using the m/z 499/99 product ion, while 1-, 3- and 4-PFOS were separated and identified using the m/z 499/419, 499/130, and 499/330 transitions, respectively (Figure B3). However, quantification of PFOS isomers were performed only using the 499/99 transition due to the low concentration of dm-, 1-, 3-, and 4-PFOS in some of our reacted samples, resulting those branches being incorrectly calculated by individual transitions. Using the 499/99 transition the four dm-PFOS (5,5-; 4,5-; 4,4-; and 3,5-PFOS, not identified individually in this study) and the

combined 1-, 3- & 4-PFOS isomers were integrated as two single peaks follow up by 5-PFOS, 6-PFOS, and L-PFOS. Limit of detection and quantified was determined and reported in Table B7.

4.3.6. Nontarget Screening for Organic Product Detection

A non-target analysis for unknown byproducts was performed using the mass accuracy of the ToF analyzer. Organic degradation products were identified using a Sciex5600 Triple Quadrapole ToF-MS equipped with a Kinetex EVO C18 (2.1 x 100 mm, 5 μ m, 100 Å) column and a Phenomenex AF0-8497 filter. Optimized source conditions are presented in Table B3 and B4. A gradient elution with 0.15% acetic acid (mobile phase A) and 20 mM ammonium acetate in methanol (mobile phase B) were used to improve byproducts separation. The solvent gradient program used are shown in Table B5. The column was maintained at a temperature of 40 °C with an injection volume of 50 μ L. The total run time was of 47 min. Samples were injected in ToF-MS scan in negative and positive ion mode. The acquisition range was m/z 50 - 1500 with a 250-ms accumulation time per averaged spectrum. All data was acquired and processed using an Analyst 1.7 and a PeakView 2.2. software, respectively. Organic products were analyzed using QToF electrospray ionization (ESI) and atmospheric pressure chemical ionization (APCI) in negative modes. In our previous study (dissertation chapter 3) several poly/per-fluorinated products were identified and confirmed with their accurate mass and fragmentation. In order to check for additional products to aid in identifying potential degradation pathways, three replicate samples were combined and concentrated by a factor of three.

4.3.7. Inorganic Products Extraction and Analysis

nNiFe⁰-AC particles were extracted three times sequentially with 10 mL of 0.02 M NaOH for 48 h in a circular tube rotator at 140 rpm and room temperature, and centrifuged (4500

rpm, 2604 g). Supernatants were combined in a PP tube and stored at 4 °C. Inorganic product concentrations were measured via ion chromatography using a Dionex ICS-3000 system equipped with a Dionex IonPac AS25 main column (4.0 x 250 mm), Dionex IonPac AS25 guard column (4.0 x 50 mm) and sodium hydroxide (NaOH) as a mobile phase. The background conductivity was suppressed with a Dionex ERS 500 system operating in recycle mode. Before each injection, the column equilibrates for 30 min until the conductivity baseline noise signal decrease to < 10 nS. The flow rate was 1.5 mL/min with an injection volume of 50 µL and a column temperature of 30 °C. F⁻ and SO₃²⁻ standards were injected first to confirm their retention time. An isocratic eluent flow-rate condition with 6 mM NaOH for 23 min and 15 mA was set for SO₃²⁻ analysis. For F⁻ measurements, the suppressor current was set to 52 mA and the eluent concentration started at 1.8 mM NaOH for the first 11 min and then increase to 21 mM NaOH to remove the excess of chloride ions for 20 min. Finally, the eluent concentration returned to initial conditions of 1.8 mM NaOH for another 10 min for re-equilibration. Before injection extracted samples were diluted to 50:50 NaOH/water to avoid matrix interferences.

4.3.8. XPS Analysis

X-ray photoelectron spectroscopy (XPS) was used to scan the surface of the particles to measure its elemental composition: Fe 2p (695-730 eV, detailed in SI).

4.4. Results and Discussion

4.4.1. Total PFOS Transformation

PFOS (linear + branched isomers) reduction by nNiFe⁰-AC at 60 °C with generation of F⁻ and SO₃²⁻ relative to initial PFOS (6 µM) over time are shown in Figure 4-1a. Seventeen moles

of F^- and one mole of SO_3^{2-} can be generated from one mole of PFOS. PFOS concentrations declined to $50.1\% \pm 6.0\%$ within the first 24 h after which no additional PFOS loss was observed. Likewise, F^- and SO_3^{2-} (quantified as SO_4^{2-}) increased rapidly with F^- plateauing at 24 h like PFOS, whereas SO_3^{2-} continued to increase from $\sim 2 \mu\text{M}$ to $\sim 3 \mu\text{M}$ over the next 96 h. The defluorination ratio $((n_{produced}^{F^-}) / (n_{initial}^{PFOS} \times 17) \times 100)$ reached $\sim 50\%$ and the desulfonation ratio $((n_{produced}^{SO_3^{2-}}) / (n_{initial}^{PFOS} \times 1) \times 100)$ reached $\sim 51\%$.

Decreasing pH and increasing ORP values after addition of PFOS correlated to PFOS degradation over time (Figure 4-1b). In the first 25 minutes, pH increased rapidly from 5.6 to 8.21 due to the anaerobic corrosion of Fe^0 followed by slower decreases in pH to 3.85 over the remaining reaction time. Under anaerobic conditions, water serves as the main oxidant forming hydroxide ions and generating hydrogen gas ($Fe^0 + 2H_2O \rightarrow Fe^{2+} + H_2 + 2OH^-$). The subsequent decrease in pH is caused by the consumption of hydroxyl ions through the precipitation of metal hydroxides. ORP and pH are inversely correlated with ORP rapidly decreasing from +266 mV to -762 mV in the first 25 min followed by increases to -500 mV at 120 h.

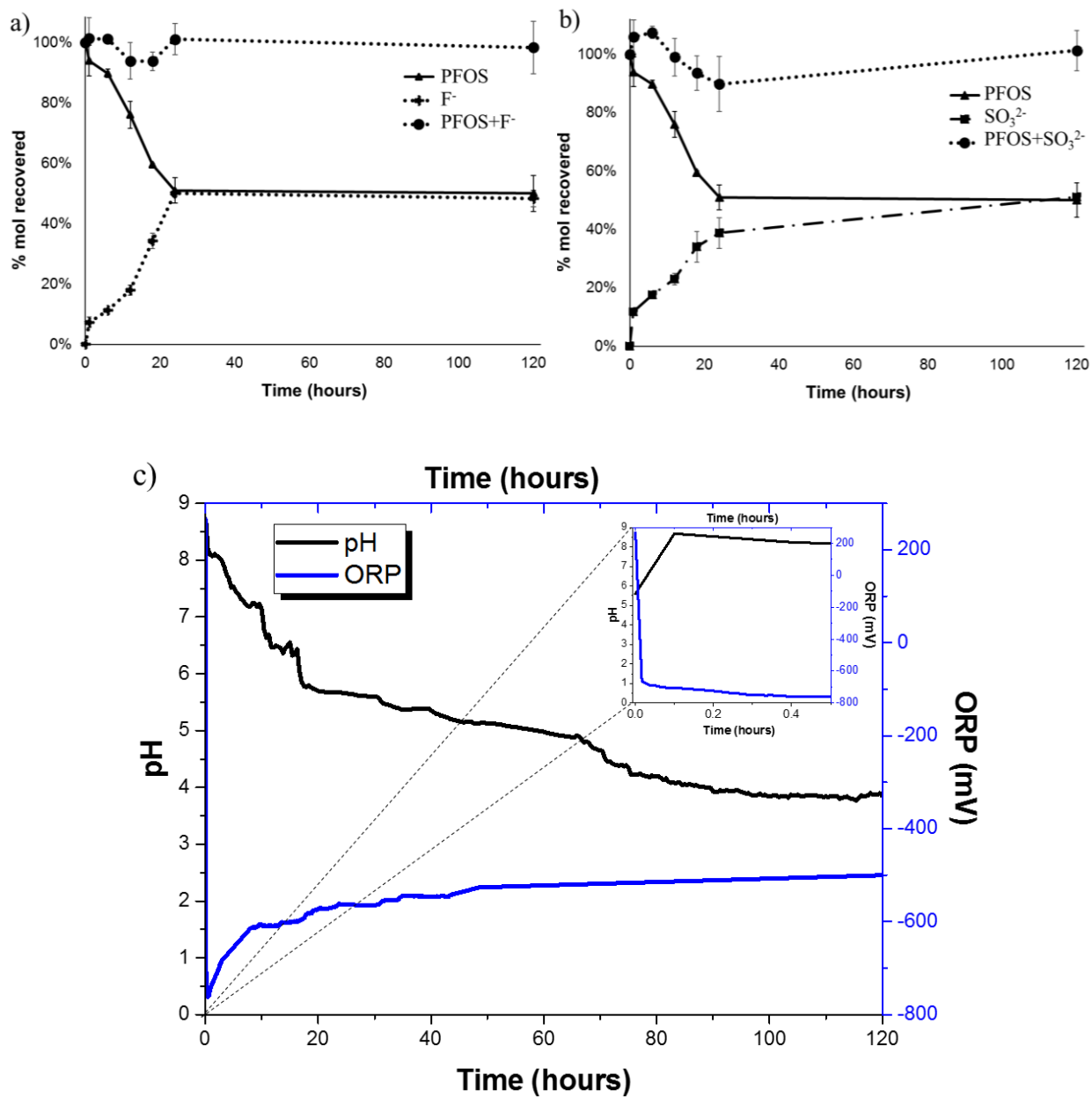


Figure 4-1. a) Mol % of total PFOS recovery and F⁻ and SO₃²⁻ generated relative to initial PFOS moles over time with nNiFe⁰-AC; 17 moles of F⁻ and one mole of SO₃²⁻ can be generated from one mole of PFOS, and b) pH and ORP (mV) measurements over time with the measurements for the matrix control being: pH = 6 and ORP = -556 meV and for the PFOS solution: pH = 5.6 and ORP = 266 meV. Particles were prepared with 3-h SST and in unbuffered deionized water with no pH adjustments. Seventeen moles of F⁻ and one mole of SO₃²⁻ can be generated from one mole of PFOS.

4.4.2. PFOS transformation kinetics

Total PFOS and L-PFOS transformation with nNiFe⁰-AC for the first 24 h were both well fitted by assuming a first-order reaction prior to the reaction plateau (Figure 4-2). Reaction rate constant between L- and Br-PFOS transformation were similar, $k_L = 0.028 \text{ h}^{-1}$ ($R^2_L=0.95$) and $k_{br} = 0.027 \text{ h}^{-1}$ ($R^2_{br}=0.97$), respectively. Ochoa-Herrera et al. (2008) also observed first order degradation kinetics (0 to 72 h) for the reductive of Br-PFOS isomers using vitamin B12 and titanium (III) citrate (Ochoa-Herrera *et al.*, 2008) with a similar first order rate constant (0.020 h^{-1}).

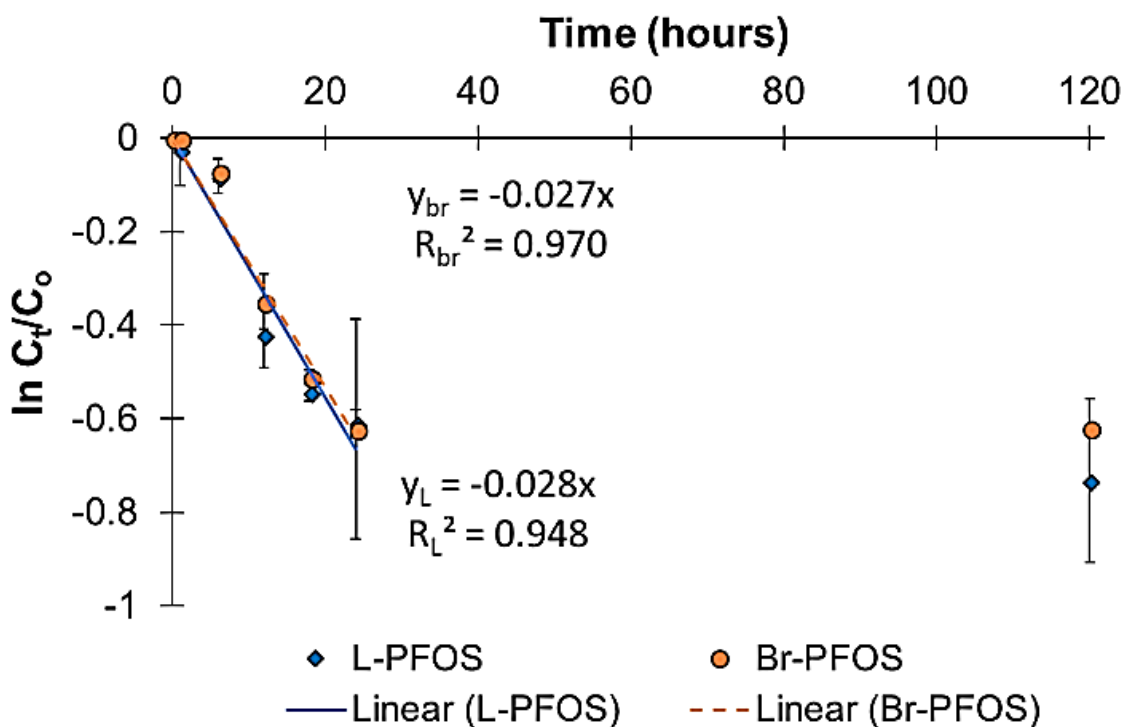


Figure 4-2. Linear regression of pseudo first-order reaction of L-PFOS and Br-PFOS isomers over time (1 h, 6 h, 12 h, 18 h, 24 h and 120 h).

4.4.3. Br-PFOS Isomers

Specific-isomer transformation was quantified and presented in Figure 4-3. In general, it appears an initial rapid decay occurs followed by a slower reaction kinetics, thus not well fit by assuming a first order reaction model as corroborated by the resulting low R^2 values. 5-PFOS appears to be the fastest reacting isomer, but it only makes up about ~3% of the total initial PFOS. The highest transformation magnitude at 1 day was observed for 6-PFOS similar to what was reported previously for both theoretical and experimental data, (Ochoa-Herrera *et al.*, 2008; S. Park *et al.*, 2017; Torres *et al.*, 2009). Computational studies, showed 6-PFOS is the isomer with the most accessible LUMO orbital of the Br-PFOS isomers, thus expected to have the highest overall reactivity.

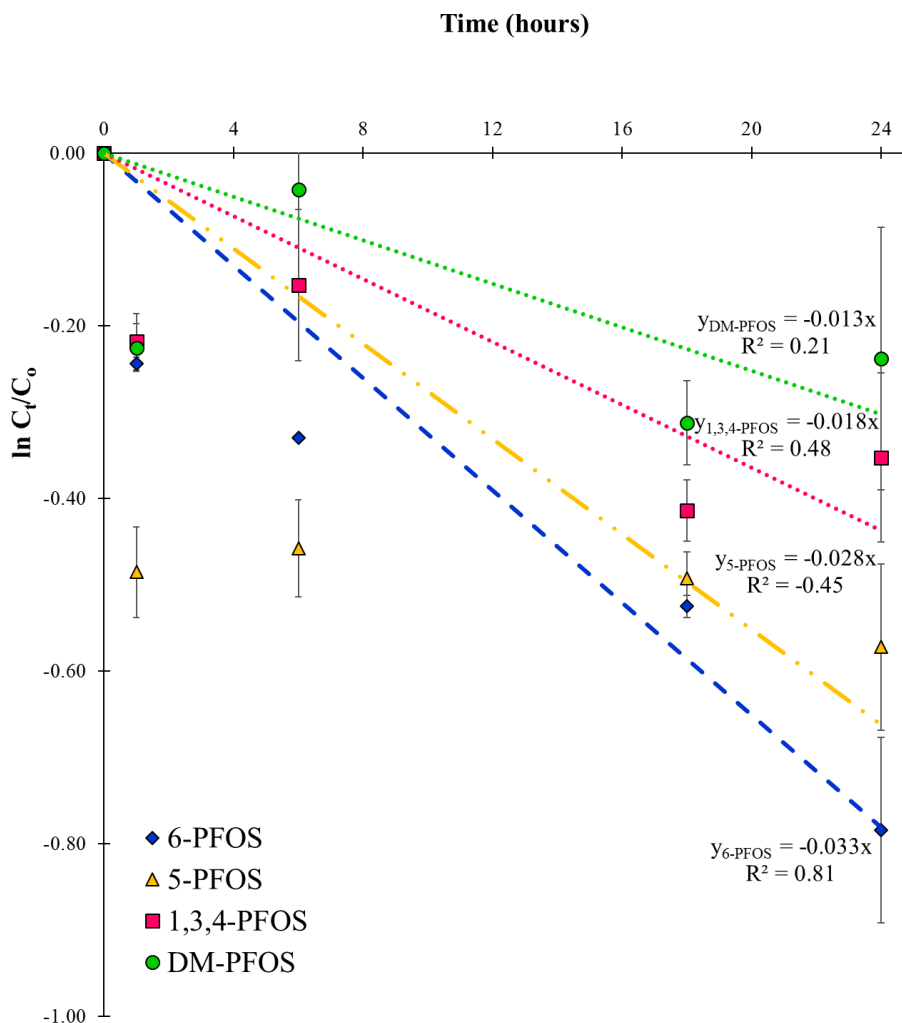


Figure 4-3. Natural logarithm of the ratio between the concentration of specific PFOS isomer at a given time relative to its concentration at $t=0$ versus reaction time. Points are an average of 3 replicates.

4.4.4. PFOS Products over time

Additional organic products in negative ESE more were identified by combining and concentrating triplicate samples (Table 4-1 and B9) including PFCAs and additional polyfluoroalkyl intermediates and one more desulfonated product. All organic products account for a low percentage of the total mass balance since >90% represent F^- and SO_3^{2-} at all timepoints. In the early stage of the reaction, $C_8HF_{16}SO_3^-$ is identified as the dominant reduction

product. The additional polyfluoroalkyl intermediates supports continued stepwise defluorination of the initial single- and double-bond C8 intermediates. After the initial transformation step, stepwise F/H exchanges is shown to occur for the first 10 fluorine atoms removed (1st and 3rd product groupings in Table 4-1). Additional shorter carbon-chain products were also detected. As previous studies have shown, Ni can catalyze the breaking of C-C bonds (Schrick *et al.*, 2002). The shorter chain intermediates [C₇ - C₄] are all polyfluoroalkane sulfonates, thus the pathway leading to this group of polyfluoroalkane sulfonates may occur after the cleavage of the C-C bond at the terminal end of the PFOS tail (tertiary carbon attached to the -CF₃ group) after the first F/H exchange. An additional reaction pathway was also encountered.

An additional reaction pathway involving desulfonation was also evident with the generation of several PFCAs and two fluorinated alkanes. PFOA, PFHpA, PFHxA, PFHeA and PFBA were found and quantified (Table B8). All the quantified PFCA products were < 0.9 ug/L, which corresponded to 0.1% of the transformed PFOS. The two fluorinated alkanes were not quantified due to the lack of commercial standards.

Table 4.1. Products detected in concentrated samples at four or more sampling times with one exception after 6 μM PFOS solution react with nNiFe⁰-AC at 60 °C. Degradation products were detected using QToF electrospray ionization (ESI) and atmospheric pressure chemical ionization (APCI), both in negative mode. The exception is m/z 431.96, which was observed only at 120 h. PFOS ($\text{C}_8\text{F}_{17}\text{SO}_3^-$, m/z 498.9297 tr = 11.34 min).

Formula	Theoretical m/z	Observed m/z	Error ^a (ppm)	Error ^b (mDa)	t _r ^c (min)
Defluorination F/H exchange					
<u>C-C Single bonds products for C8 molecules</u>					
$\text{C}_8\text{HF}_{16}\text{SO}_3^-$	480.9391	480.9355	7.49	3.60	10.56
$\text{C}_8\text{H}_2\text{F}_{15}\text{SO}_3^-$	462.9485	462.9477	1.73	0.80	10.20
* $\text{C}_8\text{H}_3\text{F}_{14}\text{SO}_3^-$	444.9579	444.9547	7.27	3.23	10.13
$\text{C}_8\text{H}_4\text{F}_{13}\text{SO}_3^-$	426.9674	426.9644	7.03	3.00	9.63
* $\text{C}_8\text{H}_5\text{F}_{12}\text{SO}_3^-$	408.9768	408.9757	2.64	1.08	9.56
$\text{C}_8\text{H}_6\text{F}_{11}\text{SO}_3^-$	390.9862	390.9844	4.60	1.80	9.43
* $\text{C}_8\text{H}_7\text{F}_{10}\text{SO}_3^-$	372.9956	372.9948	2.20	0.82	9.19
$\text{C}_8\text{H}_8\text{F}_9\text{SO}_3^-$	355.0050	355.0030	5.76	2.04	9.08
* $\text{C}_8\text{H}_9\text{F}_8\text{SO}_3^-$	337.0145	337.0142	0.79	0.26	9.05
$\text{C}_8\text{H}_{10}\text{F}_7\text{SO}_3^-$	319.0239	319.0224	4.70	1.50	8.56
<u>C-C Single bonds products with < C8 molecules</u>					
$\text{C}_7\text{HF}_{14}\text{SO}_3^-$	430.9423	430.9403	4.64	2.00	9.61
$\text{C}_6\text{HF}_{12}\text{SO}_3^-$	380.9455	380.9438	4.46	1.70	8.74
* $\text{C}_5\text{HF}_{10}\text{SO}_3^-$	330.9487	330.9469	5.35	1.77	7.50
* $\text{C}_4\text{HF}_8\text{SO}_3^-$	280.9519	280.9533	5.10	1.43	6.83
<u>C-C Double bond products (only observed for C8 molecules)</u>					
* $\text{C}_8\text{HF}_{14}\text{SO}_3^-$	442.9423	442.9402	4.70	2.08	10.25
$\text{C}_8\text{H}_2\text{F}_{13}\text{SO}_3^-$	424.952	424.9500	4.71	2.00	10.10
$\text{C}_8\text{H}_3\text{F}_{12}\text{SO}_3^-$	406.9611	406.9591	4.91	2.00	9.67
* $\text{C}_8\text{H}_4\text{F}_{11}\text{SO}_3^-$	388.9706	388.9708	0.64	0.25	9.10

Table 4-1. continued

$C_8H_5F_{10}SO_3^-$	370.9799	370.9782	4.58	1.70	8.84
$C_8H_6F_9SO_3^-$	352.9894	352.9881	3.67	1.29	8.56
$C_8H_7F_8SO_3^-$	334.9988	334.998	2.44	0.82	8.31
$C_8H_8F_7SO_3^-$	317.0082	317.0076	2.01	0.64	8.07
Perfluorocarboxylic acid products					
* $C_8F_{15}O_2^-$	412.9659	412.9681	5.39	2.23	10.32
* $C_7F_{13}O_2^-$	362.9691	362.9684	1.84	0.67	9.37
* $C_6F_{11}O_2^-$	312.9723	312.9705	5.63	1.76	8.49
* $C_4F_7O_2^-$	212.9787	212.9795	3.99	0.85	6.46
Desulfonation - SO_3^- cleavage (Paraffins)					
$C_8F_{17}O^-$	434.9678	434.9671	1.61	0.70	
$C_8F_{16}O_2^-$	431.9643	431.9633	2.41	1.04	

^a (Difference between theoretical mass and experimentally measured mass/theoretical mass) x 10⁶; ^b(Theoretical mass/(1/errorPPM*1000)). ^cRetention time. *Products detected only in the concentrated samples.

Time-dependent changes in PFOS intermediates are presented in Figures 4-4, and 4-5. Products conserving the sulfonate group, paraffins and PFCAs increased rapidly in the first 6 to 12 h and then disappeared almost completely after 24 h with a few exceptions. The peak intensities of the defluorinated C-8 intermediates with less fluorines ($C_8H_8F_9SO_3^-$, $C_8H_9F_8SO_3^-$, $C_8H_{10}F_7SO_3^-$) and the shortest carbon-chain detected ($C_4F_9SO_3^-$) appeared to continue increasing after 24 h. PFCAs and paraffins reached their maximum peak value at 12-h and 18-h, respectively, and then decreased gradually over time until they were no longer detected by 24 h except for PFBA. PFBA concentrations continued to increase throughout the 120-h reaction period.

Single bond intermediates

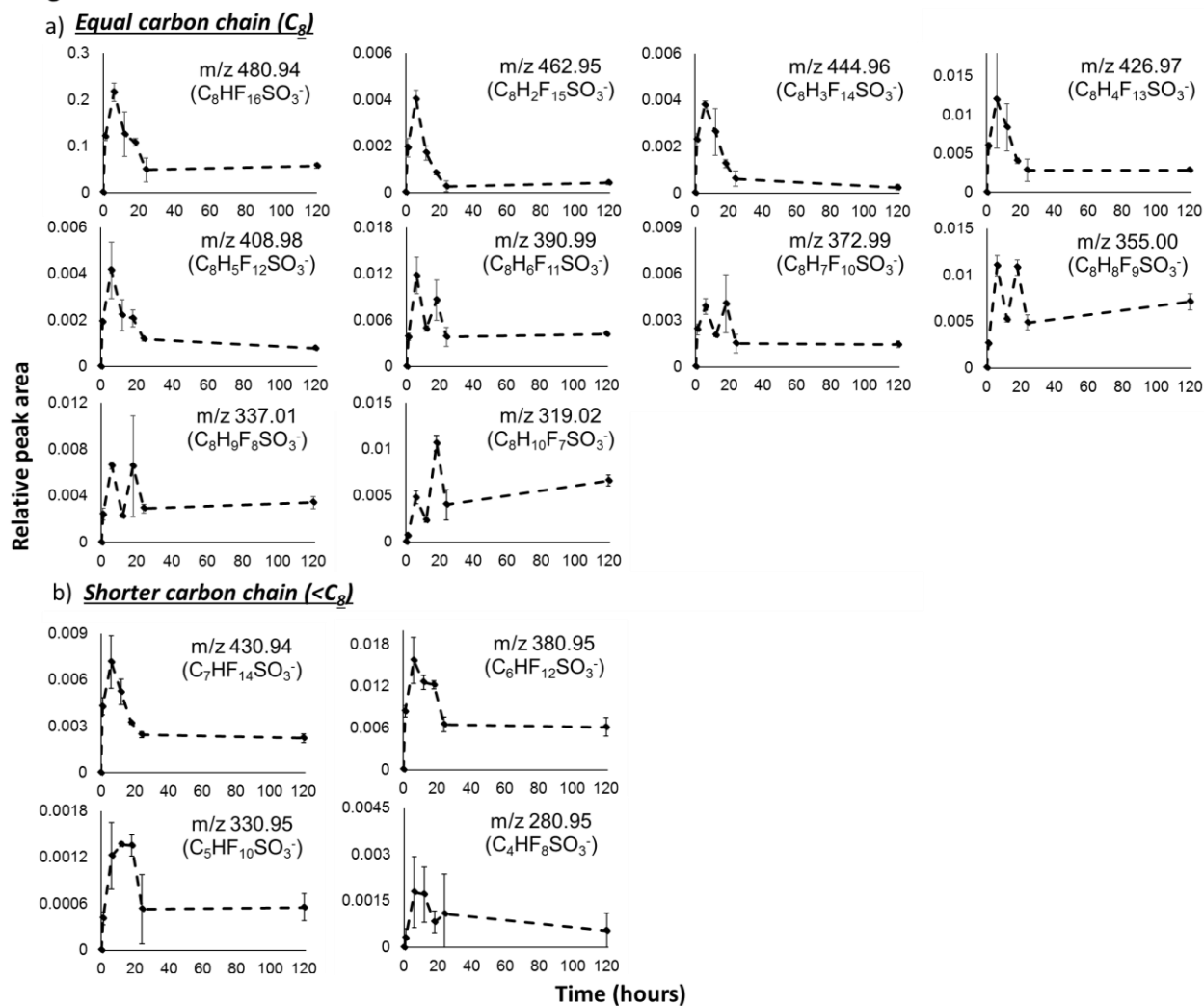


Figure 4-4. Generation of single-bond products over time from PFOS reduction. Sequential a) F/H exchanges and generation of b) shorter carbon chain [C_7 - C_4] products. Peak areas of individual products were normalized by M8PFOS IS (188 $\mu\text{g/L}$) peak area. All products shown were detected using electrospray ionization in negative mode (ESI-).

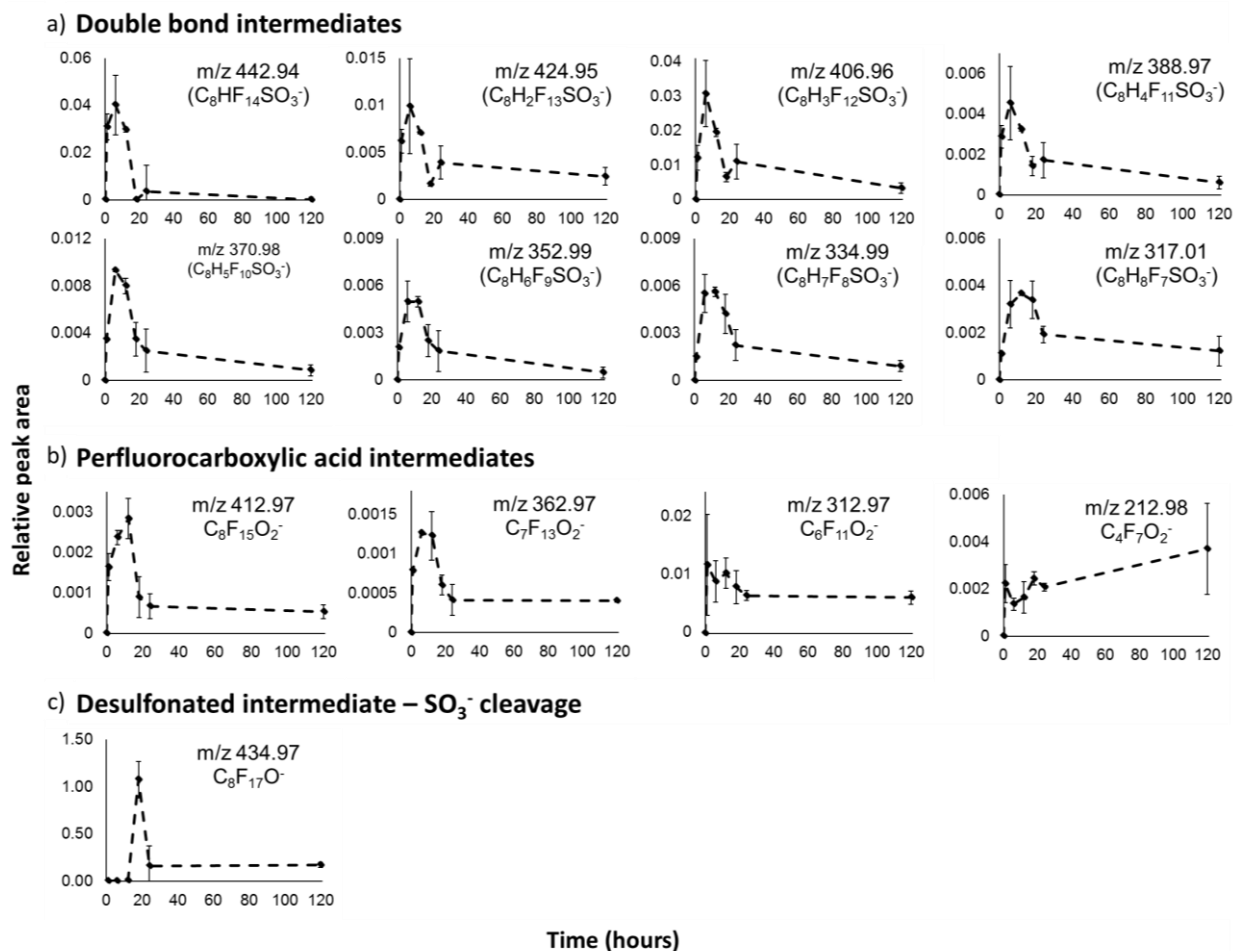


Figure 4-5. Generation over time during PFOS reduction of a) double-bond, b) PFCAs, and c) paraffin products. Peak areas of individual products were normalized by M8PFOS IS (188 $\mu\text{g/L}$) peak area. All products shown were detected using electrospray ionization in negative mode (ESI-) except for the paraffins, which required atmospheric pressure negative chemical ionization (APCI). Data for PFCAs and paraffin are from concentrated (x3) samples.

The mass balance of fluorine and sulfonate as a function of time was calculated based on quantified PFOS (seventeen F atoms and one sulfonate group), PFCAs (F atoms = $3 + 2n$ with n = carbon chain length), F^- and SO_3^{2-} relative to the initial PFOS (Table 4-2). Fluorine and sulfonate associated with the organic products generated were not included since standards were not available to quantify them. The fluorine and sulfonate corresponding mass balance over time ($t > 0$) account for $> 90\%$ as shown in Table 4-2. The relatively small fluorine and sulfonate not

captured in the mass balance are likely associated with the suite of unquantifiable organic products. Using PFOS standard curves, detected organic products were semi-quantified which resulted in their total combined contribution to the fluorine balance of 1.4% to 4.5% at the different reaction times.

Table 4-2. % F based on F content in initial PFOS (17 F/PFOS) calculated based on sum of F associated with PFOS remaining and PFCAs generated (F atoms = 3 + 2n with n = carbon chain length) and measured fluoride (F⁻).

Reaction time (h)	Remaining PFOS	F ⁻ *	SO ₃ ²⁻ **	Total F content (%)	Total SO ₃ ²⁻ content (%)
0	100.0%	0.0%	0.0%	100.0%	100.0%
1	94.0%	7.3%	11.9%	101.3%	105.9%
6	89.7%	11.4%	17.7%	101.1%	107.4%
12	76.0%	17.9%	23.0%	93.9%	99.0%
18	59.5%	34.3%	34.1%	93.8%	93.6%
24	51.0%	50.1%	38.8%	101.1%	89.8%
120	50.1%	48.3%	51.2%	98.4%	101.3%

*F⁻ yield = [(moles of F⁻ formed)/ (moles of fluorine content in initial PFOS)] x 100.

**SO₃²⁻ yield = [(moles of SO₃²⁻ formed)/ (moles of sulfate content in initial PFOS)] x 100.

4.4.5. Degradation Pathways and Potential Mechanisms

Although overall F⁻ and SO₃²⁻ mass balance was high, using the information of the organic products identified (Table 4-1) and F⁻ and SO₃²⁻ generation, four degradation pathways are proposed (Figure 4-6). Three pathways involve defluorination reactions conserving the sulfonate group while the fourth pathway involve desulfonation and the generation of fluorinated alkanes and carboxylic acids. Under anaerobic conditions, hydrogen gas and hydroxide ions (OH⁻) are produced through iron corrosion ($\text{Fe}^0 + 2\text{H}_2\text{O} \rightarrow \text{Fe}^{2+} + \text{H}_2 + 2\text{OH}^-$). Iron corrosion and formation

of Fe^{2+} was confirmed by XPS on the nanoparticle surface (Figure B4). Hydrogen is adsorbed by the Ni catalyst converting molecular hydrogen into atomic hydrogen ($\text{H}\bullet$, $E^0_{\text{H}\bullet} = -2.3 \text{ V}$) (Bokare *et al.*, 2008; Schrick *et al.*, 2002). Thus, PFOS could be reduced by direct electron transfer from Fe^0 ($E^0 = -0.44 \text{ V}$ (Burrows *et al.*, 2013)), or indirectly by Fe^{2+} ($E^0 = 0.77 \text{ V}$ (Burrows *et al.*, 2013), resulting from Fe^0 corrosion) or H-atoms ($E^0 = -2.3 \text{ V}$ (Buxton *et al.*, 1988), from the corrosion of Fe^{2+} in the presence of the Ni catalyst). The reaction may be started with the formation of the perfluoroalkyl radical $\text{C}_8\text{F}_{16}\text{SO}_3\bullet$ after fluoride is released followed by the radical reacting directly with H radicals resulting in polyfluorooctane sulfonate by direct electron transfer, $\text{C}_8\text{HF}_{16}\text{SO}_3^-$ and then loss of another F with addition of H^+ on a step-by-step basis to form polyfluoroalkyl sulfonates.

Alternatively, the C-C bond at the terminal end of the fluorocarbon chain can be broken from the polyfluorooctane molecule releasing CF_2H on a step-by-step basis and adding H^+ to form shorter chain polyfluoroalkyl sulfonates.

Double bond defluorinated products are forming only from the Br-PFOS isomers. According to theoretical studies (Torres *et al.*, 2009), the tertiary carbon attached to the $-\text{CF}_3$ group of the branched isomers is the most favorable to react. Thus, 2F atoms are released, one attached directly to tertiary carbon and the other one to the CF_3 group, forming a double bond chain and followed by another F/H replacement in the CF_3 group yielding the polyfluoroalkyl sulfonate with double bond, $\text{C}_8\text{HF}_{14}\text{SO}_3^-$.

The desulfonated mechanism may involve the formation of a perfluoroalkyl radical ($\text{C}_8\text{F}_{17}\bullet$) and the dissociation of the $\text{SO}_3\bullet$ group. Under nitrogen atmosphere, the perfluoroalkyl radical formed after dissociation, will react with hydroxyl radicals to generate the unstable perfluoroalkyl alcohol ($\text{C}_8\text{F}_{17}\text{OH}$) which then will be protonated yielding the fluorinated alkene

$C_8F_{17}H$. The unstable perfluoroalkyl alcohol will continue reacting to produce carboxylates. First it will undergo HF elimination forming $C_7F_{15}COF$ which then hydrolyzes yielding PFOA. The same mechanism is repeated forming short-chain perfluorocarboxylic acids (PFHpA, PFHxA, PFPeA, and PFBA).

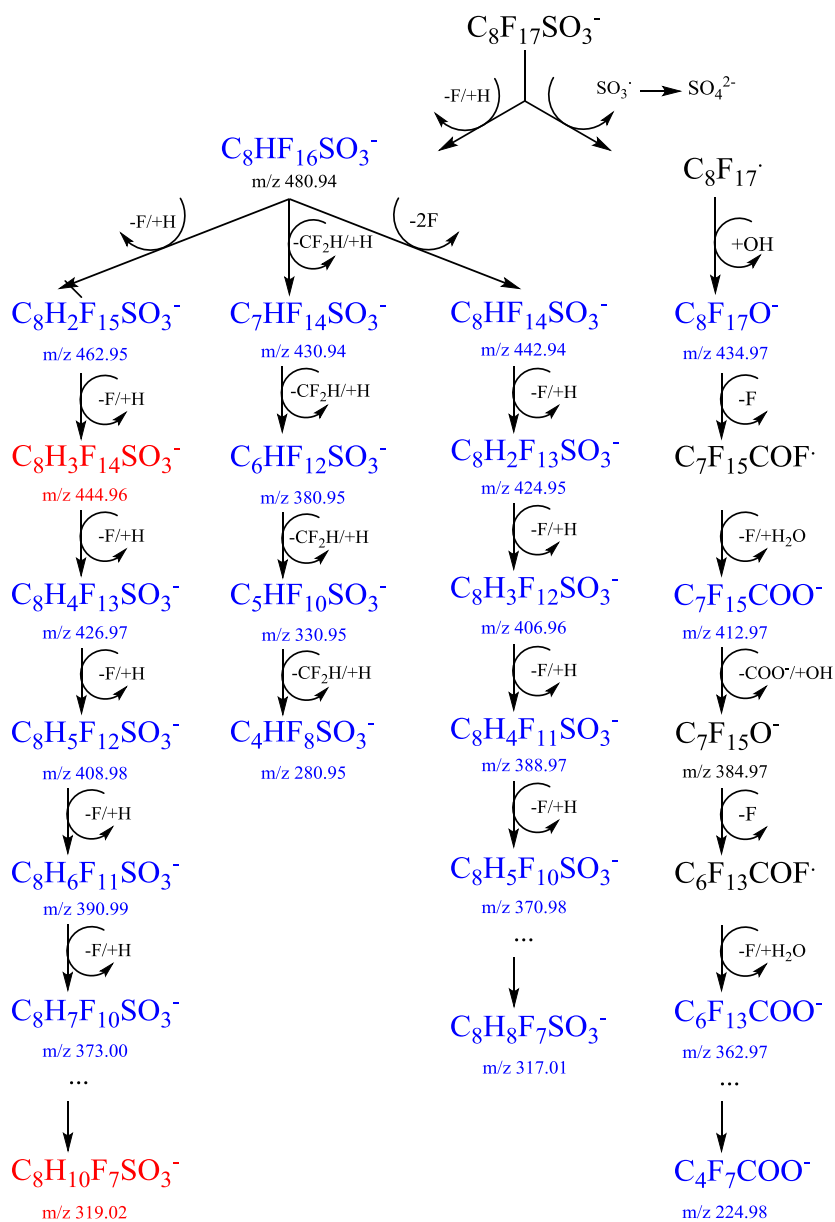


Figure 4-6. Reaction pathways proposed for PFOS reduction by nNiFe⁰-AC. Defluorination, desulfonation, and formation of single, double-bond, and paraffin products. Formulas colored with blue were confirmed with mass accuracy and fragmentation and red only with mass accuracy.

4.5. Summary

The kinetic analysis of L- and Br-PFOS degradation by nNiFe⁰-AC at 60 °C brings some unique information about PFOS reduction potential and pathways under conditions that could be amenable for in-situ remediation. Inexpensive and less toxic metals (Fe and Ni) on a carbon base support material (activated carbon) were used to transform L-PFOS and Br-PFOS. The degradation of L- and Br-PFOS isomers followed a pseudo-first-order kinetics. Contrary to other studies, L- and Br-PFOS have a similar degradation rate constants ($k_L = 0.028 \text{ h}^{-1}$ and $k_{br} = 0.027 \text{ h}^{-1}$), The reason of the similarity on degradation rates could be explained because the initial reduction is predominantly occurring through the tertiary carbon attached to the CF₃ group, of either the L- or Br- isomer. Of the branched isomers, 6-PFOS has the highest degradation correlated to theoretical studies. Organic and inorganic products were detected as an evidence of PFOS transformation. The degradation products observed in only the particle extracts reveal that continued defluorination and desulfonation reactions and that the reactions occur at the particle surface. The organic products identified are single and double bonds polyfluoroalkyl sulfonates, single bond polyfluoroalkyl sulfonates of shorter chains (C4 to C7), perfluoroalkyl carboxylic acids, and fluorinated alkanes. The mass balance of fluoride and sulfate at 120 hours of reaction, indicates that essentially all PFOS transformed was completely mineralized into F⁻ and SO₃²⁻.

CHAPTER 5. EFFECTS OF CARBON-CHAIN LENGTH, FUNCTIONAL GROUP, AND COMMON GROUNDWATER CONSTITUENTS ON PFAAS REDUCTION BY $n\text{NiFe}^0\text{-AC}$

5.1. Abstract

Perfluoroalkyl acids (PFAAs) are a class of stable chemicals recalcitrant to several degradation processes. Reductive treatment by $n\text{NiFe}^0\text{-AC}$ have been proven to degrade one of the most stable and toxic PFAA, the perfluorooctane sulfonate (PFOS). The effects of chain length ($\text{C}_3\text{-C}_8$) and functional head group ($-\text{SO}_3^-$ and $-\text{CO}_2^-$) on PFAAs degradation by $n\text{NiFe}^0\text{-AC}$ are presented here as well as $n\text{NiFe}^0\text{-AC}$ effectiveness to degrade a mixture of PFAAs in a PFAA-contaminated groundwater sample collected near a former fire-training area in Massachusetts. Similar degradation alkyl chain length trends were observed for perfluoroalkyl carboxylic (PFCAs) and sulfonic acids (PFSAs). Like PFOS, PFOA degradation plateaued by 1 d whereas shorter chains required longer time likely due to their lower sorption to reactive surfaces. F^- and SO_3^{2-} generation confirmed for both PFCA or PFSA degradation. However, measured F mass balance was higher for PFOS and PFOA (> 90% F) compared to short-chain PFAAs ($\approx 50\text{-}70\%$ F). Organic products detected for PFCAs included per- & polyfluoroalkyl carboxylates and alcohols with single and double bonds. While for PFSAs, polyfluoroalkyl sulfonates and perfluoroalkyl carboxylates with only single bonds were generated. PFAAs present in AFFF-contaminated groundwater were degraded using $n\text{NiFe}^0\text{-AC}$ at 60 °C, but appeared lower than in single-solute deionized water.

5.2. Introduction

Perfluoroalkyl acids (PFAAs) are a group of fully fluorinated molecules consisting of a hydrophobic single bonded carbon chains (2 to 18 C tail) and a charged functional group (head) attached at one end (Buck *et al.*, 2011). The most studied PFAAs are carboxylic ($-\text{CO}_2^-$) and sulfonic ($-\text{SO}_3^-$) acids (Wang *et al.*, 2017). PFAA contamination of groundwater is widespread mainly due to discharges by industrial and in firefighting activities (Hu *et al.*, 2016). Traditional remediation treatments for contaminated water and wastewater, including biological or oxidation methods are not effective in degrading PFAAs. Although some oxidative techniques have shown success for perfluoroalkyl carboxylic acids (PFCAs) such as PFOA (Giri *et al.*, 2011; Hori *et al.*, 2004; Hori *et al.*, 2007; Park *et al.*, 2016; Schroder & Meesters, 2005), perfluoroalkyl sulfonic acids (PFSAs) cannot be oxidized through reactions with hydroxyl or sulfate radicals. Production of long-chain PFAAs like PFOS and PFOA, are being replaced by their short-chain counterparts (C4 and C6 molecules) due to their lower bioaccumulation potentials and shorter elimination half-lives (Zhang *et al.*, 2013). However, shorth-chain PFAAs are equally resistant to destructive treatment, and moreover, their higher water solubilities and sorptive affinities also reduce effectiveness of their removal by adsorption processes. For example, Xiao *et al.* (Xiao *et al.*, 2017) found lower adsorption of perfluorobutanesulfonate (PFBS, $\text{C}_4\text{F}_9\text{SO}_3^-$) and perfluorobutanoic acid (PFBA, $\text{C}_4\text{F}_7\text{O}_2^-$) to granular activated carbon (GAC) compared to their longer-chain analogues (PFOS and PFOA, respectively). Zhuo *et al.* (Zhuo *et al.*, 2012) found decomposition of PFAAs with electrochemical oxidation to increase with increasing alkyl chain length for both PFCAs and PFSAs degradation. The higher degradation for the long-chain PFAAs was attributed to their higher adsorption to the hydrophobic surface of the boron-doped diamond (BDD) anode. Slower kinetics was also observed in sonochemical decomposition of

shorter chain PFCAs and PFSAs compared to their longer homologues (Campbell *et al.*, 2009; Fernandez *et al.*, 2016), which Campbell *et al.* (Campbell *et al.*, 2009) attributed to lower adsorption at the air-water interface for shorter chains. Such results highlight the need to evaluate the effects of chain length and functional groups on PFAA degradation potential when assessing a remediation technology.

The presence of common inorganic ions and other constituents present may also influence efficiency of the treatment process via competition for the released electrons. PFCAs and PFSAs are normally present as anions at environmental pH values due to their low pK_a values (< 3). Chen *et al.*, (Cheng *et al.*, 2010) showed that anions such as ClO_4^- , NO_3^- , and Cl^- had both positive and negative effects on sonochemical decomposition of PFAAs while common cations such as Ca^{2+} , Mg^{2+} , Na^+ , K^+ had negligible effects (Cheng *et al.*, 2010). For remediation technologies that use zero valent metals, atomic H or formation of a passivation oxide layer blocking pollutant access to reactive sites can also be affected by the matrix. In degradation of polychlorinated biphenyls by nPd/Fe, Cl^- and Br^- slowed degradation rates (Xu, 2005).

In our previous work (Chapters 3 and 4), degradation focused on only PFOS in batch reactions with nNiFe⁰-AC at 60 °C and deionized (DI) water. The objective of this study is to assess how carbon-chain length (C4-C8) and polar functional groups (carboxylate versus sulfonates) affect the overall reduction by nNiFe⁰-AC at 60 °C in DI water. In addition, the differences in PFAA degradation were compared between a single PFAA in DI water versus PFAAs in a contaminated groundwater from a former fire-training area in Massachusetts.

5.3. Materials and Methods

5.3.1. Chemicals

Mass-labelled and native PFCA/PFSA mixtures (MPFAC-MXA and PFAC-MXC) were acquired from Wellington Laboratories (Lenexa, KS). Iron (II) chloride tetrahydrate ($\text{FeCl}_2 \cdot 4\text{H}_2\text{O}$, 98%), sodium borohydride (NaBH_4 , 99%), nickel chloride hexahydrate ($\text{NiCl}_2 \cdot 6\text{H}_2\text{O}$, 98%), sodium fluoride (NaF , 99%), and sodium sulfate (Na_2SO_4 , 99%) were obtained from Sigma-Aldrich (St. Louis, MO). Powder activated carbon (surface area 1300 – 1400 m^2/g) was provided by Strem Chemicals (Newburyport, MA). LC-MS grade solvents, such as formic acid, ammonium acetate, acetic acid, sodium hydroxide, and methanol were purchased from Fisher Scientific (Pittsburgh, PA). All deionized (DI) water (18.2 $\text{M}\Omega \text{ cm}$) used in this study was deoxygenated by bubbling N_2 gas for 2 h. An aliquot of groundwater samples was obtained from a study conducted on western Cape Cod, Massachusetts at the U.S. Geological Survey Toxic Substances Hydrology Program Cape Cod Research site (Barber *et al.*, 2017; Weber *et al.*, 2017). Groundwater contamination was observed in the vicinity of a fire-training area and a wastewater treatment plant located on Joint Base Cape Cod. Concentrations of the analyzed PFAAs are reported in Table 5-4a). Ions concentration was provided by USGS who performed a full characterization of the studied area. Concentrations of anions and cations range from 0.07 – 6.18 mg/L and 0.61 – 3.76 mg/L, respectively (Table 5-4b).

5.3.2. Bimetals Synthesis

$n\text{NiFe}^0\text{-AC}$ particle preparation was performed under nitrogen atmosphere following the same procedure described before (dissertation chapters 3 & 4). Briefly, $\text{FeCl}_2 \cdot 4\text{H}_2\text{O}$ and AC were mixed for 10 min under N_2 purging followed by slowly adding NaBH_4 to precipitate $n\text{Fe}^0$ and

washing the particles three times with DI water. The clean $n\text{Fe}^0$ was mixed with an aqueous solution containing $\text{NiCl}_2 \cdot 6\text{H}_2\text{O}$ while stirring at 600 rpm for 3 h during which Ni was deposited on $n\text{Fe}^0$ -AC surface. Finally, particles were sonicated for 30 min and the final nanocomposite $n\text{NiFe}^0$ -AC washed three times to remove residual impurities. Characterization of the $n\text{NiFe}^0$ -AC particles has been previously described (dissertation chapter 3).

5.3.3. Batch Experiments

The differences in the effectiveness of $n\text{NiFe}^0$ -AC to transform PFAAs as a function of carbon-chain length and polar function group in single solute DI water systems as well as compared to a mixed PFAA contaminated groundwater were investigated in batch experiments under N_2 atmosphere in an anaerobic chamber. Five PFAAs were selected for this study including: perfluorohexane sulfonic acid (PFH_xS , $\text{C}_6\text{F}_{13}\text{SO}_3^-$), perfluorobutane sulfonic acid (PFBS , $\text{C}_4\text{F}_9\text{SO}_3^-$), perfluorooctanoic acid (PFOA , $\text{C}_7\text{F}_{15}\text{COO}^-$), perfluorohexanoic acid (PFH_xA , $\text{C}_5\text{F}_{11}\text{COO}^-$), and perfluorobutyric acid (PFBA , $\text{C}_3\text{F}_7\text{COO}^-$). PFOS results from chapters 3 & 4 will be used for comparison. The reactions were initiated by adding 0.2 g of $n\text{NiFe}^0$ -AC and 10 mL of either DI water containing individual PFAA ($6 \mu\text{M}$) or PFAA-contaminated groundwater. Reaction took place in a 60-mL high-density polyethylene (HDPE) vials hermetically sealed with rubber crimp caps. After sealed, vials were shaken (150 rpm) for 1 d or 5 d at $60 \text{ }^\circ\text{C}$ using a temperature-controlled chamber. Two controls, PFAA solution with no particles and matrix with particles but no PFAAs, were prepared identically in vials. All experiments were performed in unbuffered and unadjusted solutions except the groundwater sample and deoxygenated before adding the particles. Reactions were carried out for 1 d and 5 d for the single solute experiments and 5 d for the PFAA-contaminated groundwater.

5.3.4. Extractions

Postreaction, water (~ 10 mL) was removed and particles extracted. For PFAAs and organic products, particles were extracted using 10 mL of acidified methanol (1% acetic acid in DI water: methanol 10:90 v/v). The vials were then placed on the rotator shaker (140 rpm) for 24 h. Repeated acidified methanol extractions were performed until no more PFAAs were observed in the solvent. Control vials were always extracted using the same method as the samples. From each vial, an aliquot of about 50 μL was dilute and adjusted with 50:50 MeOH/H₂O to a final volume of 1.5 mL in a HPLC vial for PFAAs quantification and organic product identification. For inorganic products (F⁻ and SO₄²⁻), sequential extractions of were performed using 10 mL of 0.02 M NaOH for 48 h. All vials were placed on a rotator shaker at room temperature (22 \pm 1 $^{\circ}\text{C}$) and shaken at 140 rpm. Then, the NPs were separated from the solution by centrifugation at 4,500 rpm (2604 g) and storage at 4 $^{\circ}\text{C}$ until analysis. All experiments were performed in triplicate.

5.3.5. Analytical Methods

Concentration of PFAAs and ions were quantified using an Agilent 6460 Triple-Quad mass spectrometer with online SPE and an ICS-3000 ion chromatography system, respectively.

5.3.6. LCMS

Separation was achieved using a reversed phase poroshell 120 EC-C18 column (3.0 mm x 50 mm), a binary gradient of 2 mM ammonium acetate in water (A) and 2 mM ammonium acetate in methanol (B) and a 300 μL injection volume as described previously (dissertation chapter 4). Solvents for the online SPE consisted of 0.1% formic acid in water and 100%

methanol. Gradient details, temperature and MS/MS conditions are described in Table C1 and C2. For PFAA quantification, a 10-point calibration curve was generated in the range of 50 – 1,500 ng/L.

5.3.7. ICS

F⁻ and SO₄²⁻ quantification was performed using suppressed conductivity detection on a Dionex ICS-3000 ion chromatograph equipped with a DC chromatography compartment, DP gradient pump, Dionex ERS-500 membrane suppressor operated in the autosuppression recycle mode, conductivity detector and an AS autosampler. Anion separation was performed on a Dionex IonPac AS25 column (4.0 x 250 mm) with the corresponding guard column (4.0 x 50 mm). The isocratic and gradient elution conditions, column temperature and eluent concentration for F⁻ and SO₄²⁻ analysis were optimized to minimize analysis time and to maximize resolution. The column temperature was set up to 30 °C and the NaOH eluent flow rate was of 1.0 mL/min. All the analytes were detected using suppressed conductivity detection at 30 °C and an injection volume of 50 µL. Separation of residual Cl⁻ from NP's synthesis and F⁻ was performed by gradient elution (Table C3). While an isocratic elution of 6 mM NaOH for 15 min was used for SO₄²⁻. elution (Table C3). While an isocratic elution of 6 mM NaOH for 15 min was used for SO₄²⁻.

5.4. Results and Discussion

5.4.1. Transformation of PFCAs and PFSA's in single solute DI water

The average reductive transformation of individual PFSA's and PFCAs in DI water are shown in Figure 5-1a and 5-1b, respectively, for 1-d and 5-d reaction times. In 1-d reactions, less

transformation was observed with decreasing alkyl chain length for both PFSA and PFCAs, whereas by 5 d, % loss was similar for all PFAAs. This is because there was additional loss of PFBS, PFHxS, PFBA and PFHxA between 1-d and 5-d reaction times whereas additional losses of PFOS and PFOA were not statistically different (Table C6). While for PFCAs and PFSAs with the same alkyl chain length, PFCAs had the higher transformation rate in a good agreement with those reported previously for electrochemical oxidation (Zhuo *et al.*, 2012) and sonochemical decomposition (Campbell *et al.*, 2009). However, at 5 d no significant differences were observed among PFAAs with different carbon-chains or functional group. Given that the reaction happens at the surface and the shorter-chain PFAAs sorb less, sorption appears to be the rate-limiting step. For example, Zhao *et al.* (Zhao *et al.*, 2011) attributed the higher adsorption of long chain PFAAs to the extra -CF₂ units in their structure, which will increase their hydrophobicity increasing its adsorption to GAC. It was also noted that the final pH values after the reaction process at 1 or 5 d were lower than that of control solutions (Table C6).

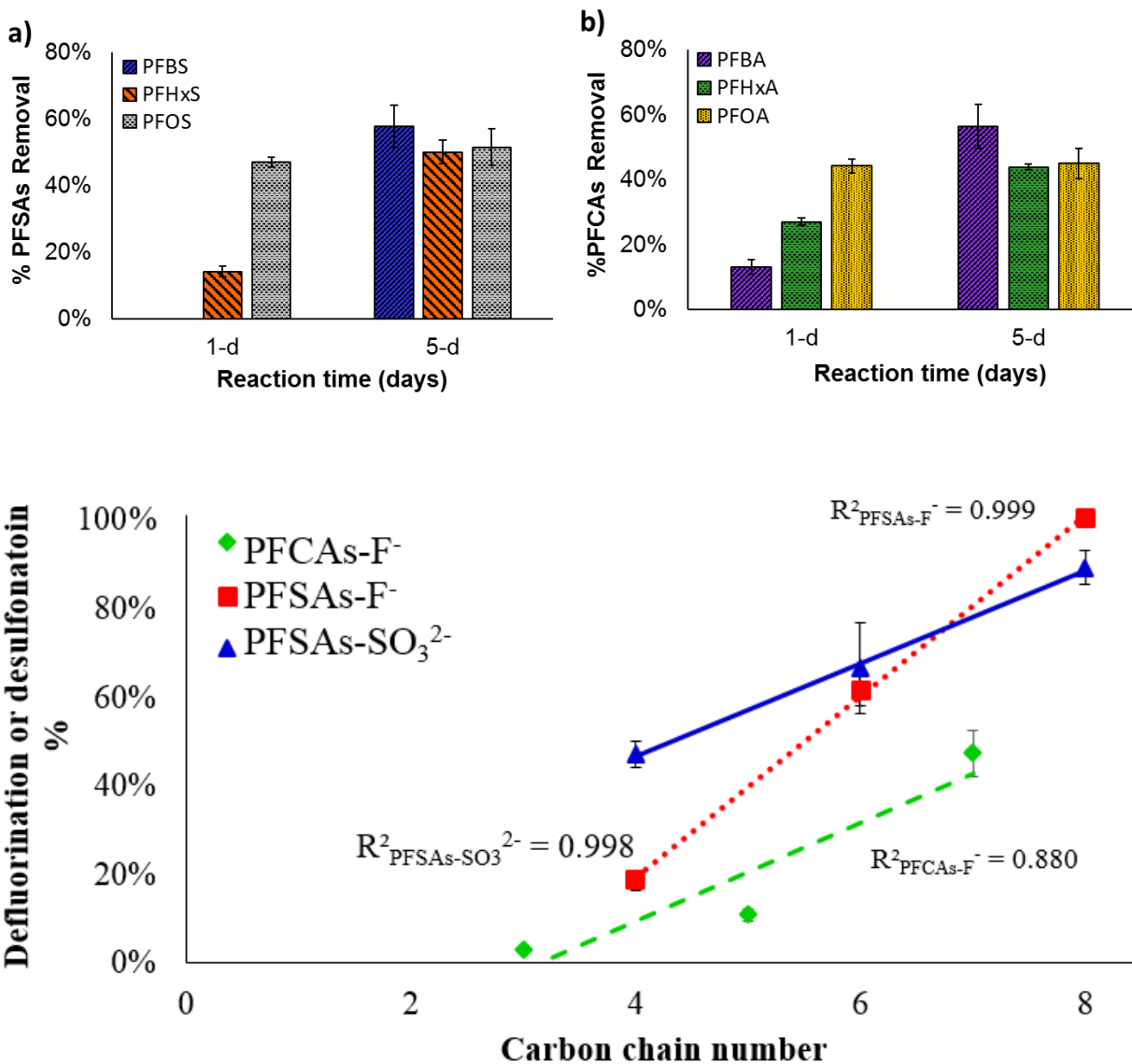


Figure 5-1. Transformation of a) PFSA and b) PFCAs at 1-d and 5-d of reaction, and c) generation of inorganic products F⁻ and/or SO₃²⁻ (quantified as SO₄²⁻) after 5-d. Average and standard deviation (bars) of three replicates.

5.4.1.1. PFCAs and PFSA inorganic byproducts

Recovery of inorganic products (F⁻ and SO₄²⁻) and subsequent trends from the reduction of individual PFAAs are summarized in Figure 5-1c and Table C4. The % defluorination and % desulfonation was calculated by the moles of F⁻ or SO₃²⁻ produced relative to the moles of fluorine per mole of PFAA transformed (e.g., CF₃(CF₂)_n-X has 3+2n fluorine atoms that can

become fluoride as $\text{CF}_3(\text{CF}_2)_n\text{-X}$ is transformed). Defluorination % and desulfonation % increased with increasing alkyl chain length and for a given chain length, greater defluorination occurs for the PFSA's. The lower defluorination observed for PFBS and PFBA may suggest that the CF_2 unzipping cycle is harder to occur for the shorter fluorocarbon chains.

5.4.1.2. Organic transformation products from PFAA reduction

In addition to F^- and SO_3^{2-} generation, several organic degradation products were identified using QToF ESI-MS. PFSA's and PFCAs products are summarized in Tables 5-1 and 5-2, respectively, and their MS/MS fragmentation reported in Tables C7 and C8, respectively.

Degradation products from PFOS decomposition was detailed in chapters 3 & 4. In brief, single and double bond polyfluoroalkyl sulfonates and single bond perfluoroalkyl carboxylates with 4 to 8 carbons; and fluorinated alkanes with 8 carbons were the main degradation products detected. Similar to PFOS, polyfluoroalkyl sulfonates and perfluoroalkyl carboxylates with only single bonds were the main degradation products for PFHxS and PFBS. A set of 3 peaks at m/z 380.95, 330.95, and 280.95 for PFHxS and 1 peak at m/z 280.95 for PFBS were assigned to polyfluoroalkyl sulfonates, explicitly, $[\text{C}_n\text{HF}_{2n}\text{SO}_3]^-$ ($n = 4 - 6$ for PFHxS and $n = 4$ for PFBS). PFHxA and PFBA were detected in the reduction of PFHxS and PFBA from PFBS decomposition.

Per & polyfluoroalkyl carboxylates and alcohols with single and double bonds were identified for PFCAs. A stepwise defluorination was observed with formation of polyfluoroalkyl carboxylates reflecting the loss of up to 12 fluorine atoms for PFOA and 4 for PFHxA. Short chain perfluorocarboxylic acids were detected, forming PFHpA, PFHxA and PFBA from PFOA degradation; and PFPeA and PFBA from PFHxA degradation. However, the concentration of shorter-chain products was too low to be quantified probably likely due to their fast

decomposition and higher limits of detection. No per- or polyfluoroalkyl carboxylates were generated on PFBA reactions. Additionally, a series of peaks at m/z 346.97, 296.98, 246.98, 196.98, and 146.99 were assigned to perfluoroalkyl alcohols with double bond, namely, $[C_nF_{2n-1}O]^-$ resulting from dissociation of CF_2 in a stepwise manner. For PFOA, PFHxA and PFBA the n range goes from [3 – 7], [4 – 6], and [3], respectively. Only one polyfluoroalkyl alcohol with double bond was detected for PFOA with m/z 328.98 assigned to polyfluoroheptanol $[C_7HF_{12}O]^-$. Extra peaks were observed at m/z 284.98 from PFHxA degradation, and 184.98 from PFBA degradation, which were assigned to perfluoropentanol $[C_5F_{11}O]^-$ and perfluoropropanol $[C_3F_7O]^-$, respectively.

Mass balances for fluorine and sulfonate (Table 5-3) were calculated based on quantified PFOS (17 F^- and 1 SO_3^{2-}), F^- and SO_3^{2-} concentration relative to the initial PFOS. Fluorine atoms in the organic products generated during reaction were not included due to the lack of standards and LOQ. The imbalance mass balances for F and SO_3^{2-} are associate to the unquantifiable or undetectable fluorinated products or loss of partially defluorinated or desulfonated species to the gas phase. As reported in Table C5, the final pH after 5 d of reaction decreased to 3.03 and 3.17 for PFBA and PFHxA, respectively, which is below the pK_a value for HF ($pK_{a_HF} = 3.2$). Thus, the low concentration of F in the C4 and C6 PFCAs may be due to volatilization of HF.

Table 5-1. Products detected after individual 6 μM solutions of PFBS and PFHxS reacted with nNiFe⁰-AC at 60 °C for 1 d or 5 d. Degradation products were detected using Q-ToF ESI. All samples were concentrated 3 times to increase product detection.

PFSA s	Molecular Formula	Theoretical m/z	Observed m/z	Error (ppm)	RT (min)
PFBS (C ₄ F ₉ SO ₃ ⁻ : m/z 298.9416) RT = 7.68 min	Polyfluoroalkyl sulfonate with single bond				
	C ₄ HF ₈ SO ₃ ⁻	280.9519	280.9521	0.80	6.83
	Perfluorobutane sulfonate with single bond				
	C ₄ F ₇ O ₂ ⁻	212.9787	212.9789	1.12	6.45
PFHxS (C ₆ F ₁₃ SO ₃ ⁻ : m/z 398.9373) RT = 9.48 min	Polyfluoroalkyl sulfonate with single bond				
	C ₆ HF ₁₂ SO ₃ ⁻	380.9455	380.9450	1.25	9.16
	C ₅ HF ₁₀ SO ₃ ⁻	330.9487	330.9487	0.08	7.90
	C ₄ HF ₈ SO ₃ ⁻	280.9519	280.9534	5.46	7.43
	Perfluoroalkyl carboxylate with single bond				
	C ₆ F ₁₁ O ₂ ⁻	312.9723	312.9730	2.35	8.43
	C ₄ F ₇ O ₂ ⁻	212.9787	212.9788	0.70	6.42

Table 5-2. Products detected after individual 6 μM solutions of PFBA, PFHxA, PFOA reacted with nNiFe⁰-AC at 60 °C for 1 d or 5 d. Degradation products were detected using Q-ToF ESI. All samples were concentrated 3 times to increase product detection.

PFCAs	Molecular Formula	Theoretical m/z	Observed m/z	Error (ppm)	RT (min)
PFBA (C ₄ F ₇ O ₂ ⁻ : m/z 212.9787) RT = 6.45 min	Perfluoropropanol with single bond				
	C ₃ F ₇ O ⁻	184.9837	184.9840	1.43	6.45
	Perfluoropropanol with double bond				
	C ₃ F ₅ O ⁻	146.9869	146.9870	0.48	6.45
PFHxA (C ₆ F ₁₁ O ₂ ⁻ : m/z 312.9723) RT = 8.45 min	Perfluoropentanol with single bond				
	C ₅ F ₁₁ O ⁻	284.9773	284.9774	0.18	8.42
	Perfluoroalkyl alcohol with double bond				
	C ₆ F ₁₁ O ⁻	296.9773	296.9767	2.18	8.42
	C ₅ F ₉ O ⁻	246.9805	246.9808	1.05	8.42
	C ₄ F ₇ O ⁻	196.9837	196.9841	1.85	7.56
	Perfluoroalkyl carboxylate with single bond				
	C ₅ F ₉ O ₂ ⁻	262.9755	262.9758	1.30	7.55
	C ₄ F ₇ O ₂ ⁻	212.9787	212.9786	0.24	6.44
	Polyfluoroalkyl carboxylate with single bond				
	C ₆ H ₄ F ₇ O ₂ ⁻	241.0100	241.0095	1.87	8.27
PFOA (C ₈ F ₁₅ O ₂ ⁻ : m/z 412.9659) RT = 10.22 min	Perfluoroalkyl carboxylate with single bond				
	C ₇ F ₁₃ O ₂ ⁻	362.9691	362.9696	1.46	9.35
	C ₆ F ₁₁ O ₂ ⁻	312.9723	312.9708	4.67	8.46
	C ₄ F ₇ O ₂ ⁻	212.9787	212.9791	2.11	6.45
	Perfluoroalkyl alcohol with double bond				
	C ₇ F ₁₃ O ⁻	346.9742	346.9750	2.44	9.36
	C ₆ F ₁₁ O ⁻	296.9773	296.9779	1.86	8.45
	C ₄ F ₇ O ⁻	196.9837	196.9845	3.88	7.58
	C ₃ F ₅ O ⁻	146.9869	146.9874	3.20	6.47
	Polyfluoroalkyl carboxylates with single bond				
	C ₈ HF ₁₄ O ₂ ⁻	394.9753	394.9761	2.03	9.88
	C ₈ H ₂ F ₁₃ O ₂ ⁻	376.9847	376.9853	1.54	9.55
	C ₈ H ₃ F ₁₂ O ₂ ⁻	358.9941	358.9945	1.00	9.32
	C ₈ H ₄ F ₁₁ O ₂ ⁻	341.0036	341.0036	0.11	8.69

Table 5-2. continued

PFCAs	Molecular Formula	Theoretical m/z	Observed m/z	Error (ppm)	RT (min)
PFOA (C ₈ F ₁₅ O ₂ ⁻ : m/z 412.9659) RT = 10.22 min	Polyfluoroalkyl carboxylates with single bond				
	C ₈ H ₅ F ₁₀ O ₂ ⁻	323.0130	323.0137	2.21	8.42
	C ₈ H ₆ F ₉ O ₂ ⁻	305.0224	305.0225	0.30	7.98
	C ₈ H ₇ F ₈ O ₂ ⁻	287.0318	287.0317	0.45	7.78
	C ₈ H ₈ F ₇ O ₂ ⁻	269.0413	269.0415	0.93	7.74
	C ₈ H ₉ F ₆ O ₂ ⁻	251.0507	251.0514	2.90	7.70
	C ₈ H ₁₁ F ₄ O ₂ ⁻	215.0695	215.0698	1.32	7.47
	C ₈ H ₁₂ F ₃ O ₂ ⁻	197.0789	197.0791	0.82	7.45
	C ₇ HF ₁₂ O ₂ ⁻	344.9785	344.9801	4.66	7.36
	C ₆ HF ₁₀ O ₂ ⁻	294.9817	294.9808	3.00	7.36
	Polyfluoroheptanol with double bond				
	C ₇ HF ₁₂ O ⁻	328.9836	328.9829	2.05	8.99

Table 5-3. F and SO₃²⁻ mass balance from 5-d reactions with PFCAs (PFBA, PFHxA, and PFOA) and PFSAs (PFBS and PFHxS). All experiments were performed using DI water.

*PFOS data reported in chapter 4 was used for comparison.

PFAAs	Remaining PFAAs	F ⁻	SO ₄ ²⁻	Total F content (%)	Total SO ₄ ²⁻ content (%)
PFBA	43.7%	4.0%	-	47.7%	-
PFHxA	55.8%	7.4%	-	63.2%	-
PFOA	67.0%	24.1%	-	91.2%	-
PFBS	46.3%	20.3%	45.2%	66.6%	91.5%
PFHxS	34.6%	40.4%	29.6%	74.9%	64.2%
*PFOS	42.0%	57.6%	57.2%	100.0%	99.2%

5.4.1.3. Proposed degradation pathways

Reductive pathways are proposed for PFOA as a representative of the PFCAs and for PFHxS as a representative of the PFSA's since a proposed PFOS pathway was detailed previously in chapter 4. PFHxA, PFBA, and PFBS pathways follow a similar pattern to their longer-chain analogues. The proposed pathways in the sequential reductive defluorination of PFOA is shown in Figure 5-2 according to the byproduct analysis. PFOA can be degraded gradually following two main pathways. The first pathway occurs through a stepwise reductive defluorination mechanism, starting with the loss of one fluorine atom to form $C_8HF_{14}O_2^-$ with sequential F/H replacement ending to $C_8H_{12}F_3O_2^-$. The second pathway was previously detailed by several authors (Chen & Zhang, 2006; Chen *et al.*, 2006; Hori *et al.*, 2004; Moriwaki *et al.*, 2005; Trautmann *et al.*, 2015) for other types of destructive technologies (UV-activated persulfate, UV/TiO₂, UV/H₂O₂, sonolysis, and electrochemical oxidation). This pathway consists of the cleavage of the C-C bond between C₇F₁₅ and COOH and the addition of OH following by the loss of CF₂ on a step-by-step basis to form short-chain PFCAs and alcohols. Briefly, an unstable perfluoroalkyl radical (C₇F₁₅•) is formed after the cleavage of the CO₂ group. Then, the perfluoroalkyl radical reacts with OH to form perfluoroalkyl alcohol, explicitly, C₇F₁₅OH. The unstable perfluoroalkyl alcohol undergoes HF elimination forming C₆F₁₃COF and then hydrolyzed to form PFHpA and F⁻. PFHpA further degrades to produce PFCA with one less CF₂ unit (PFHxA). Following the same process, PFBA was formed. A side degradation pathway was also found from the formation of the perfluoroalkyl alcohols. For example, C₇F₁₅OH is converted to C₇F₁₃OH due to the repetitive cleavage of a C-F bond and the addition of an H atom in a twostep process. Finally, a series of 4 perfluoroalkyl alcohols with double bonds including [C₇F₁₃O]⁻, [C₆F₁₁O]⁻, [C₄F₇O]⁻, and [C₃F₅O]⁻ were formed during PFOA degradation.

A proposed PFH_xS pathway is presented in figure 5-3. PFH_xS decomposes forming polyfluoroalkyl sulfonates and perfluoroalkyl carboxylates with shorter-carbon chains similar to what was observed for PFOS. The reaction may be started with the formation of the perfluoroalkyl radical, C₆F₁₂SO₃• after a F atom is released. The perfluoroalkyl radical can react directly with H radicals forming the polyfluorohexane sulfonate (C₆HF₁₂SO₃⁻). Then the formation of shorter chain polyfluoroalkyl sulfonates occurs when the C-C bond at the terminal end is broken releasing the CF₂H fragment and replace it by another H+ resulting in the polyfluoropentane sulfonate (C₅HF₁₀SO₃⁻). Following the same process, C₄HF₈SO₃⁻ is formed.

A second pathway leads to formation of PFCAs (C3 and C5 PFCAs) with the cleavage of the C-S bond and addition of OH forming C₆F₁₃OH. As described previously for PFOS in chapter 4, the C₆F₁₃OH alcohol undergoes HF elimination to form C₅F₁₂COF and then hydrolyzed to give PFH_xA. PFH_xA is then decomposed forming short-chain PFCAs by stepwise removal of CF₂ such as PFBA.

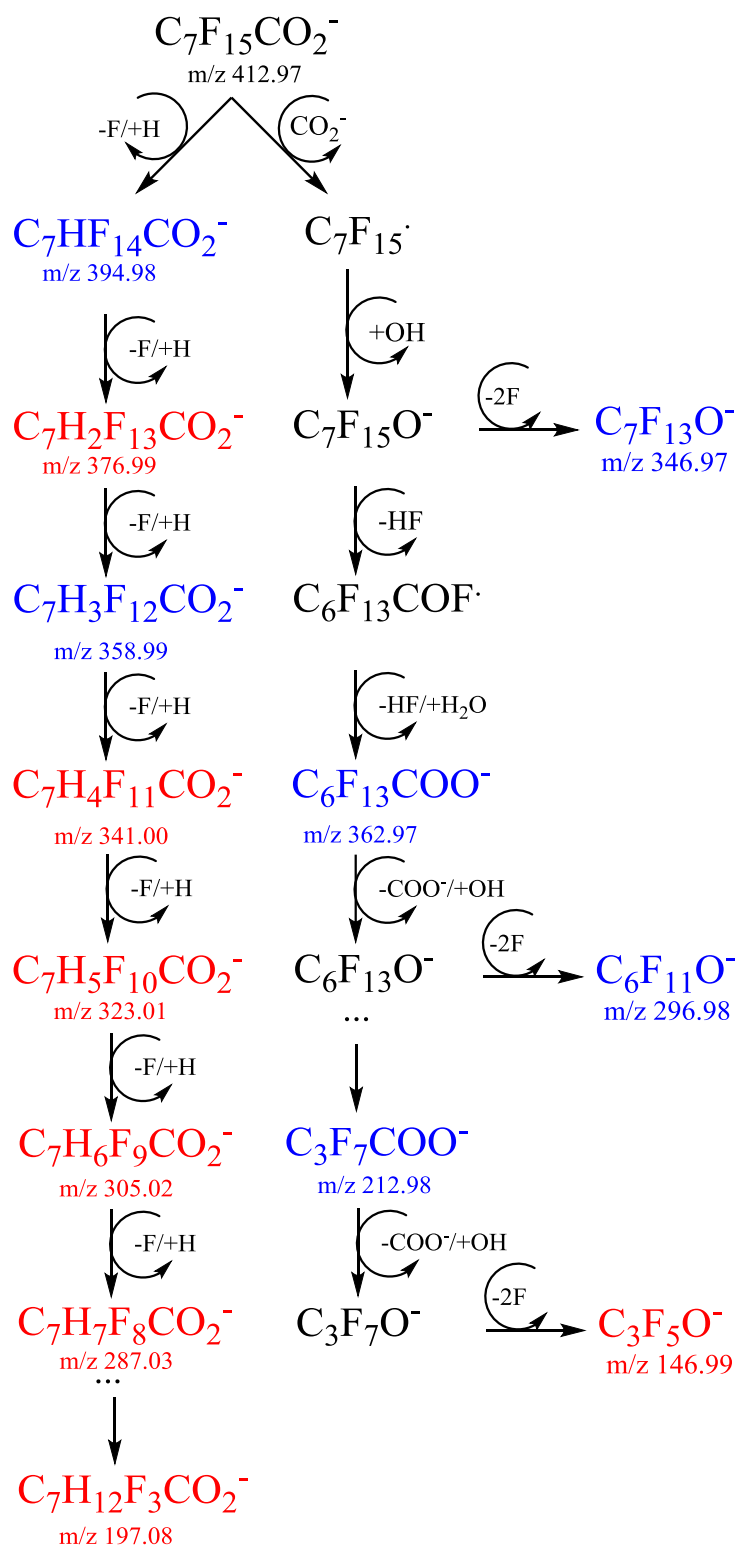


Figure 5-2. PFOA degradation pathway. Formulas colored with blue were confirmed with mass accuracy and fragmentation and red only with mass accuracy.

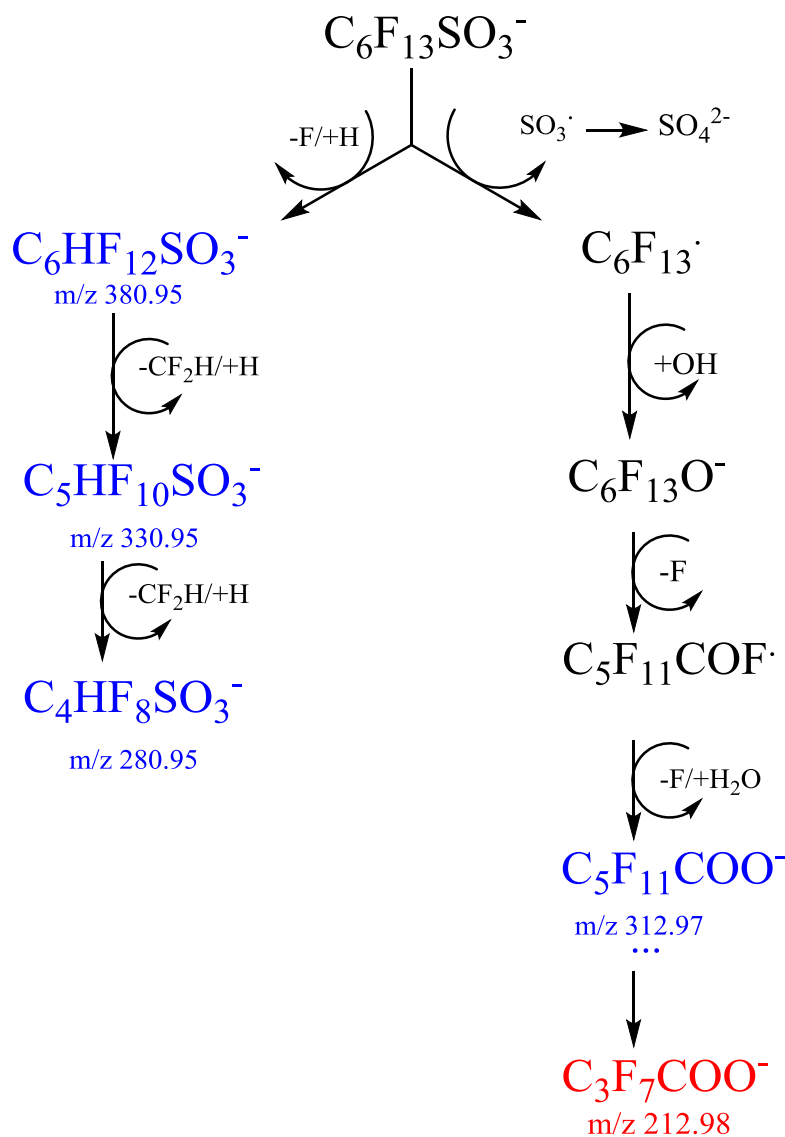


Figure 5-3. PFHxS degradation pathway. Formulas colored with blue were confirmed with mass accuracy and fragmentation and red only with mass accuracy.

5.4.2. Transformation of PFAAs in a PFAA-contaminated groundwater

$nNiFe^0$ -AC was able to transform PFAAs in the groundwater samples from the former fire-training area in Massachusetts, but overall, the % transformation for a given PFAA was generally lower than what was observed in single PFAA DI water solutions. The % removed for all the PFAAs quantified are summarize in Figure 5-4 and Table C4. Initial PFAAs concentration

vary from 0.20 to 38 nM with PFOS having the highest concentration (Table 5-4a), well below the concentration used in the single solute studies of 6 μM . In a pseudo-first order reaction, lower initial concentration will result in a lower overall reaction rate. Several anions (Cl^- , Br^- , SO_4^{2-} , and NO_3^-) and cations (K^+ , Na^+ , Mg^{2+} , and Ca^{2+}) were quantified with concentrations ranging from 0.92 to 341 μM (Table 5-4b) that may have inhibited the reactions. There may also have been some dissolved organic matter in the groundwater samples that coated the particles or competed for electrons; organic matter was not made measured for this groundwater sample.

The PFAAs quantifiable include six PFCAs: PFBA, PFPeA, PFHxA, PFHpA, PFOA, and perfluorononanoic acid (PFNA, $\text{C}_9\text{F}_{17}\text{O}_2^-$); five PFSAs: PFBS, perfluoropentanesulfonate (PFPeS, $\text{C}_5\text{F}_{11}\text{SO}_3^-$), PFHxS, perfluoroheptanesulfonate (PFHpS, $\text{C}_7\text{F}_{15}\text{SO}_3^-$), and PFOS; and two PFAAs precursors: 6:2 and 8:2 fluorotelomer sulfonates (6:2 FtS, $\text{C}_8\text{H}_4\text{F}_{13}\text{SO}_3^-$ and 8:2 FtS, $\text{C}_{10}\text{H}_4\text{F}_{17}\text{SO}_3^-$). For the groundwater sample, except for one anomaly with PFBA, PFAA transformation was less than observed in the single PFAA DI water systems (Figure 5-5). Cheng *et al.* 2009 also saw reduced effectiveness in sonochemical degradation of PFAAs in groundwater from near a landfill compared to DI water. The increase of concentration of three PFCAs (PFNA, PFOA, and PFHxA) suggest that PFCAs are produced during the reductive treatment. Fluorotelomer precursors commonly degrade to PFCAs rather than PFSAs (Carrillo-Abad *et al.*, 2018; Shaw *et al.*, 2019; Urtiaga *et al.*, 2018). Harding-Marjanovic *et al.* (Harding-Marjanovic *et al.*, 2015) found that 8:2 FtS can be transformed producing PFOA, PFHpA, and PFHxA, while 6:2 FtS degradation generate PFHxA, PFPeA, and PFBA. The increased concentration of PFNA points to the present of other precursors not measured in this study. The intermediates/products recovered were among those identified in the batch studies previously (e.g., $\text{C}_5\text{F}_{11}\text{SO}_3^-$).

Table 5-4. a) Initial PFAS concentration and b) ions measured in the groundwater sample. Ions data was provided from Barber et al. and Weber et al. (Barber *et al.*, 2017; Weber *et al.*, 2017).

a)	PFAs	nM	b)	Ions	μM
	PFBA	0.58		Chloride	174.42
	PFPeA	1.34		Bromide	0.92
	PFHxA	3.47		Sulfate	147.76
	PFHpA	1.43		Nitrate	83.44
	PFOA	2.68		Potassium	31.86
	PFNA	0.20		Sodium	341.37
	PFBS	1.20		Magnesium	86.40
	PFPeS	3.64		Calcium	62.44
	PFHxS	13.95			
	PFHpS	0.23			
	PFOS	38.08			
	6:2 FtS	0.99			
	8:2 FtS	3.77			

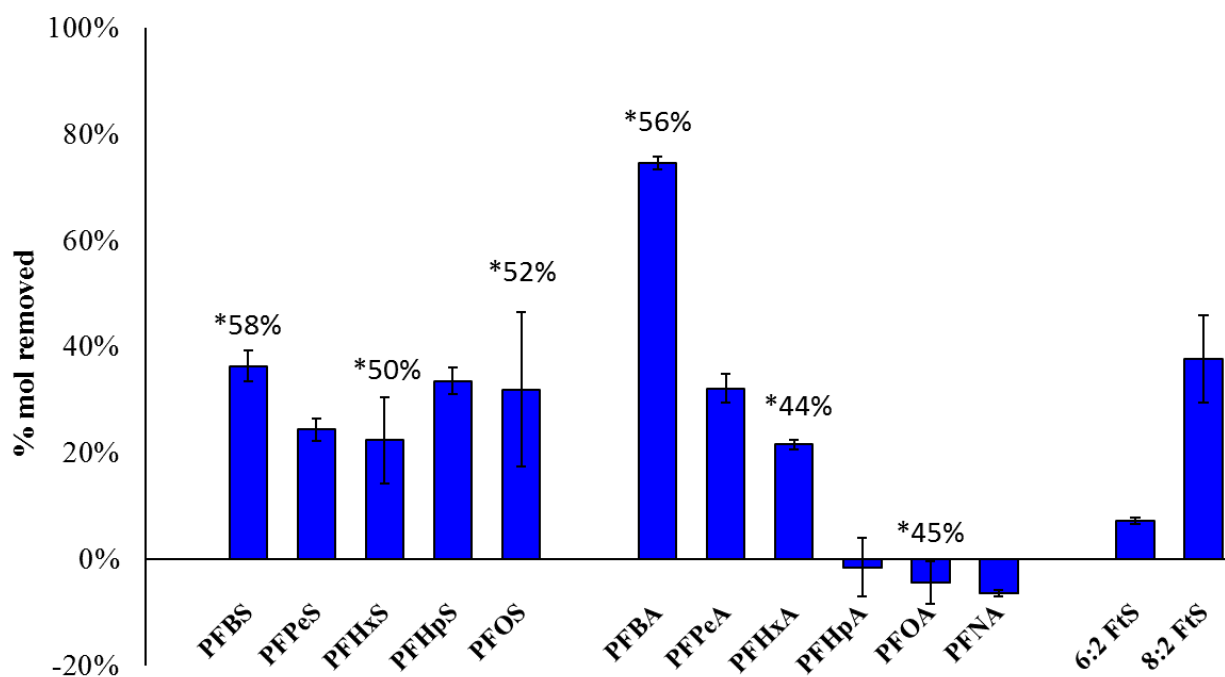


Figure 5-4. PFASs and PFCAs degradation using contaminated groundwater sampled from a former fire training area in Massachusetts. Reaction time: 5-d.

*% mol removed in controlled studies with single solute in Milli-Q water for comparison.

CHAPTER 6. CONCLUSIONS AND FUTURE WORK

6.1. Conclusion

Perfluoroalkyl acids (PFAAs) are a group of synthetic chemicals resistant to typical environmental degradation processes. Their chemical and physical properties vary depending on the length of their fluorinated alkyl tail and the functional group of their head. They are the active ingredient of aqueous film-forming foam (AFFF), the main source of PFAS contamination in groundwater. PFAAs accumulation, particularly in groundwater, is of increasing environmental concern. Long-chain PFAAs such as PFOS, PFHxS and PFOA and their short-chain analogues PFBA and PFBS are the most studied PFAAs due to their potential toxicity, mobility, and bioaccumulation. PFAAs have not been shown to be biodegradable, in fact they can be generated from microbial degradation of PFAAs precursors such as fluorotelomer sulfonates. Thus abiotic processes was the focus of this PhD study. A reductive treatment to transform PFOS targeting the linear PFOS isomer as a representative PFAA and identified as the most stable was then proposed. Differences on degradation rates due to their carbon-chain length and functional groups were also investigated as well as the effects of groundwater constituents. Batch experiments were carried out using Milli-Q water and PFAS contaminated groundwater to test the degree of degradation using nanoparticles (NPs) of nickel as a catalyst in the presence of iron as the reducing agent, both supported in activated carbon ($n\text{NiFe}^0\text{-AC}$). Effectiveness of $n\text{NiFe}^0\text{-AC}$ NPs was assessed by quantifying PFOS loss in both solution and solid phase extracts and generation of inorganic and organic byproducts. Different approaches to enhance NPs reactivity like heat, addition of bimetal catalyst, and a carbon material as a support to increase surface area were evaluated. The $n\text{NiFe}^0\text{-AC}$ (2 wt% Ni) particles synthesized for 3 h resulted in

the greatest loss of PFOS. Transformation of both L- and Br- isomers were observed over time with ~50% total PFOS transformed within 5 d and at 60 °C. PFOS degradation is correlated to the decrease of pH and the increase of ORP. The main intermediates during the degradation of PFOS were F⁻ and SO₄²⁻. Also, several poly/per-fluorinated products with single and double-bonds were identified using quadrupole time-of-flight mass spectrometry (QToF-MS) with ESI⁻ or APCI as the ionization method and MS/MS fragmentation confirmation. Experiments using total PFOS and only L-PFOS isomers reveal that double-bond byproducts are forming only from Br-PFOS degradation while single-bond intermediates are generated from the degradation of L- and Br- PFOS isomers. The main pathways of PFOS degradation is its defluorination and desulfonation via electron transfer mechanism from the electron-rich nanocomposite.

Effects of carbon-chain length and functional group on PFCAs and PFSAs degradation was evaluated. Degradation magnitude at a 1-d reaction time showed chain-length dependence with more degraded for PFAAs with the longer alkyl chain and for a given chain length, degradation was greater for PFCAs compared to PFSAs. However, after reacting for 5 d, no significant differences were observed with alkyl chain length or functional group. For longer-chain PFAAs, reactions plateaued by 1 d while the short-chain PFAAs continued to degrade, which was attributed to the extra time needed to sorb prior to degradation. Numerous organic metabolites were detected including per- & polyfluoroalkyl carboxylates and alcohols with single and double bonds for PFCAs, and polyfluoroalkyl sulfonates and perfluoroalkyl carboxylates with single bonds for PFSAs.

PFAA degradation in PFAS-contaminated groundwater was generally lower than observed in single-solute Milli-Q water, which may be as a result of inorganic ion competition of the released electrons and/or hydrogen atoms or more rapid formation of a passivation layer on

the NP's surface. PFOA and PFHpA concentrations increased above their initial concentrations, which is likely due to their generation in the degradation of PFOS as observed in chapter 4 with PFOS degradation in DI water with nNiFe⁰-AC. However, the increase of PFNA may suggest degradation of the PFAAs precursors 6:2 FtS and 8:2 FtS and/or the presence of other precursors not measured in this study. Detection of the same byproducts identified in the single-solute experiments, such as C₅F₁₁SO₃⁻ and C₆F₁₁O₂⁻, supports that nNiFe⁰-AC at 60 °C is able to degrade PFAAs in groundwater containing a complex inorganic matrix.

6.2. Future work

The results of this work provide insight into a potential NiFe⁰-AC for both in-situ and ex-situ treatment of PFAS-contaminated groundwater and offer a starting point for further optimization of a nNiFe⁰-AC treatment system. There are numerous aspects from mechanism to feasibility that warrant further studies of which some are exemplified below.

Material/heterogenous catalyst development:

- (1) Evaluate the of nanocomposite concentration on PFAA degradation. Increasing the mass of nanocomposite increases the rate and magnitude of the reaction if the limitation is surface area or available reactive surface sites.
- (2) The biggest limitation of metallic nanoparticles is the aggregation of the nanoparticles forming bulk metals. In order to increase their catalytic activity, supported materials are commonly used. In this Ph.D. study, activated carbon was used as the support material due to their large surface area. Other materials including carbonaceous (graphene or carbon nanotube) and porous materials (zeolite) could be tested to see if they lead to increased access to reactive surfaces. However, the additional cost may not be warranted unless reactivity and particle longevity are substantially improved.

Transformation mechanisms and particle regeneration:

- (3) The batch studies presented in this research were targeted at assessing the potential for nNiFe⁰-AC to transform PFAAs and not designed to clarify the reaction mechanisms, which can aid in development of the current or future technologies. For example, clarifying the role of Fe in the reaction; is it serving to shuttle electrons or generate H₂ gas? The latter can be tested by purging with H₂ gas in a Fe-free Ni-AC system.
- (4) Temperature effects should be further evaluated given that only 2 temperatures were tested in the current work. Is 60 °C required to initiate the reaction or can a lower temperature or does that just increase reaction rates? Can a temperature between the 22 °C and 60 °C yield similar results, which would lead to lower energy costs when implemented in the field?
- (5) Future work should be done in steady-state flow column systems under different flow conditions (residence times) to simulate permeable reactive barriers (PRBs) which will offer insight into the mass load that can be captured and transformed by the nNiFe⁰-AC and clarify if the plateau effect observed in batch systems was a poisoning effect due to the closed system.
- (6) Future work should evaluate the shelf life of the nanocomposite and possible regeneration approaches to reactivate aged particles and if this process can be done on-situ.

Treatment train/simulation of field conditions

- (7) The PFAS contaminated groundwater samples used for this research provided a snapshot of the potential for field application. Because of this, it is unclear which constituent (anions, cations, PFAAs precursors or other co-contaminants) will significantly impact the transformation rates and magnitudes by nNiFe⁰-AC. Conducting additional studies

where individual constituents are controlled (PFFA mix vs single in deionized water; single PFAA with or without specific ions, etc.) as well as probe other types of PFAA-contaminated groundwater.

- (8) Future work should also investigate the reduction of precursors under controlled conditions and identification of their degradation products after reaction with $n\text{NiFe}^0\text{-AC}$. Precursors are commonly detected in AFFF-impacted groundwater and soils and it is imperative to understand their transformation pathway.
- (9) Evaluate potential for reductive/oxidative treatment trains. Considering that several defluorinated intermediates/products were generated in the reductive reaction between PFAAs and $n\text{NiFe}^0\text{-AC}$ NPs, coupling reductive processes with oxidation treatments such as heat activated persulfate should be investigated. Partial defluorinated products are molecules containing C-H bonds that are more susceptible to attack by strong oxidants (e.g., oxidation of 6:2 FtS by heat-activated persulfate).

Overall, this reductive treatment approach has potential for use in ex-situ and in-situ applications. The main advantage $n\text{NiFe}^0\text{-AC}$ N is the complete removal of PFAAs and the extractability of the PFAAs from the nanocomposite. Another advantage of this treatment is that PFAA transformation does not appear to be pH-dependent although reactions tested were limited to unadjusted and unbuffered pH solutions. $n\text{NiFe}^0\text{-AC}$ was able to mineralize PFAAs. The materials used for nanoparticle synthesis have low toxicity and are inexpensive increasing their potential for in-situ applications. However, particles aggregation, catalyst poisoning, passivation and competition with reactive sites on the nanoparticle surface could limit its application, and requires additional research.

**APPENDIX A. SUPPORTING INFORMATION: EVIDENCE OF REDUCTIVE
TRANSFORMATION OF PERFLUOROOCTANE SULFONATE BY NIFE⁰
NANOPARTICLES SYNTHESIZED ONTO ACTIVATED CARBON**

Organic Product Detection and Identification

Products in the headspace

Identification of desulfonated products

Tables

Table A1. Agilent 6460 Triple-Quad LC/MS source parameters

Table A2. MS/MS conditions for PFOS and M8PFOS quantification

Table A3. QToF and MS/MS source parameters

Table A4. SWATH parameters

Table A5. APCI optimized parameters

Table A6. Identification of single bond products

Table A7. Identification of double bond products

Table A8. Identification of desulfonated products

Figures

Figure A1. HPLC/MS/MS chromatogram of linear and branched PFOS.

Figure A2. XPS spectra of F 1s and S 2p3 for PFOS powder and 1-h SST nNiFe⁰-AC reacted with PFOS before and after extractions.

Figure A3. TEM images of 1-h SST nNiFe⁰-AC

Figure A4. SEM images and size distribution histograms for nNiFe⁰-AC prepared with 1-h SST, 2-h SST, and 3-h SST

Figure A5 Ion chromatograms for 1-h and 3-h SST reactions

Figure A6. Identification process for PFOS transformation products

Figure A7. Fragmentation pattern of the 434.96 in APCI negative mode

Organic Product Detection and Identification

Products in the headspace

Volatile organic products were expected after the cleavage of the sulfonate group. To capture the headspace, two approaches were used for volatile product capture from 60-mL crimped bottles with butyl rubber stoppers: direct injection of headspace and extraction of volatile products on a C₁₈ cartridge. For direct injection, 10 mL of headspace in samples reacted with PFOS and in the matrix and PFOS stock controls were injected manually into a Shimadzu 17A gas chromatography (GC) system with an electron capture detection (ECD). High production of H₂ gas inside each bottles (40-60 mL) resulted in variability between injections (data not shown). For the C₁₈ cartridge approach, headspace was pulled with a 100-mL gastight syringe and passed through a 600 mg C₁₈ dry solid phase extraction (SPE) cartridges followed by elution with 5 mL of MeOH, and injection into the LC-QToF in positive and negative modes. The high pressure generated inside the bottles where PFOS was reacted with the nNiFe⁰-AC particles caused syringe plunger to move when the 100-mL gastight syringe was inserted into the septa after the 5-d reaction. The gas generated was variable, but on average, the plunger moved to the 40-60 mL mark after which an additional 10 mL was manually drawn up prior to passing through the C₁₈ cartridge. Several unidentified peaks were detected in headspace samples particularly in positive mode. However, their search and identification has been challenging due to the likelihood of the formation of adducts, complexes or reaction in the ESI source.

Identification of desulfonated products

A perfluorooctane (C₈F₁₈) standard was used to identify desulfonated products. A 2310 ppm C₈F₁₈ solution dissolved in methanol was injected directly into the APCI probe of the source

at 50 $\mu\text{L}/\text{min}$ via a syringe to determine the main ions in positive and negative modes using different parameters. The final parameters given in Table A5 were optimized for the ion 434.97 in negative mode. The positive mode was less sensitive and did not provide m/z allowing straightforward identification of C_8F_{18} , therefore only negative mode was selected. Different mobile phases, including 0.15% acetic acid in water and 20 mM of ammonium acetate in methanol, were tested in addition to the flowing solution in methanol. For the same flow rate, 0.15% acetic acid in water provided the highest sensitivity for the main ion of C_8F_{18} in negative mode, and the minimum flow rate was ideal (0.05 ml/min was selected). The highest peaks detected were m/z 434.9707 ($[\text{C}_8\text{F}_{17}\text{O}]^-$ exact mass: 434.9683, 5.5 ppm error) and m/z 445.9760. After applying a collision energy, m/z 434.9707 fragmented into several daughter ions including $[\text{C}_6\text{F}_{13}]^-$, $[\text{C}_5\text{F}_{11}]^-$, $[\text{C}_4\text{F}_9]^-$, $[\text{C}_3\text{F}_7]^-$, and $[\text{C}_2\text{F}_5]^-$ (Table A8). The ion m/z 445.9760 fragmented into mainly $[\text{C}_4\text{F}_9\text{O}]^-$, C_3F_7^- , and CF_3O^- . The peaks present in the MS spectrum remained the same regardless of the APCI parameters tested, only intensities of the peaks were modified. The standard solution was also injected via the TurboIonSpray probe to compare with electrospray ionization. In negative ESI mode, m/z 445.9760 was detected, but not 434.9707. Because of the nature of the DuoSpray source containing both ESI and APCI probes, ESI ions may also be present when using the APCI probe. However, no APCI ions are present when using the TurboIonSpray probe since in this mode no current is applied to the Corona needle. Therefore, m/z 445.9760 is likely produced by ESI, while m/z 434.9707 is specifically an APCI produced ion. This was confirmed by using a “pure” APCI source connected to an ion trap low resolution. No matter the parameters or the ionization mode, C_8F_{18} was modified in the source, either by fragmentation, or by exchange of atoms. No adduct of the full molecule, nor $[\text{C}_8\text{F}_{18}]^-$, were observed. Perfluoroalkanes such as perfluorooctane are known not to be ionized by ESI and weakly ionized by APCI (Schutz *et al.*, 2015). A couple

studies (Marotta *et al.*, 2004; Schutz *et al.*, 2015) have looked into the reactivity of perfluoroalkanes in the APCI source, and they both found $[M+O-F]^-$ ions to be the main ions formed, which correspond to the main ion detected in our experiment (m/z 434.9707, $[C_8F_{17}O]^-$).

A stock solution of $C_8F_{17}Br$ was prepared in methanol and injected with the same APCI parameters optimized for $[C_8F_{18}]^-$, and the ion m/z 434.9672 ($[C_8F_{17}O]^-$, exact mass: 434.9683, 3.5 ppm error) was also detected. The only ions detected containing Br were at very low intensity: m/z 494.8869 ($[C_8F_{16}^{78}BrO]^-$ exact mass: 494.8883, 3 ppm error) and 496.8849 ($[C_8F_{16}^{80}BrO]^-$ exact mass: 496.8876, 5 ppm error), confirming that the exchange of Br for O in APCI is easier than the exchange of F with O. The ion at m/z 445.98 was not detected in the $C_8F_{17}Br$ solution (Figure A7). Extracted samples with 3-hSST and 5d reaction were injected in flow injection acquisition (FIA) mode into the APCI source with dependent MS-MS scans programmed with mass defect filtering. An additional peak was detected only in the 3-hSST sample with a m/z 431.9633, which exact mass and fragmentation correspond to $[C_8F_{16}O_2]^-$.

Table A1. Agilent 6460 Triple-Quad LC/MS source parameters for negative ion mode.

Parameter	values
Gas temperature (°C)	300
Gas flow (L/min)	11
Nebulizer gas (psi)	45
Capillary voltage (V)	3750

Table A2. MS/MS conditions for PFOS and M8PFOS (internal standard) quantification using an Agilent 6460 Triple-Quad LC/MS.

Parameter	PFOS	M8PFOS
Precursor Ion Mass	498.9 m/z	506.9 m/z
Product Ion Mass	80 m/z	80 m/z
	99 m/z	99 m/z
Fragmentor	210 V	205 V
Collision Energy	55 V	55 V
Cell Accelerator Voltage	2 V	2 V
Polarity	Negative	Negative

Table A3. Quadrupole time of flight (QToF) negative and positive electrospray ionization (ESI⁻ and ESI⁺, respectively) source parameters.

Parameter	QToF (ESI⁻)	QToF (ESI⁺)
Curtain gas (CUR)	25	25
Ion Source Gas 1 (GS1)	50	50
Ion Source Gas 2 (GS2)	60	60
IonSpray Voltage Floating (ISVF)	4500	5000
Temperature (TEM)	500	500
Collision energy (CE)	-60	60
Collision gas (CAD)	6	6
Collision energy spread (CES)	30	30
Declustering potential (DP)	-50	50
Ion release delay (IRD)	67	67
Ion release width (IRW)	25	25

Table A4. SWATH parameters used for unknown identification.

Experiment #	Mass range (m/z)	CE (eV)	Dwell time (ms)
1	100-175	30	50
2	174-225	30	50
3	224-275	30	50
4	274-320	30	50
5	319-345	30	50
6	344-375	30	50
7	374-420	30	50
8	419-445	30	50
9	444-475	30	50
10	474-520	30	50
11	519-545	30	50
12	544-594	30	50
13	593-643	30	50
14	642-795	30	50
15	794-845	30	50
16	844-1000	30	50
17	1000-1200	30	50

Table A5. Negative mode APCI (APCI⁻) optimized parameters for negative mode of C₈F₁₈ analysis.

Parameters	(APCI⁻)
Ion source gas 1 (GS1)	10
Ion source gas 2 (GS2)	50
Temperature (TEM)	500
IonSpray voltage floating (ISVF)	-4400
Collision energy (CE)	-22
Collision gas (CAD)	6
Ion release delay (IRD)	60
Ion release width (IRW)	23
Nebulizer current	-5

Table A6. Single bond defluorinated transformation products identified after nNiFe⁰-AC reacted with PFOS using accurate-mass identification. Precursor and daughter ions were identified by QToF. In column one, the number in parenthesis is the observed m/z of the precursor ions.

MS Precursor		MS/MS fragments									
C ₈ HF ₁₆ SO ₃ ⁻ (480.9388)	Theoretical mass	79.9568	98.9552	118.9920	129.9536	168.9888	179.9504	218.9856	229.9472	279.9440	329.9408
	Measured mass	79.9587	98.9558	118.9917	129.9539	168.9888	179.9491	218.9831	229.9468	279.9443	329.9359
	Error (ppm)	23.8417	6.1983	2.3734	2.0309	0.2341	7.2556	11.7582	1.8565	0.8912	15.0042
	Formula	SO ₃ ⁻	FSO ₃ ⁻	C ₂ F ₅ ⁻	CF ₂ SO ₃ ⁻	C ₃ F ₇ ⁻	C ₂ F ₄ SO ₃ ⁻	C ₄ F ₉ ⁻	C ₃ F ₆ SO ₃ ⁻	C ₄ F ₈ SO ₃ ⁻	C ₅ F ₁₀ SO ₃ ⁻
C ₈ H ₂ F ₁₅ SO ₃ ⁻ (462.9471)	Theoretical mass	68.9952	79.9568	98.9552	118.9920	229.9472	442.9423				
	Measured mass	68.9960	79.9573	98.9553	118.9906	229.9436	442.9431				
	Error (ppm)	11.9736	6.3335	0.3960	11.5236	15.7476	1.8188				
	Formula	CF ₃ ⁻	SO ₃ ⁻	FSO ₃ ⁻	C ₂ F ₅ ⁻	C ₃ F ₆ SO ₃ ⁻	C ₈ HF ₁₄ SO ₃ ⁻				
C ₈ H ₄ F ₁₃ SO ₃ ⁻ (426.9672)	Theoretical mass	79.9568	82.9603	98.9552	216.9888						
	Measured mass	79.9588	82.9605	98.9577	216.9885						
	Error (ppm)	24.8938	2.0324	24.8059	1.5193						
	Formula	SO ₃ ⁻	FSO ₂ ⁻	FSO ₃ ⁻	C ₄ H ₂ F ₅ SO ₂ ⁻						
C ₈ H ₆ F ₁₁ SO ₃ ⁻ (390.9856)	Theoretical mass	61.9968	68.9952	79.9568	98.9552	282.9981	370.9800				
	Measured mass	61.9971	68.9970	79.9584	98.9556	282.9962	370.9753				
	Error (ppm)	5.3115	25.2787	20.4232	4.2978	6.5473	12.7147				
	Formula	C ₂ F ₂ ⁻	CF ₃ ⁻	SO ₃ ⁻	FSO ₃ ⁻	C ₆ H ₂ F ₁₁ ⁻	C ₈ H ₅ F ₁₀ SO ₃ ⁻				

Table A6. continued

C ₈ H ₈ F ₉ SO ₃ ⁻ (355.0050)	Theoretical mass	79.9568	82.9603	98.9552	129.9536					
	Measured mass	79.9585	82.9599	98.9559	129.9534					
	Error (ppm)	21.0139	4.4055	7.3082	1.5255					
	Formula	SO ₃ ⁻	FSO ₂ ⁻	FSO ₃ ⁻	CF ₂ SO ₃ ⁻					
C ₆ HF ₁₂ SO ₃ ⁻ (380.9462)	Theoretical mass	61.9968	79.9568	98.9552	183.0045	130.9920	230.9862	280.9824	310.9430	360.9398
	Measured mass	61.9961	79.9582	98.9564	183.0053	130.9932	230.9875	280.9829	310.9402	360.9364
	Error (ppm)	11.3809	17.2968	11.6566	4.7996	9.0540	5.6280	1.7277	9.0049	-9.4199
	Formula	C ₂ F ₂ ⁻	SO ₃ ⁻	FSO ₃ ⁻	C ₄ H ₂ F ₇ ⁻	C ₃ F ₅ ⁻	C ₅ F ₉ ⁻	C ₆ F ₁₁ ⁻	C ₅ F ₉ SO ₃ ⁻	C ₆ F ₁₁ SO ₃ ⁻
C ₇ HF ₁₄ SO ₃ ⁻ (430.9459)	Theoretical mass	79.9568	410.9366							
	Measured mass	79.9583	410.9376							
	Error (ppm)	18.5475	2.4335							
	Formula	SO ₃ ⁻	C ₇ F ₁₃ SO ₃ ⁻							

Table A7. Double bond defluorinated transformation products identified after nNiFe⁰-AC reacted with PFOS using accurate-mass identification. Precursor and daughter ions were identified by QToF. In column one, the number in parenthesis is the observed m/z of the precursor ions.

MS Precursor		MS/MS fragments					
C ₈ H ₂ F ₁₃ SO ₃ ⁻ (424.9517)	Theoretical mass	79.9568	98.9552	129.9536			
	Measured mass	79.9581	98.9555	129.9539			
	Error (ppm)	16.4126	2.8674	2.3770			
	Formula	SO ₃ ⁻	FSO ₃ ⁻	CF ₂ SO ₃ ⁻			
C ₈ H ₃ F ₁₂ SO ₃ ⁻ (406.9611)	Theoretical mass	79.9568	82.9603	98.9552	386.9549		
	Measured mass	79.9585	82.9613	98.9556	386.9560		
	Error (ppm)	20.4952	11.8621	4.1322	2.9324		
	Formula	SO ₃ ⁻	FSO ₂ ⁻	FSO ₃ ⁻	C ₈ H ₂ F ₁₁ SO ₃ ⁻		
C ₈ H ₅ F ₁₀ SO ₃ ⁻ (370.9786)	Theoretical mass	79.9568	82.9603	98.9552	121.0265	129.9536	
	Measured mass	79.9586	82.9622	98.9559	121.0253	129.9537	
	Error (ppm)	22.9239	23.2245	6.7148	9.8987	0.9538	
	Formula	SO ₃ ⁻	FSO ₂ ⁻	FSO ₃ ⁻	C ₅ H ₄ F ₃ ⁻	CF ₂ SO ₃ ⁻	
C ₈ H ₆ F ₉ SO ₃ ⁻ (352.9893)	Theoretical mass	79.9568	98.9552				
	Measured mass	79.9584	98.9552				
	Error (ppm)	20.2088	0.2388				
	Formula	SO ₃ ⁻	FSO ₃ ⁻				
C ₈ H ₇ F ₈ SO ₃ ⁻ (334.9989)	Theoretical mass	79.9568	98.9552	150.9982	154.9978		
	Measured mass	79.9584	98.9539	151.0005	154.9969		
	Error (ppm)	19.4071	13.1830	14.7731	6.0427		
	Formula	SO ₃ ⁻	FSO ₃ ⁻	C ₃ HF ₆ ⁻	C ₄ H ₅ F ₂ SO ₂ ⁻		

Table A7. continued.

C ₈ H ₈ F ₇ SO ₃ ⁻ (317.0081)	Theoretical mass	79.9568	82.9603	98.9552	121.0265	129.9536	136.0500
	Measured mass	79.9586	82.9612	98.9569	121.0252	129.9525	136.0504
	Error (ppm)	22.6838	11.0380	17.1236	10.4698	8.4742	2.7413
	Formula	SO ₃ ⁻	FSO ₂ ⁻	FSO ₃ ⁻	C ₅ H ₄ F ₃ ⁻	CF ₂ SO ₃ ⁻	C ₆ H ₇ F ₃ ⁻

Table A8. Paraffin product identified after nNiFe⁰-AC reacted with PFOS using accurate-mass identification. Precursor and daughter ions were identified by QToF. In column one, the number in parenthesis is the observed m/z of the precursor ions.

MS Precursor		MS/MS fragments					
C ₈ F ₁₇ O ⁻ (434.9661)	Theoretical mass	118.9920	168.9888	218.9856	268.9824	318.9792	368.9766
	Measured mass	118.9904	168.9898	218.9851	268.9817	318.9791	368.9757
	Error (ppm)	13.5723	-5.7933	2.4066	2.7251	0.4358	2.4392
	Formula	C ₂ F ₅ ⁻	C ₃ F ₇ ⁻	C ₄ F ₉ ⁻	C ₅ F ₁₁ ⁻	C ₆ F ₁₃ ⁻	C ₇ F ₁₅ ⁻
C ₈ F ₁₆ O ₂ ⁻ (431.9633)	Theoretical mass	330.9792	399.9744				
	Measured mass	330.9784	399.9744				
	Error (ppm)	2.5349	0.1200				
	Formula	C ₇ F ₁₃ ⁻	C ₈ F ₁₆ ⁻				

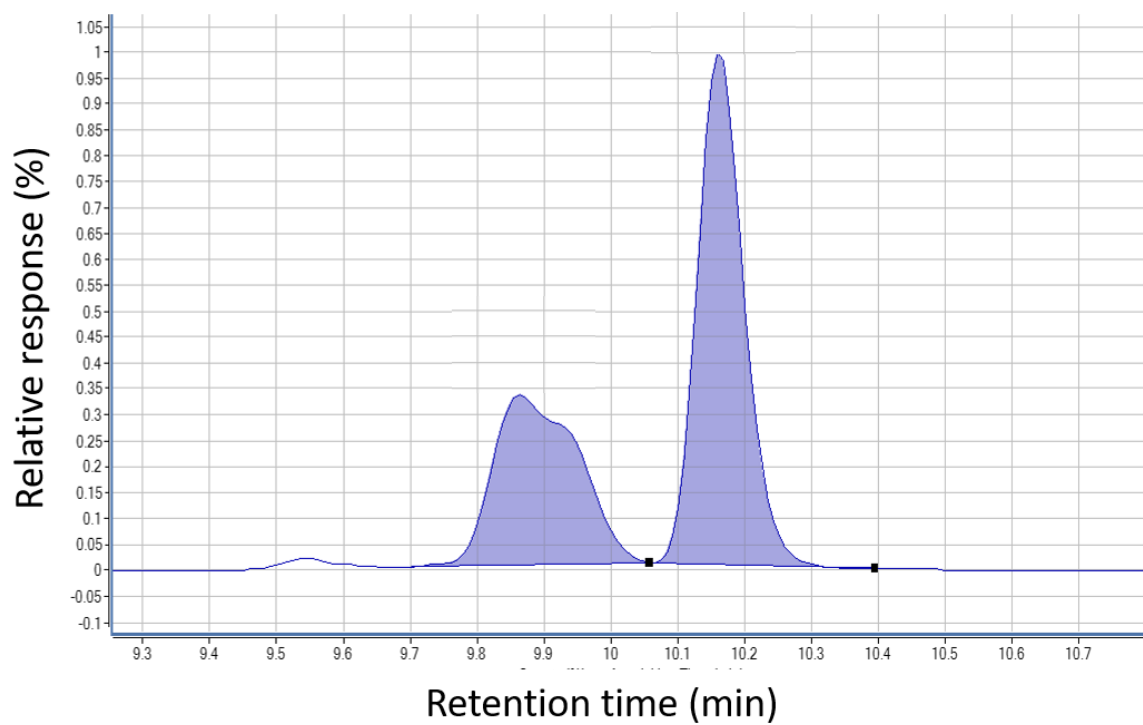


Figure A1. HPLC/MS/MS chromatogram of linear PFOS (the peak on the right) and branched PFOS (the peaks on the left) with intensity on the y-axis and retention time.

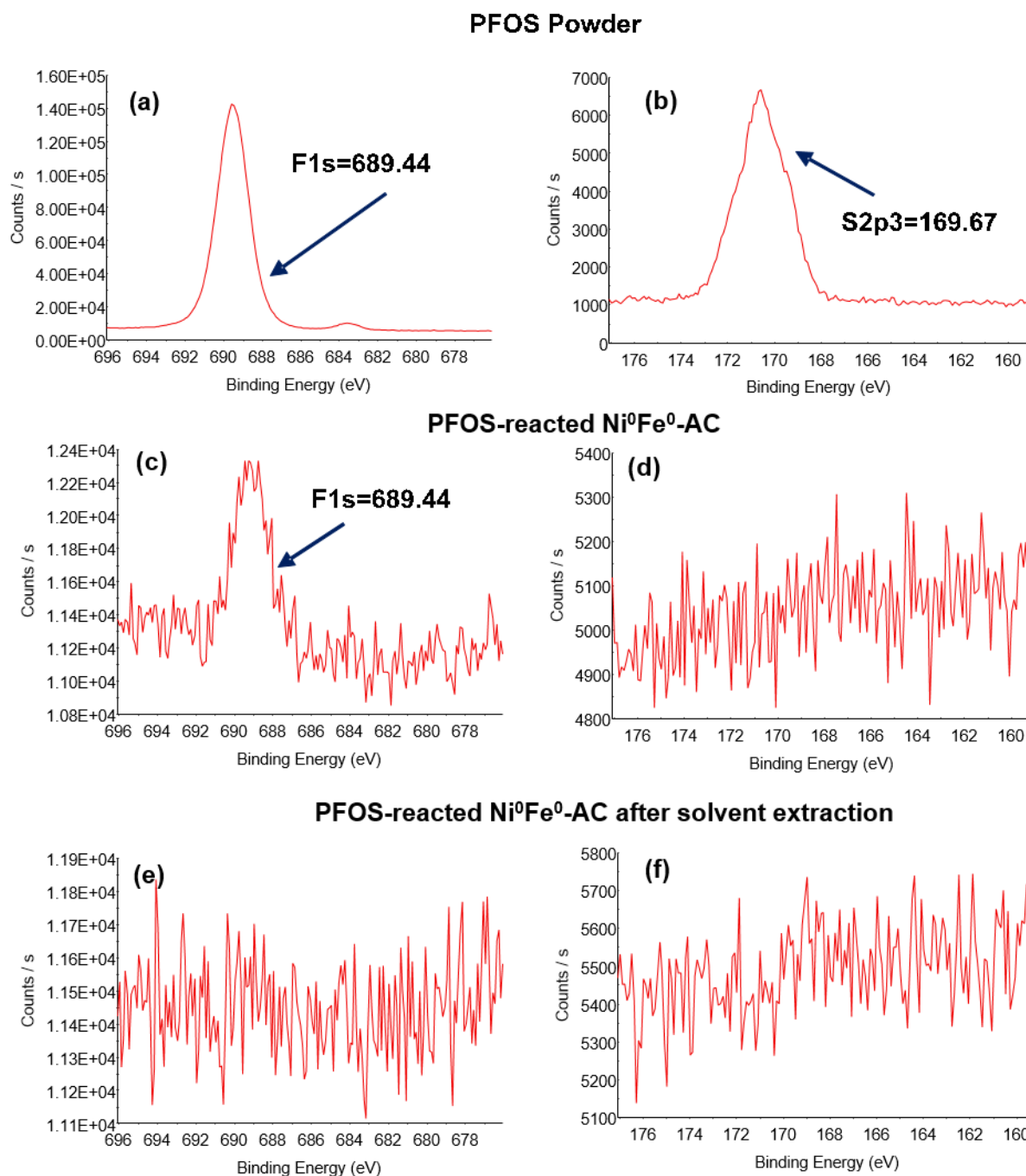


Figure A2. XPS spectra of (a-b) PFOS powder, (c-d) PFOS-reacted nNiFe⁰-AC; and (e-f) PFOS-reacted nNiFe⁰-AC after solvent extraction showing F 1s (675-695 eV) in the left column of graphs and S 2p₃ (158-178 eV) in the right column of graphs. Reaction was for 5-d at 60 °C with PFOS and nNiFe⁰-AC that were synthesized with a 1-h stirring time.

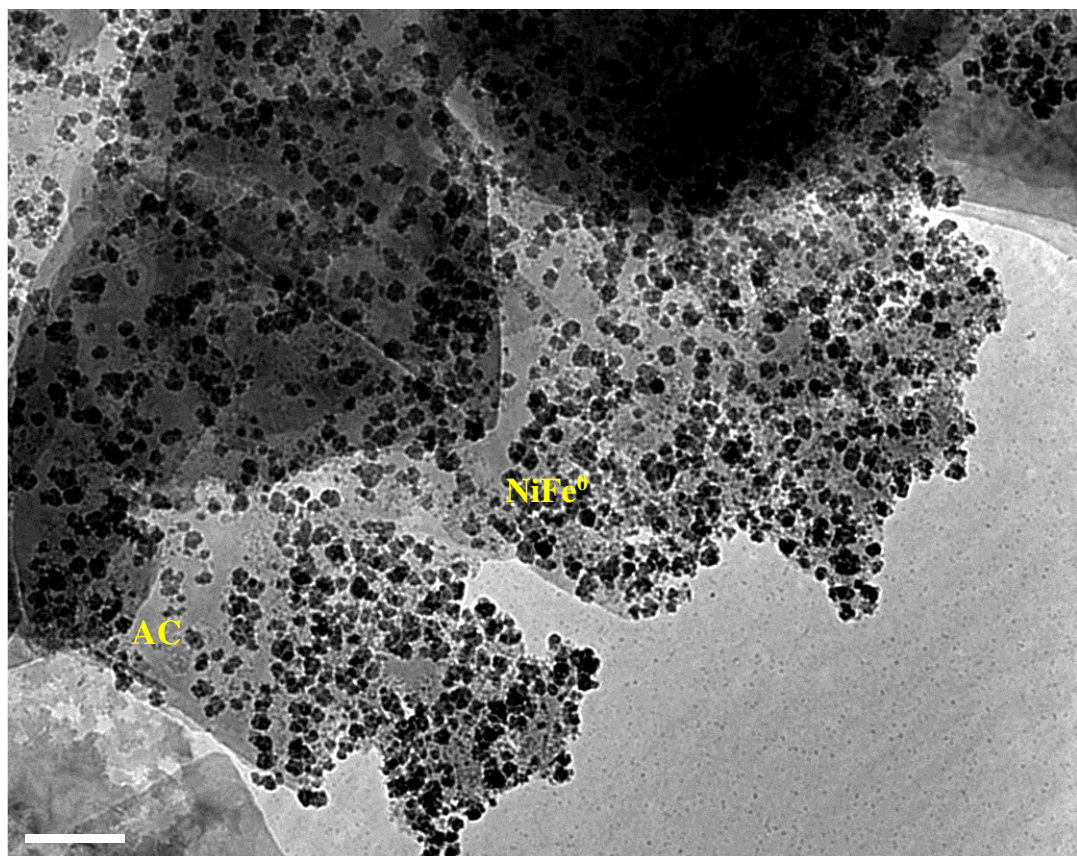


Figure A3. TEM images of 1-h SST nNiFe⁰-AC NPs after a 5-d reaction with PFOS at 60 °C. The gray sheets are AC, and the black NPs are nNiFe⁰.

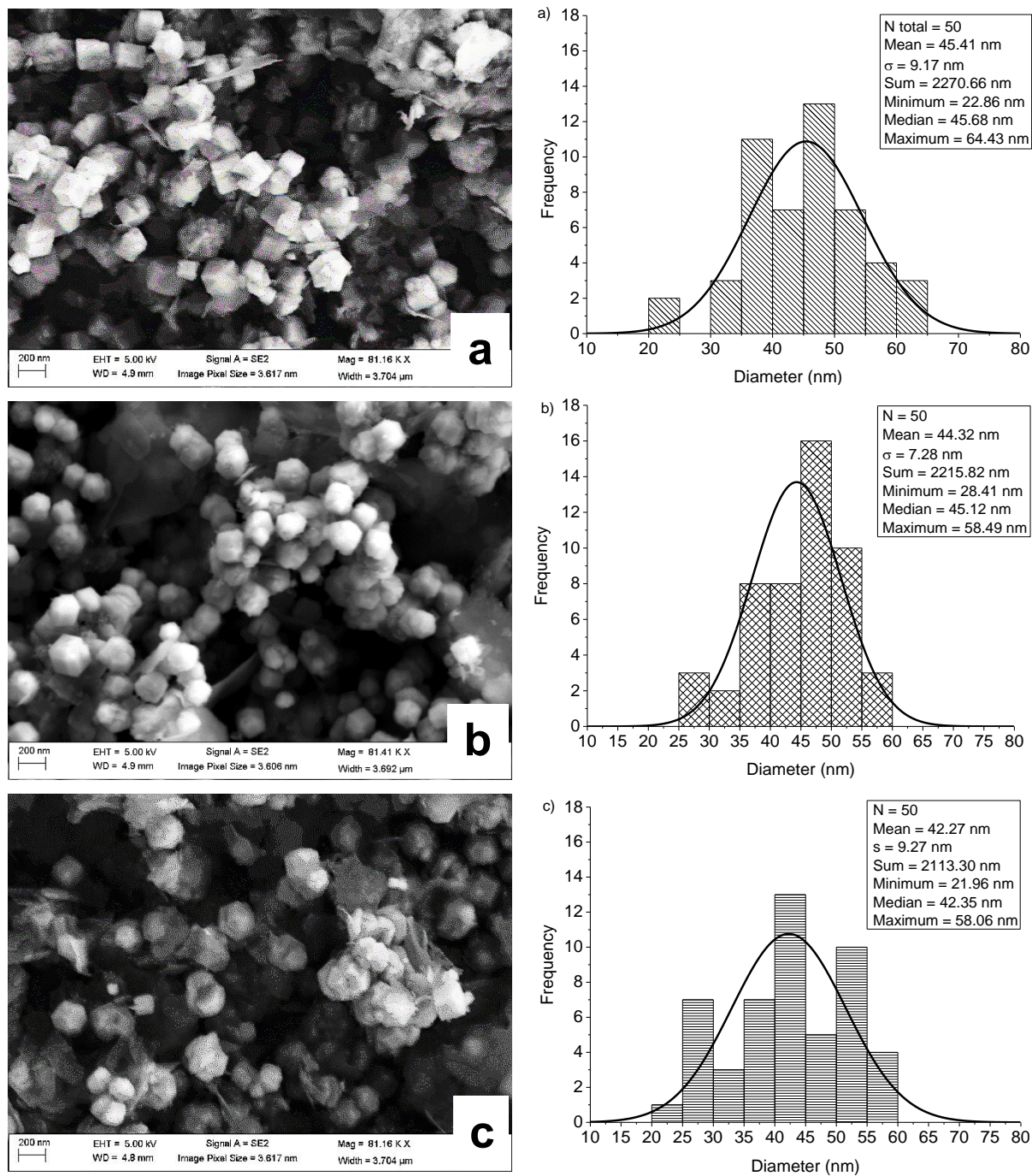


Figure A4. SEM images of the morphology and associated size distribution histograms determined of AC-supported nNiFe⁰ synthesized with different stirring time (SST) after a 5-d reaction period with PFOS (~ 6 μM) in unbuffered and unadjusted pH solutions at 60 °C: a) 1-h SST; b) 2-h SST; and c) 3-h SST.

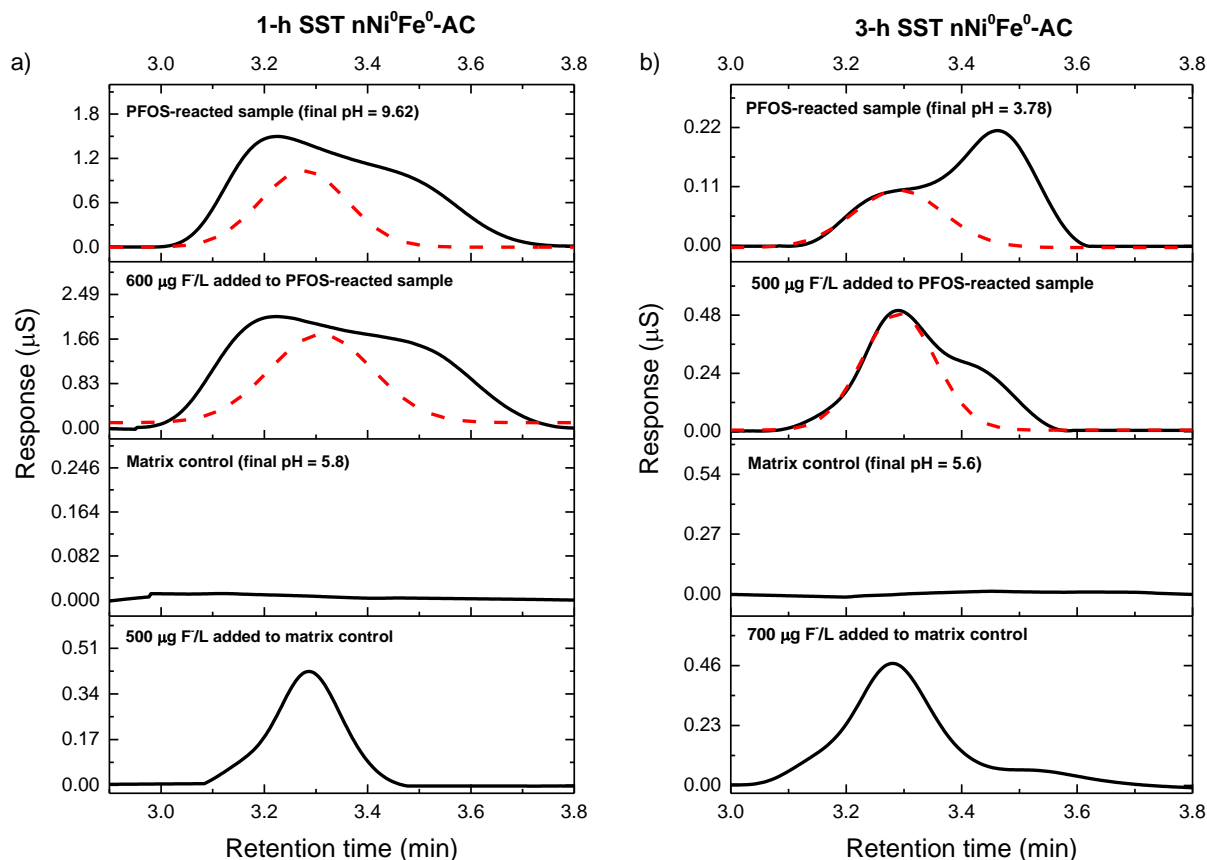


Figure A5. Ion chromatograms for solutions associated with $n\text{NiFe}^0\text{-AC}$ ($\text{Ni} = 2 \text{ wt\% of Fe}^0$) particles prepared with different synthesis stirring time (SST): a) 1-h SST $n\text{NiFe}^0\text{-AC}$ and b) 3-h SST $n\text{NiFe}^0\text{-AC}$. Upper two graphs are chromatograms after a 5-d reaction at 60°C in unbuffered solutions containing PFOS ($\sim 6 \mu\text{M}$, $\sim 3 \text{ mg/L}$) with and without a fluoride (F^-) standard addition, respectively. Red dashed line represents where the F^- peak should be located in the chromatogram. In Fig A5b, fluoride concentration was estimated to be $170 \mu\text{g/L}$ from the F^- standard curve. Based on the standard addition, F^- concentration after the 5-day PFOS reaction with 3-h SST $n\text{NiFe}^0\text{-AC}$ was estimated by Gaussian fitting using OriginPro 2016 software.

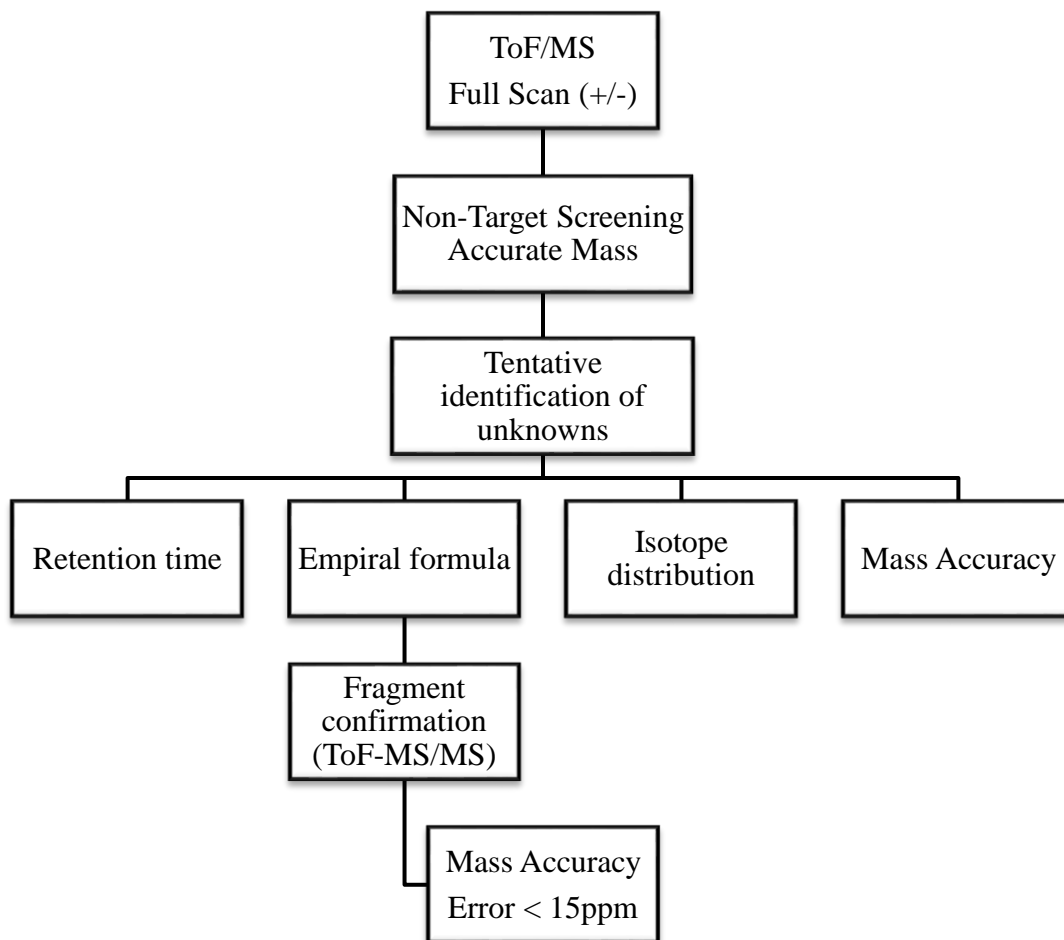
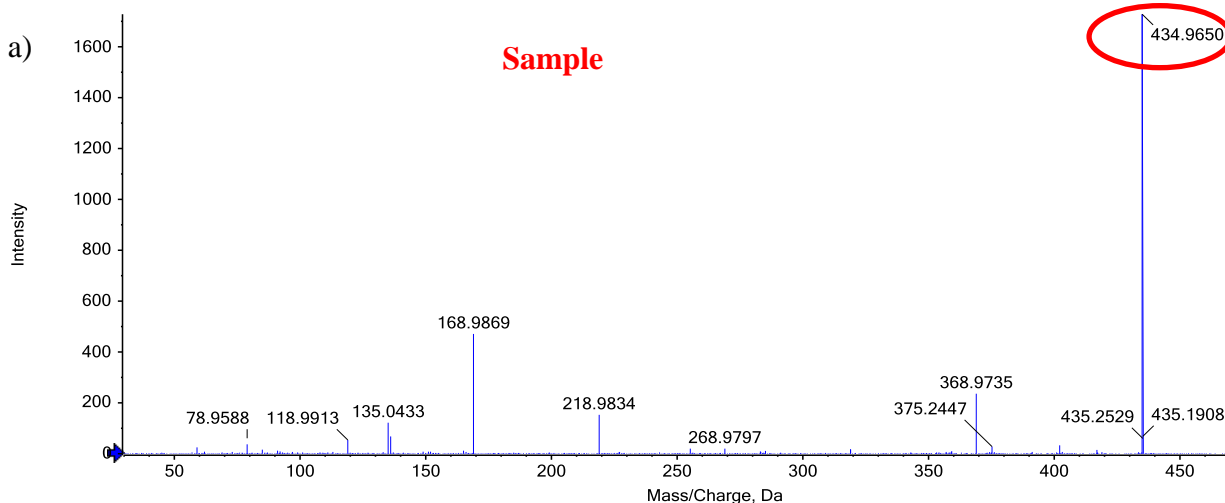


Figure A6. Identification process for PFOS transformation products using QToF/MS.

Spectrum from 040218_APCI_syringe_027.wiff (sample 1) - Jenny's sample MSMS 434.97, -TOF MS² of 435.0 (30 - 500)



Spectrum from 012918_FIA_C8F18_20.wiff (sample 1) - APCI C8F18 in MeOH 23 ppm FIA test 20, Experiment 2, -TOF MS² (10 - 1500) from 0.361 min
Precursor: 435.0 Da

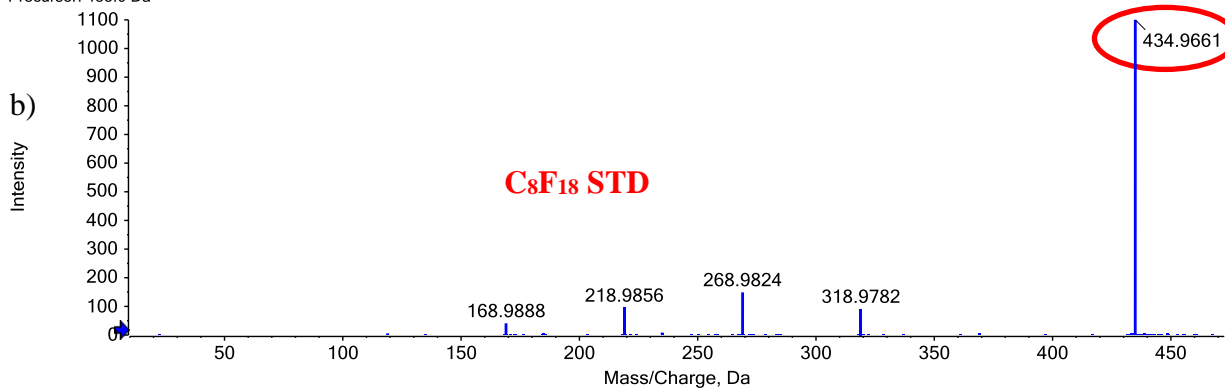


Figure A7. MS-MS spectrum of m/z 435 precursor ion in the a) sample and in the b) 23 ppm perfluorooctane (C₈F₁₈) standard solution injected in flow injection mode. The sample was injected directly in the syringe in APCI negative mode.

**APPENDIX B. SUPPORTING INFORMATION: KINETICS AND MECHANISM OF
REDUCTIVE TRANSFORMATION OF PERFLUOROOCCTANE SULFONATE BY
NIFE⁰-AC PARTICLES**

Analytical Methods

Organic intermediate product analysis

X-ray photoelectron spectrometer (XPS) analysis

Tables

Table B1. Agilent 6460 Triple-Quad LC/MS source optimized parameters

Table B2. QToF source parameters for PFOS isomers separation

Table B3. QToF source parameters ESI-

Table B4. QToF source parameters APCI-

Table B5. Gradient program for separation of organic byproducts

Table B6. Retention time of PFOS isomers

Table B7. Limit of detection and quantification of PFOS isomers

Table B8. Limit of detection and quantification of PFCAS

Table B9. Fragmentation of the transformation products identified for PFOS

Figures

Figure B1. Chemical structure of linear and branched PFOS

Figure B2. Chromatograms of PFOS isomers

Figure B3. XPS spectra of Fe at the nanoparticle surface

Analytical Methods

Organic intermediate product analysis

A triple quadrupole time-of-flight MS couple with a shimadzu ultra-high performance reverse-phase liquid chromatography (HPLC) was used for organic byproducts identification as described previously (dissertation chapter 3). Two ionization techniques were used including electrospray ionization (ESI) and atmospheric pressure chemical ionization (APCI), both in negative mode (Table B3 and Table B4). The target products were chromatographed using a Kinetex EVO C18 column (2.1 x 100 mm, 5 μ m, 100 Å) and a Phenomenex AF0-8497 filter with a mobile phase containing 0.15% acetic acid and 20 mM ammonium acetate in methanol and an oven temperature of 40 °C. The gradient program is given in Table B5.

X-ray photoelectron spectrometer (XPS) analysis.

XPS spectra was collected by Thermal Scientific K-Alpha XPS instrument. The instrument was equipped with a monochromatic Al K α X-ray source. The XPS analysis chamber was evacuated to a pressure of 5×10^{-8} or lower before collecting XPS spectra. The spot size was of 400 μ m and individual element scans were collected. Nanoparticles were dried overnight at 90 °C and mounted on a small carbon tape of 0.5 cm by 0.5 cm prior to analysis.

Table B1. Optimized LCMS parameters for quantification of PFCAs and PFOS (linear and branched).

Name	Formula	Internal Standard	Precursor Ion Mass	Product Ion Mass	Fragmentor Voltage (V)	Collision Energy (V)
PFOA	C ₈ F ₁₅ O ₂ ⁻	[¹³ C ₄] PFOA	413	369	80	2
				169		10
PFHpA	C ₇ F ₁₃ O ₂ ⁻	[¹³ C ₂] PFHxA	363	319	70	2
				169		10
				119		18
PFHxA	C ₆ F ₁₁ O ₂ ⁻	[¹³ C ₂] PFHxA	313	269	70	2
				119		14
PFPeA	C ₅ F ₉ O ₂ ⁻	[¹³ C ₂] PFHxA	263	219	60	2
PFBA	C ₄ F ₇ O ₂ ⁻	[¹³ C ₄] PFBA	213	169	60	2
PFOS	C ₈ F ₁₇ SO ₃ ⁻	[¹³ C ₈] PFOS	499	80	200	50
				99		60

Table B2. Quadrupole time of flight (QToF) source parameters used for PFOS isomers separation.

Parameter	Value
Curtain gas (CUR)	25
Ion Source Gas 1 (GS1)	40
Ion Source Gas 2 (GS2)	40
IonSpray Voltage Floating (ISVF)	4300
Temperature (TEM)	510
Collision energy (CE)	-50
Collision gas (CAD)	6
Collision energy spread (CES)	0
Declustering potential (DP)	-80
Ion release delay (IRD)	30
Ion release width (IRW)	12

Table B3. Quadrupole time of flight (QToF) source parameters using electrospray ionization in negative mode (ESI-) for identification of organic products.

Parameter	ESI-
Curtain gas (CUR)	25
Ion Source Gas 1 (GS1)	40
Ion Source Gas 2 (GS2)	40
IonSpray Voltage Floating (ISVF)	3800
Temperature (TEM)	510
Collision energy (CE)	-45
Collision gas (CAD)	6
Collision energy spread (CES)	15
Declustering potential (DP)	-80
Ion release delay (IRD)	60
Ion release width (IRW)	24

Table B4. Quadrupole time of flight (QToF) source parameters using atmospheric pressure chemical ionization (APCI) for identification of organic byproducts.

Parameters	APCI-
Ion source gas 1 (GS1)	10
Ion source gas 2 (GS2)	50
Temperature (TEM)	500
IonSpray voltage floating (ISVF)	-4400
Collision energy (CE)	-22
Collision gas (CAD)	6
Ion release delay (IRD)	60
Ion release width (IRW)	23
Nebulizer current	-5

Table B5. Gradient program of the mobile phase for separation of PFOS byproducts using QToF.

Time (min)	Flow (mL/min)	%A	%B
2.5	0.5	97	3
3.5	0.5	75	25
4.5	0.5	55	45
6	0.5	45	55
7	0.4	40	60
15	0.4	20	80
20	0.4	15	85
23	0.4	10	90
24	0.4	5	95
25	0.5	0	100
32	0.5	0	100
34	0.5	0	100
47	0.5	97	3

Table B6. PFOS isomers retention time (min) separated using QToF-MS.

Abbreviation	Scientific name	Formula	RT (min)
L-PFOS	n-Perfluoro--1-octanesulfonate	$\text{CF}_3\text{CF}_2\text{CF}_2\text{CF}_2\text{CF}_2\text{CF}_2\text{CF}_2\text{CF}_2\text{SO}_3\text{H}$	10.63
6-PFOS	Perfluoro-6-methylheptane sulfonate	$\text{CF}_3\text{CF}(\text{CF}_3)\text{CF}_2\text{CF}_2\text{CF}_2\text{CF}_2\text{CF}_2\text{SO}_3\text{H}$	10.30
5-PFOS	Perfluoro-5-methylheptane sulfonate	$\text{CF}_3\text{CF}_2\text{CF}(\text{CF}_3)\text{CF}_2\text{CF}_2\text{CF}_2\text{CF}_2\text{SO}_3\text{H}$	10.10
4-PFOS	Perfluoro-4-methylheptane sulfonate	$\text{CF}_3\text{CF}_2\text{CF}_2\text{CF}(\text{CF}_3)\text{CF}_2\text{CF}_2\text{CF}_2\text{SO}_3\text{H}$	9.90
3-PFOS	Perfluoro-3-methylheptane sulfonate	$\text{CF}_3\text{CF}_2\text{CF}_2\text{CF}_2\text{CF}(\text{CF}_3)\text{CF}_2\text{CF}_2\text{SO}_3\text{H}$	9.80
1-PFOS	Perfluoro-1-methylheptane sulfonate	$\text{CF}_3\text{CF}_2\text{CF}_2\text{CF}_2\text{CF}_2\text{CF}_2\text{CF}(\text{CF}_3)\text{SO}_3\text{H}$	9.84
dm-PFOS	Perfluoro-5,5-dimethylhexane sulfonate	$\text{CF}_3\text{C}(\text{CF}_3)_2\text{CF}_2\text{CF}_2\text{CF}_2\text{CF}_2\text{SO}_3\text{H}$	9.2 – 9.7
	Perfluoro-4,5-dimethylhexane sulfonate	$\text{CF}_3\text{CF}(\text{CF}_3)\text{CF}(\text{CF}_3)\text{CF}_2\text{CF}_2\text{CF}_2\text{SO}_3\text{H}$	
	Perfluoro-4,4-dimethylhexane sulfonate	$\text{CF}_3\text{CF}_2\text{C}(\text{CF}_3)_2\text{CF}_2\text{CF}_2\text{CF}_2\text{SO}_3\text{H}$	
	Perfluoro-3,5-dimethylhexane sulfonate	$\text{CF}_3\text{CF}_2\text{CF}(\text{CF}_3)\text{CF}(\text{CF}_3)\text{CF}_2\text{CF}_2\text{SO}_3\text{H}$	

Table B7. Limit of detection (LOD) and quantification (LOQ) of PFOS isomers using QToF-MS. The highest and lowest concentrations detected in the samples are reported in $\mu\text{g/L}$.

Name	PFOS composition (%)	Limit of detection ($\mu\text{g/L}$)	Limit of quantification ($\mu\text{g/L}$)	Lowest Concentration detected ($\mu\text{g/L}$)	Highest Concentration detected ($\mu\text{g/L}$)
L-PFOS	69.6 ± 4.7	1.0	4.8	16	642
6-PFOS	10.0 ± 2.0	1.0	4.8	7	187
5-PFOS	3.0 ± 0.5	1.0	4.8	< LOQ	66
1,3,4-PFOS	15.1 ± 2.1	4.8	10.0	10	260
DM-PFOS	2.3 ± 0.6	1.0	10.0	< LOQ	58

Table B8. Limit of detection (LOD) and quantification (LOQ) of the perfluorocarboxylic acid products detected in the concentrated samples using LCMS. The highest and lowest product concentrations in ng/L were also reported.

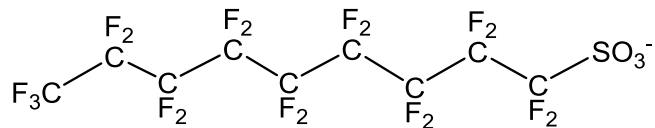
Name	Formula	Limit of detection (ng/L)	Limit of quantification (ng/L)	Lowest Concentration detected (ng/L)	Highest Concentration detected (ng/L)
PFOA	$\text{C}_8\text{F}_{15}\text{O}_2^-$	2	10	20.79	130.50 ± 3.60
PFHpA	$\text{C}_7\text{F}_{13}\text{O}_2^-$	2	10	14.75	57.66 ± 3.74
PFHxA	$\text{C}_6\text{F}_{11}\text{O}_2^-$	2	10	38.53	660.93 ± 873.38
PFPeA	$\text{C}_5\text{F}_9\text{O}_2^-$	2	10	<LOQ	30.13 ± 3.09
PFBA	$\text{C}_4\text{F}_7\text{O}_2^-$	2	10	<LOQ	20.10 ± 4.79

Table B9. Fragmentation of the transformation products identified for PFOS.

MS Precursor		MS/MS Fragments					
C-C Single bonds products for C8 molecules							
C ₈ H ₅ F ₁₂ SO ₃ ⁻ (408.9768)	Exact mass	79.9568					
	Accurate mass	79.9575					
	Error (ppm)	8.5421					
	Formula	SO ₃ ⁻					
C ₈ H ₇ F ₁₀ SO ₃ ⁻ (372.9956)	Exact mass	79.9568	98.9552	218.9856	229.9472		
	Accurate mass	79.9577	98.9551	218.9848	229.9468		
	Error (ppm)	11.0435	1.2127	3.7765	1.8917		
	Formula	SO ₃ ⁻	FSO ₃ ⁻	C ₄ F ₉ ⁻	C ₃ F ₆ SO ₃ ⁻		
C-C Single bonds products with < C8 molecules							
C ₅ HF ₁₀ SO ₃ ⁻ (330.9487)	Exact mass	79.9568	98.9552	260.9456			
	Accurate mass	79.9579	98.9554	260.9482			
	Error (ppm)	13.5448	1.8190	9.8181			
	Formula	SO ₃ ⁻	FSO ₃ ⁻	C ₄ F ₇ SO ₃ ⁻			
C ₄ HF ₈ SO ₃ ⁻ (280.9519)	Exact mass	79.9568	98.9552	260.9456			
	Accurate mass	79.9581	98.9551	260.9450			
	Error (ppm)	16.0462	1.2127	2.4450			
	Formula	SO ₃ ⁻	FSO ₃ ⁻	C ₄ F ₇ SO ₃ ⁻			
C-C Double bond products (only observed for C8 molecules)							
C ₈ HF ₁₄ SO ₃ ⁻ (442.9423)	Exact mass	79.9568	98.9552	118.9920	180.9888	230.9856	330.9792
	Accurate mass	79.9581	98.9551	118.9924	180.9888	230.9871	330.9802
	Error (ppm)	16.0462	1.2127	3.2355	0.1160	6.3770	2.9035
	Formula	SO ₃ ⁻	FSO ₃ ⁻	C ₂ F ₅ ⁻	C ₄ F ₇ ⁻	C ₅ F ₉ ⁻	C ₇ F ₁₃ ⁻
C ₈ H ₄ F ₁₁ SO ₃ ⁻ (388.9706)	Exact mass	79.9568	98.9552				
	Accurate mass	79.9589	98.9579				
	Error (ppm)	26.0516	27.0830				
	Formula	SO ₃ ⁻	FSO ₃ ⁻				

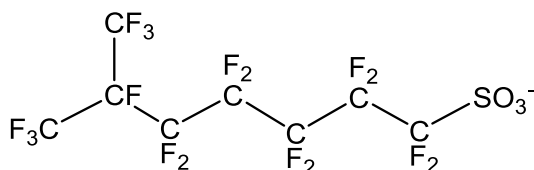
Linear isomer

L-PFOS

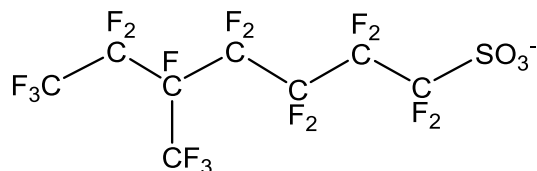


Perfluoromethyl isomers

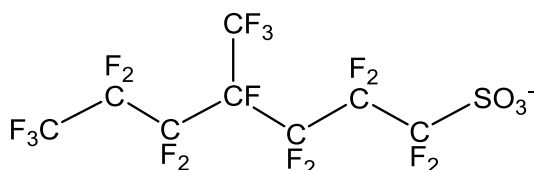
6-PFOS



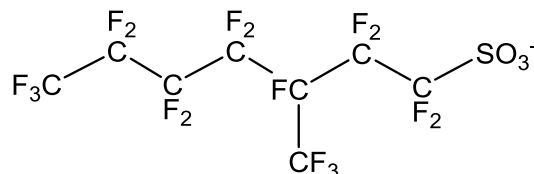
5-PFOS



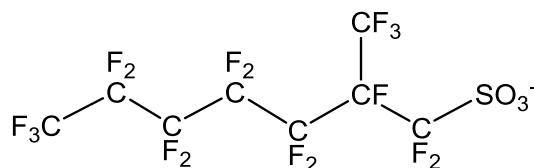
4-PFOS



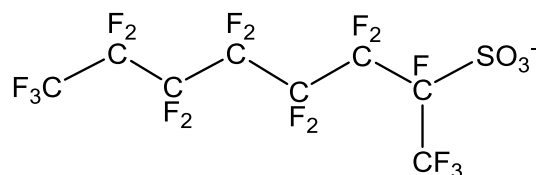
3-PFOS



2-PFOS

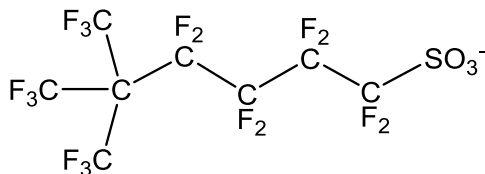


1-PFOS

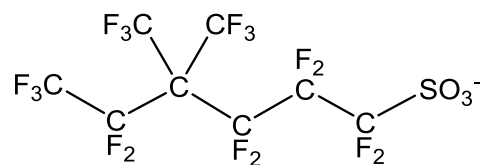


Diperfluoromethyl isomers (dm-PFOS)

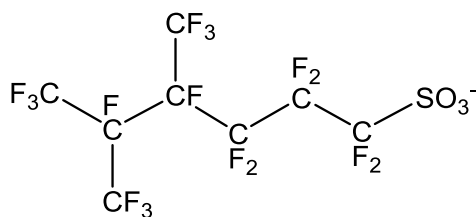
5,5-PFOS



4,4-PFOS



4,5-PFOS



3,5-PFOS

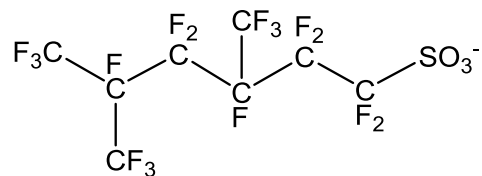


Figure B1. L- and Br-PFOS present in the technical PFOS used to perform batch experiments.

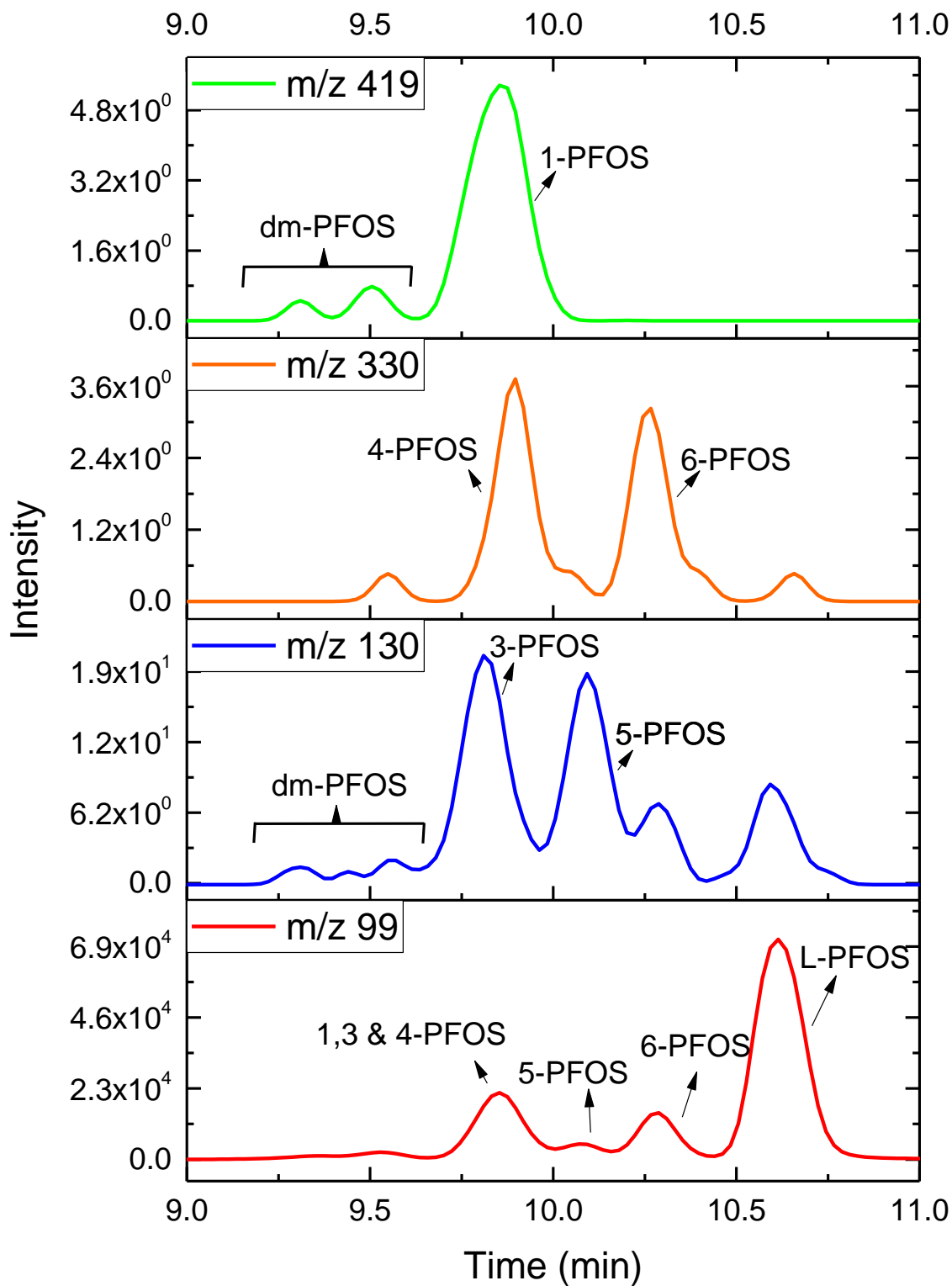


Figure B2. PFOS isomers and specific product ion used for isomers identification.

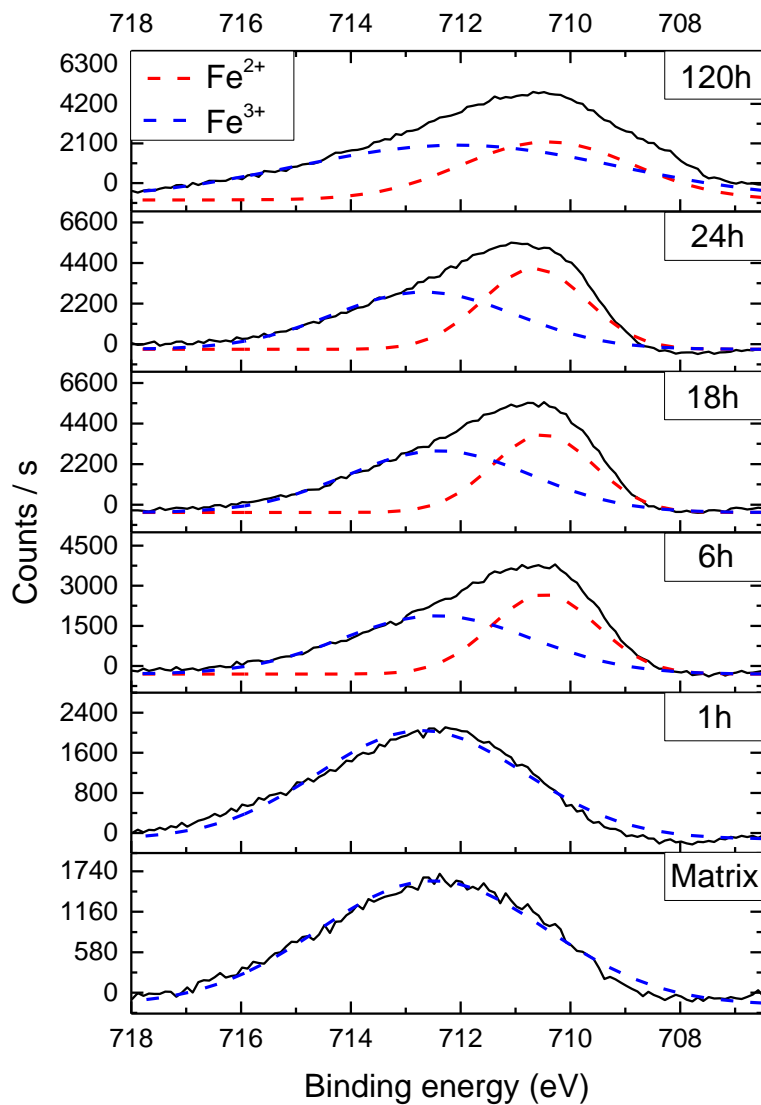


Figure B3. Fe 2p_{3/2} XPS spectra of nNiFe⁰-AC nanoparticles at different reaction times (1 h, 6 h, 18 h, 24 h, and 120 h) and matrix control (NPs and water mixed for 120 h).

**APPENDIX C. SUPPORTING INFORMATION: EFFECTS OF CARBON-CHAIN
LENGTH, FUNCTIONAL GROUP, AND COMMON GROUNDWATER
CONSTITUENTS ON PFAAS REDUCTION BY NIFE⁰-AC**

Tables

Table C1. LCMS parameters for PFAS quantification

Table C2. LCMS gradient conditions

Table C3. IC gradient conditions

Table C4. % Transformation of PFSAAs and PFCAs

Table C5. Final pH after PFAAs reaction with nNiFe⁰-AC for 1 or 5 d

Table C6. Fragmentation of the transformation products identified for PFCAs

Table C7. Fragmentation of the transformation products identified for PFSAAs

Table C1. LCMS conditions for PFAAs quantification.

Name	Formula	Internal Standard	Precursor Ion (m/z)	Product Ion (m/z)	Fragmentor Voltage (V)	Collision Energy (V)
PFNA	C ₉ F ₁₇ O ₂ ⁻	M9PFNA	463	169	75	14
				219		10
				419		2
PFOA	C ₈ F ₁₅ O ₂ ⁻	M8PFOA	413	369	80	2
				169		10
PFHpA	C ₇ F ₁₃ O ₂ ⁻	M4PFHpA	363	369	70	2
				169		10
				119		18
PFHxA	C ₆ F ₁₁ O ₂ ⁻	M5PFHxA	313	269	70	2
				119		14
PFPeA	C ₅ F ₉ O ₂ ⁻	M5PFPeA	263	219	60	2
PFBA	C ₄ F ₇ O ₂ ⁻	MPFBA	213	169	60	2
PFOS	C ₈ F ₁₇ SO ₃ ⁻	M8PFOS	499	80	200	50
				99		60
PFHpS	C ₇ F ₁₅ SO ₃ ⁻	MPFHxS	449	80	180	54
				99		42
PFHxS	C ₆ F ₁₃ SO ₃ ⁻	MPFHxS	399	80	135	58
				99		34
PFPeS	C ₅ F ₁₁ SO ₃ ⁻	MPFHxS	349	80	140	38
				99		30
PFBS	C ₄ F ₉ SO ₃ ⁻	M3PFBS	302	80	95	38
				99		30
6:2 FtS	C ₈ H ₄ F ₁₃ SO ₃ ⁻	M2-6:2 FtS	427	81	135	34
				407		18
8:2 FtS	C ₁₀ H ₄ F ₁₇ SO ₃ ⁻	M2-8:2 FtS	527	81	180	42
				507		26

Table C2. LCMS gradient conditions for PFAAs quantification.

Time (min)	A [%]	B [%]
0.00	97.0	3.0
0.85	97.0	3.0
3.50	46.0	54.0
16.00	15.0	85.0
16.50	0.0	100.0
17.50	0.0	100.0

Table C3. IC gradient separation for F⁻ and SO₄²⁻ quantification. [A] = Water and [B] = 30 mM NaOH.

Time (min)	A [%]	B[%]
0.00	94.0	6.0
11.00	94.0	6.0
20.00	30.0	70.0
20.00	94.0	6.0
30.00	94.0	6.0

Table C4. % Transformation of PFSA's and PFCAs at 1-d and 5-d of reaction.

PFAAs	1 d	5 d	Defluorination %*
PFBS	0.0%	57.7 ± 6.3%	19 ± 2.3%
PFHxS	14.3 ± 1.6%	50.1 ± 3.6%	62 ± 3.5%
PFOS	47.0 ± 1.4%	51.6 ± 5.5%	100 ± 0.6%
PFBA	13.1 ± 2.3%	56.5 ± 6.8%	3 ± 0.3%
PFHxA	27.1 ± 1.2%	44.0 ± 1.0%	11 ± 1.3%
PFOA	44.3 ± 2.1%	45.0 ± 4.6%	47 ± 5.2%

*Defluorination was calculated after 5 d of reaction.

Table C5. Final pH measured at 1 d or 5 d after reaction of PFAAs with nNiFe⁰-AC.

PFAA	Final pH	
	1 d	5 d
PFOA	4.47 ± 0.38	4.48 ± 0.59
PFHxA	3.77 ± 0.16	3.17 ± 0.18
PFBA	3.54 ± 0.14	3.03 ± 0.23
PFOS	3.48 ± 0.49	3.78 ± 0.53
PFHxS	4.28 ± 0.21	3.32 ± 0.28
PFBS	3.96 ± 0.56	3.80 ± 0.47

Table C6. Transformation products identified after nNiFe⁰-AC reacted with PFSA's using accurate-mass identification. Precursor and daughter ions were identified by QToF. In column one, the number in parenthesis is the observed m/z of the precursor ions.

PFSA's	Molecular Formula	Theoretical m/z	Observed m/z	Error (ppm)	Molecular Formula
PFBS C ₄ F ₉ SO ₃ ⁻ m/z 298.9416	C ₄ HF ₈ SO ₃ ⁻	79.9574	79.9581	8.75	SO ₃ ⁻
		98.9552	98.9555	2.83	FSO ₃ ⁻
PFHxS C ₆ F ₁₃ SO ₃ ⁻ m/z 398.9373	C ₆ HF ₁₂ SO ₃ ⁻	79.9574	79.9574	0.00	SO ₃ ⁻
		98.9552	98.9543	9.30	FSO ₃ ⁻
		118.9926	118.9915	9.24	C ₂ F ₅ ⁻
		168.9894	168.9885	5.33	C ₃ F ₇ ⁻
		298.9424	298.9411	4.35	C ₄ F ₉ SO ₃ ⁻
	C ₅ HF ₁₀ SO ₃ ⁻	79.9574	79.9577	3.75	SO ₃ ⁻
		98.9552	98.9554	1.82	FSO ₃ ⁻
	C ₄ HF ₈ SO ₃ ⁻	79.9574	79.9573	1.25	SO ₃ ⁻
		98.9552	98.9550	2.22	FSO ₃ ⁻
	C ₆ F ₁₁ O ₂ ⁻	68.9958	68.9967	13.04	CF ₃ ⁻
		118.9926	118.9918	6.72	C ₂ F ₅ ⁻
		268.9824	268.9814	3.84	C ₅ F ₁₁ ⁻
	C ₄ F ₇ O ₂ ⁻				

Table C7. Transformation products identified after nNiFe⁰-AC reacted with PFCAs using accurate-mass identification. Precursor and daughter ions were identified by QToF. In column one, the number in parenthesis is the observed m/z of the precursor ions.

PFCAs	Molecular Formula	Theoretical m/z	Observed m/z	Error (ppm)	Molecular Formula
PFBA (C ₄ F ₇ O ₂ ⁻ : m/z 212.9787) RT = 6.45 min	C ₃ F ₇ O ⁻	68.9958	68.9975	24.6	CF ₃ ⁻
		134.9869	134.985	14.3	C ₂ F ₅ O ⁻
	C ₃ F ₅ O ⁻				
PFHxA (C ₆ F ₁₁ O ₂ ⁻ : m/z 312.9723) RT = 8.45 min	C ₅ F ₁₁ O ⁻	118.9926	118.9922	3.4	C ₂ F ₅ ⁻
		168.9894	168.9878	9.5	C ₃ F ₇ ⁻
	C ₆ F ₁₁ O ⁻	130.9920	130.9916	3.1	C ₃ F ₅ ⁻
		180.9888	180.9884	2.3	C ₄ F ₇ ⁻
		230.9856	230.9860	1.6	C ₅ F ₉ ⁻
	C ₅ F ₉ O ⁻	84.990124	84.9895	7.3	CF ₃ O ⁻
		118.9926	118.9923	2.5	C ₂ F ₅ ⁻
		130.9920	130.9921	0.7	C ₃ F ₅ ⁻
		146.9869	146.9876	4.6	C ₃ F ₅ O ⁻
		180.9888	180.9885	1.8	C ₄ F ₇ ⁻
		196.9837	196.9826	5.8	C ₄ F ₇ O ⁻
	C ₄ F ₇ O ⁻				
	C ₄ F ₇ O ₂ ⁻	118.9926	118.9921	4.2	C ₂ F ₅ ⁻
C ₆ H ₄ F ₇ O ₂ ⁻					
PFOA (C ₈ F ₁₅ O ₂ ⁻ : m/z 412.9659) RT = 10.22 min	C ₇ F ₁₃ O ₂ ⁻	68.9958	68.9958	0.0	CF ₃ ⁻
		118.9919	118.9918	0.8	C ₂ F ₅ ⁻
		168.9894	168.9882	7.1	C ₃ F ₇ ⁻
		318.9792	318.9796	1.1	C ₆ F ₁₃ ⁻
	C ₆ F ₁₁ O ₂ ⁻	118.9919	118.9931	10.1	C ₂ F ₅ ⁻
	C ₄ F ₇ O ₂ ⁻	118.9926	118.9921	4.2	C ₂ F ₅ ⁻
	C ₇ F ₁₃ O ⁻	68.9958	68.9964	8.7	CF ₃ ⁻
		84.9901	84.9908	8.0	CF ₃ O ⁻
		118.9926	118.9922	3.4	C ₂ F ₅ ⁻
		130.9920	130.9921	0.7	C ₃ F ₅ ⁻
		134.9869	134.9869	0.2	C ₂ F ₅ O ⁻

Table C7. continued.

PFASs	Molecular Formula	Theoretical m/z	Observed m/z	Error (ppm)	Molecular Formula
PFOA C ₈ F ₁₅ O ₂ ⁻ m/z 412.9659	C ₇ F ₁₃ O ⁻	146.9869	146.9869	0.2	C ₃ F ₅ O ⁻
		168.9894	168.988	8.3	C ₃ F ₇ ⁻
		180.9888	180.9882	3.4	C ₄ F ₇ ⁻
		184.9837	184.9849	6.3	C ₃ F ₇ O ⁻
		196.9837	196.9823	7.3	C ₄ F ₇ O ⁻
		218.9862	218.9876	6.4	C ₄ F ₉ ⁻
		230.9856	230.9856	0.1	C ₅ F ₉ ⁻
		280.9824	280.9832	2.7	C ₆ F ₁₁ ⁻
	C ₆ F ₁₁ O ⁻	118.9919	118.9919	0.0	C ₂ F ₅ ⁻
		130.9920	130.9924	3.0	C ₃ F ₅ ⁻
		134.9869	134.9851	13.6	C ₂ F ₅ O ⁻
		168.9894	168.991	9.5	C ₃ F ₇ ⁻
		180.9888	180.9885	1.8	C ₄ F ₇ ⁻
		230.9856	230.9857	0.3	C ₅ F ₉ ⁻
	C ₄ F ₇ O ⁻	130.9920	130.9912	6.2	C ₃ F ₅ ⁻
	C ₃ F ₅ O ⁻				
	C ₈ HF ₁₄ O ₂ ⁻	68.9958	68.9971	18.8	CF ₃ ⁻
		118.9926	118.9923	2.5	C ₂ F ₅ ⁻
		168.9894	168.9896	1.2	C ₃ F ₇ ⁻
	C ₈ H ₂ F ₁₃ O ₂ ⁻				
	C ₈ H ₃ F ₁₂ O ₂ ⁻	68.9958	68.995	11.6	CF ₃ ⁻
		118.9926	118.9932	5.0	C ₂ F ₅ ⁻
	C ₈ H ₄ F ₁₁ O ₂ ⁻				
	C ₈ H ₅ F ₁₀ O ₂ ⁻				
	C ₈ H ₇ F ₈ O ₂ ⁻				
	C ₈ H ₈ F ₇ O ₂ ⁻				
	C ₈ H ₉ F ₆ O ₂ ⁻				
	C ₈ H ₁₁ F ₄ O ₂ ⁻				
	C ₈ H ₁₂ F ₃ O ₂ ⁻				
	C ₇ HF ₁₂ O ₂ ⁻	130.992	130.9928	6	C ₃ F ₅ ⁻

Table C7. continued.

PFASs	Molecular Formula	Theoretical m/z	Observed m/z	Error (ppm)	Molecular Formula
PFOA $C_8F_{15}O_2^-$ m/z 412.9659	$C_7HF_{12}O_2$	280.9824	280.9841	5.9	$C_6F_{11}^-$
	$C_6HF_{10}O_2^-$	230.9856	230.9833	10.1	$C_5F_9^-$
	$C_7HF_{12}O^-$	180.9888	180.9944	13.8	$C_4F_7^-$

REFERENCES

- 3M. (2000). Voluntary use and exposure information profile for perfluorooctanesulfonic acid and various salt forms. .
- 3M. (2008). *Screening level human exposure assessment report*. Retrieved from 3M Decatur, Alabama facility PFOA site-related environmental monitoring program:
- Ahrens, L., Harner, T., Shoeib, M., Lane, D. A., & Murphy, J. G. (2012). Improved Characterization of Gas-Particle Partitioning for Per- and Polyfluoroalkyl Substances in the Atmosphere Using Annular Diffusion Denuder Samplers. *Environmental Science & Technology*, *46*(13), 7199-7206. doi:10.1021/es300898s
- Ahrens, L., Hedlund, J., Dürig, W., Tröger, R., & Wiberg, K. (2016). *Screening of PFASs in groundwater and surface water*. Retrieved from
- Alsmeyer, Y. W., Childs, W. V., Flynn, R. M., Moore, G. G. I., & Smeltzer, J. C. (1994). *Electrochemical fluorination and its applications*. In: Banks, R. E., Smart, B. E., Tatlow, J.C., editors. *Organofluorine chemistry: Principles and commercial applications*. New York (NY): Plenum.
- Ananikov, V. P. (2015). Nickel: The “spirited horse” of transition metal catalysis. *Acs Catalysis*, *5*(3), 1964-1971. doi:10.1021/acscatal.5b00072
- Appleman, T. D., Higgins, C. P., Quiñones, O., Vanderford, B. J., Kolstad, C., Zeigler-Holady, J. C., & Dickenson, E. R. V. (2014). Treatment of poly- and perfluoroalkyl substances in U.S. full-scale water treatment systems. *Water Research*, *51*, 246-255. doi:10.1016/j.watres.2013.10.067
- Armitage, J. M., MacLeod, M., & Cousins, I. T. (2009). Comparative Assessment of the Global Fate and Transport Pathways of Long-Chain Perfluorocarboxylic Acids (PFCAs) and Perfluorocarboxylates (PFCs) Emitted from Direct Sources. *Environmental science & technology*, *43*(15), 5830-5836. doi:10.1021/es900753y
- Backe, W. J., Day, T. C., & Field, J. A. (2013). Zwitterionic, Cationic, and Anionic Fluorinated Chemicals in Aqueous Film Forming Foam Formulations and Groundwater from US Military Bases by Nonaqueous Large-Volume Injection HPLC-MS/MS. *Environmental Science & Technology*, *47*(10), 5226-5234. doi:10.1021/es3034999
- Bao, J., Yu, W. J., Liu, Y., Wang, X., Jin, Y. H., & Dong, G. H. (2019). Perfluoroalkyl substances in groundwater and home-produced vegetables and eggs around a fluorochemical industrial park in China. *Ecotoxicology and Environmental Safety*, *171*, 199-205. doi:10.1016/j.ecoenv.2018.12.086
- Barber, L. B., Weber, A. K., LeBlanc, D. R., Hull, R. B., Sunderland, E. M., & Vecitis, C. D. (2017). *Poly-and Perfluoroalkyl Substances in Contaminated Groundwater, Cape Cod, Massachusetts, 2014-2015*. U.S. Geological Survey: Reston, VA
- Becker, A. M., Gerstmann, S., & Frank, H. (2008). Perfluorooctane surfactants in waste waters, the major source of river pollution. *Chemosphere*, *72*(1), 115-121. doi:10.1016/j.chemosphere.2008.01.009
- Becker, A. M., Suchan, M., Gerstmann, S., & Frank, H. (2010). Perfluorooctanoic acid and perfluorooctane sulfonate released from a waste water treatment plant in Bavaria, Germany. *Environmental Science and Pollution Research*, *17*(9), 1502-1507. doi:10.1007/s11356-010-0335-x

- Benitez, F. J., Beltran-Heredia, J., Acero, J. L., & Rubio, F. J. (2001). Oxidation of several chlorophenolic derivatives by UV irradiation and hydroxyl radicals. *Journal of chemical technology and biotechnology.*, 76(3), 312-320. doi:10.1002/jctb.384
- Benskin, J. P., Ikononou, M. G., Gobas, F., Woudneh, M. B., & Cosgrove, J. R. (2012). Observation of a Novel PFOS-Precursor, the Perfluorooctane Sulfonamido Ethanol-Based Phosphate (SAmPAP) Diester, in Marine Sediments. *Environmental Science & Technology*, 46(12), 6505-6514. doi:10.1021/es300823m
- Boiteux, V., Dauchy, X., Rosin, C., & Munoz, J. F. (2012). National Screening Study on 10 Perfluorinated Compounds in Raw and Treated Tap Water in France. *Archives of Environmental Contamination and Toxicology*, 63(1), 1-12. doi:10.1007/s00244-012-9754-7
- Bokare, A. D., Chikate, R. C., Rode, C. V., & Paknikar, K. M. (2008). Iron-nickel bimetallic nanoparticles for reductive degradation of azo dye Orange G in aqueous solution. *Applied Catalysis B-Environmental*, 79(3), 270-278. doi:10.1016/j.apcatb.2007.10.033
- Brendel, S., Fetter, É., Staude, C., Vierke, L., & Biegel-Engler, A. (2018). Short-chain perfluoroalkyl acids: environmental concerns and a regulatory strategy under REACH. *Environmental sciences Europe.*, 30(1), 9. doi:10.1186/s12302-018-0134-4
- Buck, R. C., Franklin, J., Berger, U., Conder, J. M., Cousins, I. T., de Voogt, P., . . . van Leeuwen, S. P. J. (2011). Perfluoroalkyl and polyfluoroalkyl substances in the environment: Terminology, classification, and origins. *Integrated environmental assessment and management.*, 7(4), 513-541. doi:10.1002/ieam.258
- Burrows, A., Holman, J., Parsons, A., Pilling, G., & Price, G. (2013). *Chemistry³: Introducing Inorganic, Organic and Physical Chemistry*: Oxford University Press.
- Buxton, G. V., Greenstock, C. L., Helman, W. P., & Ross, A. B. (1988). Critical-review of rate constants for reactions of hydrated electrons, hydrogen-atoms and hydroxyl radicals (.OH/.O-) in aqueous-solution. *J. Phys. Chem. Ref. Data*, 17(2), 513-886. doi:10.1063/1.555805
- Campbell, T. Y., Vecitis, C. D., Mader, B. T., & Hoffmann, M. R. (2009). Perfluorinated Surfactant Chain-Length Effects on Sonochemical Kinetics. *Journal of Physical Chemistry A*, 113(36), 9834-9842. doi:10.1021/jp903003w
- Carrillo-Abad, J., Perez-Herranz, V., & Urtiaga, A. (2018). Electrochemical oxidation of 6:2 fluorotelomer sulfonic acid (6:2 FTSA) on BDD: electrode characterization and mechanistic investigation. *Journal of Applied Electrochemistry*, 48(6), 589-596. doi:10.1007/s10800-018-1180-8
- Carter, K. E., & Farrell, J. (2008). Oxidative destruction of perfluorooctane sulfonate using boron-doped diamond film electrodes. *Environmental Science & Technology*, 42(16), 6111-6115. doi:10.1021/es703273s
- Chen, J., & Zhang, P. (2006). Photodegradation of perfluorooctanoic acid in water under irradiation of 254 nm and 185 nm light by use of persulfate. *Water Science and Technology*, 54(11-12), 317-325. doi:10.2166/wst.2006.731
- Chen, J., Zhang, P. Y., & Zhang, L. (2006). Photocatalytic decomposition of environmentally persistent perfluorooctanoic acid. *Chemistry Letters*, 35(2), 230-231. doi:10.1246/cl.2006.230
- Chen, K. F., Li, S. L., & Zhang, W. X. (2011). Renewable hydrogen generation by bimetallic zero valent iron nanoparticles. *Chemical Engineering Journal*, 170(2-3), 562-567. doi:10.1016/j.cej.2010.12.019

- Cheng, J., Vecitis, C. D., Park, H., Mader, B. T., & Hoffmann, M. R. (2010). Sonochemical Degradation of Perfluorooctane Sulfonate (PFOS) and Perfluorooctanoate (PFOA) in Groundwater: Kinetic Effects of Matrix Inorganics. *Environmental Science & Technology*, 44(1), 445-450. doi:10.1021/es902651g
- Cheng, S. F., & Wu, S. C. (2000). The enhancement methods for the degradation of TCE by zero-valent metals. *Chemosphere*, 41(8), 1263-1270. doi:10.1016/s0045-6535(99)00530-5
- Cho, Y., & Choi, S. I. (2010). Degradation of PCE, TCE and 1,1,1-TCA by nanosized FePd bimetallic particles under various experimental conditions. *Chemosphere*, 81(7), 940-945. doi:10.1016/j.chemosphere.2010.07.054
- Chu, S. G., & Letcher, R. J. (2017). Side-chain fluorinated polymer surfactants in aquatic sediment and biosolid-augmented agricultural soil from the Great Lakes basin of North America. *Science of the Total Environment*, 607, 262-270. doi:10.1016/j.scitotenv.2017.06.252
- CONCAWE. (2017). Environmental Fate and Effects of Poly and Perfluoroalkyl Substances (PFAS). *Network for Industrially Contaminated Land in Europe, CONCAWE*.
- Cottrell, T. L. (1958). *The strengths of chemical bonds*. London: Butterworths Publications Ltd., London.
- Cousins, I. T., Vestergren, R., Wang, Z. Y., Scheringer, M., & McLachlan, M. S. (2016). The precautionary principle and chemicals management: The example of perfluoroalkyl acids in groundwater. *Environment International*, 94, 331-340. doi:10.1016/j.envint.2016.04.044
- Damjanovic, L., Majchrzak, M., Bennici, S., & Auroux, A. (2011). Determination of the heat evolved during sodium borohydride hydrolysis catalyzed by Co(3)O(4). *International Journal of Hydrogen Energy*, 36(3), 1991-1997. doi:10.1016/j.ijhydene.2010.11.041
- Dasu, K., Lee, L. S., Turco, R. F., & Nies, L. F. (2013). Aerobic biodegradation of 8:2 fluorotelomer stearate monoester and 8:2 fluorotelomer citrate triester in forest soil. *Chemosphere*, 91(3), 399-405. doi:10.1016/j.chemosphere.2012.11.076
- Dauchy, X., Boiteux, V., Colin, A., Bach, C., Rosin, C., & Munoz, J. F. (2019). Poly- and Perfluoroalkyl Substances in Runoff Water and Wastewater Sampled at a Firefighter Training Area. *Archives of Environmental Contamination and Toxicology*, 76(2), 206-215. doi:10.1007/s00244-018-0585-z
- Ding, G. H., & Peijnenburg, W. (2013). Physicochemical Properties and Aquatic Toxicity of Poly- and Perfluorinated Compounds. *Critical Reviews in Environmental Science and Technology*, 43(6), 598-678. doi:10.1080/10643389.2011.627016
- Du, Z. W., Deng, S. B., Bei, Y., Huang, Q., Wang, B., Huang, J., & Yu, G. (2014). Adsorption behavior and mechanism of perfluorinated compounds on various adsorbents-A review. *Journal of hazardous materials*, 274, 443-454. doi:10.1016/j.jhazmat.2014.04.038
- Duenas Fadic, M. E. (2013). *Estudio DFT del Rol de la Vitamina B12 en la dehalogenación reductiva de contaminantes orgánicos perfluorinados persistentes*. UNIVERSIDAD SAN FRANCISCO DE QUITO,
- EPA. (2015). *Short-chain polyfluoroalkyl substances (PFAS)*. Retrieved from Strandgade 29, 1401 Copenhagen K, Denmark:

- Ericson, I., Domingo, J. L., Nadal, M., Bigas, E., Llebaria, X., van Bavel, B., & Lindstrom, G. (2009). Levels of Perfluorinated Chemicals in Municipal Drinking Water from Catalonia, Spain: Public Health Implications. *Archives of Environmental Contamination and Toxicology*, 57(4), 631-638. doi:10.1007/s00244-009-9375-y
- Eriksson, U., Haglund, P., & Karrman, A. (2017). Contribution of precursor compounds to the release of per- and polyfluoroalkyl substances (PFASs) from waste water treatment plants (WWTPs). *Journal of Environmental Sciences*, 61, 80-90. doi:10.1016/j.jes.2017.05.004
- Fei, C., McLaughlin, J. K., Lipworth, L., & Olsen, J. (2008). Prenatal exposure to perfluorooctanoate (PFOA) and perfluorooctanesulfonate (PFOS) and maternally reported developmental milestones in infancy. *Environmental Health Perspectives*, 116(10), 1391-1395. doi:10.1289/ehp.11277
- Fernandez, N. A., Rodriguez-Freire, L., Keswani, M., & Sierra-Alvarez, R. (2016). Effect of chemical structure on the sonochemical degradation of perfluoroalkyl and polyfluoroalkyl substances (PFASs). *Environmental Science-Water Research & Technology*, 2(6), 975-983. doi:10.1039/c6ew00150e
- Ghaedi, M., Heidarpour, S., Kokhdan, S. N., Sahraie, R., Daneshfar, A., & Brazesh, B. (2012). Comparison of silver and palladium nanoparticles loaded on activated carbon for efficient removal of Methylene blue: Kinetic and isotherm study of removal process. *Powder Technology*, 228, 18-25. doi:10.1016/j.powtec.2012.04.030
- Ghisi, R., Vamerali, T., & Manzetti, S. (2019). Accumulation of perfluorinated alkyl substances (PFAS) in agricultural plants: A review. *Environmental Research*, 169, 326-341. doi:10.1016/j.envres.2018.10.023
- Giri, R. R., Ozaki, H., Morigaki, T., Taniguchi, S., & Takanami, R. (2011). UV photolysis of perfluorooctanoic acid (PFOA) in dilute aqueous solution. *Water Science and Technology*, 63(2), 276-282. doi:10.2166/wst.2011.050
- Gottschall, N., Topp, E., Edwards, M., Russell, P., Payne, M., Kleywegt, S., . . . Lapen, D. R. (2010). Polybrominated diphenyl ethers, perfluorinated alkylated substances, and metals in tile drainage and groundwater following applications of municipal biosolids to agricultural fields. *Science of the Total Environment*, 408(4), 873-883. doi:10.1016/j.scitotenv.2009.10.063
- Gu, Y. R., Liu, T. Z., Wang, H. J., Han, H. L., & Dong, W. Y. (2017). Hydrated electron based decomposition of perfluorooctane sulfonate (PFOS) in the VUV/sulfite system. *Science of the Total Environment*, 607, 541-548. doi:10.1016/j.scitotenv.2017.06.197
- Han, Y., & Yan, W. (2014). Bimetallic nickel-iron nanoparticles for groundwater decontamination: Effect of groundwater constituents on surface deactivation. *Water Research*, 66, 149-159. doi:10.1016/j.watres.2014.08.001
- Harding-Marjanovic, K. C., Houtz, E. F., Yi, S., Field, J. A., Sedlak, D. L., & Alvarez-Cohen, L. (2015). Aerobic Biotransformation of Fluorotelomer Thioether Amido Sulfonate (Lodyne) in AFFF-Amended Microcosms. *Environmental Science & Technology*, 49(13), 7666-7674. doi:10.1021/acs.est.5b01219
- Hayashi, R., Obo, H., Takeuchi, N., & Yasuoka, K. (2015). Decomposition of Perfluorinated Compounds in Water by DC Plasma within Oxygen Bubbles. *Electrical Engineering in Japan*, 190(3), 9-16. doi:10.1002/eej.22499
- Hingston, F. J., Quirk, J. P., & Posner, A. M. (1972). Anion adsorption by goethite and gibbsite .1. Role of proton in determining adsorption envelopes. *J. Soil Sci.*, 23(2), 177-&. Retrieved from <Go to ISI>://WOS:A1972N076700006

- Hori, H., Hayakawa, E., Einaga, H., Kutsuna, S., Koike, K., Ibusuki, T., . . . Arakawa, R. (2004). Decomposition of environmentally persistent perfluorooctanoic acid in water by photochemical approaches. *Environmental Science & Technology*, 38(22), 6118-6124. doi:10.1021/es049719n
- Hori, H., Nagaoka, Y., Yamamoto, A., Sano, T., Yamashita, N., Taniyasu, S., . . . Arakawa, R. (2006). Efficient decomposition of environmentally persistent perfluorooctanesulfonate and related fluorochemicals using zerovalent iron in subcritical water. *Environmental Science & Technology*, 40(3), 1049-1054. doi:10.1021/es0517419
- Hori, H., Yamamoto, A., Koike, K., Kutsuna, S., Osaka, I., & Arakawa, R. (2007). Photochemical decomposition of environmentally persistent short-chain perfluorocarboxylic acids in water mediated by iron(II)/(III) redox reactions. *Chemosphere*, 68(3), 572-578. doi:10.1016/j.chemosphere.2006.12.038
- Hotze, E. M., Phenrat, T., & Lowry, G. V. (2010). Nanoparticle aggregation: Challenges to understanding transport and reactivity in the environment. *Journal of Environmental Quality*, 39(6), 1909-1924. doi:10.2134/jeq2009.0462
- Houtz, E. F., Higgins, C. P., Field, J. A., & Sedlak, D. L. (2013). Persistence of Perfluoroalkyl Acid Precursors in AFFF-Impacted Groundwater and Soil. *Environmental Science & Technology*, 47(15), 8187-8195. doi:10.1021/es4018877
- Houtz, E. F., & Sedlak, D. L. (2012). Oxidative Conversion as a Means of Detecting Precursors to Perfluoroalkyl Acids in Urban Runoff. *Environmental Science & Technology*, 46(17), 9342-9349. doi:10.1021/es302274g
- Houtz, E. F., Sutton, R., Park, J.-S., & Sedlak, M. (2016). Poly- and perfluoroalkyl substances in wastewater: Significance of unknown precursors, manufacturing shifts, and likely AFFF impacts. *Water Research*, 95, 142-149. doi:10.1016/j.watres.2016.02.055
- Hu, X. D. C., Andrews, D. Q., Lindstrom, A. B., Bruton, T. A., Schaidler, L. A., Grandjean, P., . . . Sunderland, E. M. (2016). Detection of poly- and perfluoroalkyl substances (PFASs) in US drinking water linked to industrial sites, military fire training areas, and wastewater treatment plants. *Environmental Science & Technology Letters*, 3(10), 344-350. doi:10.1021/acs.estlett.6b00260
- Jin, L., Zhang, P. Y., Shao, T., & Zhao, S. L. (2014). Ferric ion mediated photodecomposition of aqueous perfluorooctane sulfonate (PFOS) under UV irradiation and its mechanism. *Journal of hazardous materials*, 271, 9-15. doi:10.1016/j.jhazmat.2014.01.061
- Kaiser, M. A. (2010). Understanding Potential Exposure Sources of Perfluorinated Carboxylic Acids in the Workplace. *The annals of occupational hygiene.*, 54(8), 915. doi:10.1093/annhyg/meq066
- Kaiser, M. A., Larsen, B. S., & Kao, C. P. C. (2005). Vapor pressures of perfluorooctanoic, -nonanoic, -decanoic, -undecanoic, and -dodecanoic acids. *Journal of Chemical & Engineering Data*, 50, 1841 - 1843.
- Kauck, E. A., & Diesslin, A. R. (1951). Some properties of perfluorocarboxylic acids. *Industrial and Engineering Chemistry*, 43(10), 2332-2334. doi:10.1021/ie50502a044
- Kim, H., Hong, H.-J., Jung, J., Kim, S.-H., & Yang, J.-W. (2010). Degradation of trichloroethylene (TCE) by nanoscale zero-valent iron (nZVI) immobilized in alginate bead. *Journal of hazardous materials*, 176(1-3), 1038-1043. doi:10.1016/j.jhazmat.2009.11.145

- Kim, Y. H., & Carraway, E. R. (2000). Dechlorination of pentachlorophenol by zero valent iron and modified zero valent irons. *Environmental Science & Technology*, *34*(10), 2014-2017. doi:10.1021/es991129f
- Kim, Y. H., Shin, W. S., & Ko, S. O. (2004). Reductive dechlorination of chlorinated biphenyls by palladized zero-valent metals. *Journal of Environmental Science and Health Part A-Toxic/Hazardous Substances & Environmental Engineering*, *39*(5), 1177-1188. doi:10.1081/ese-120030302
- Kirchgeorg, T., Dreyer, A., Gabrielli, P., Gabrieli, J., Thompson, L. G., Barbante, C., & Ebinghaus, R. (2016). Seasonal accumulation of persistent organic pollutants on a high altitude glacier in the Eastern Alps. *Environmental Pollution*, *218*, 804-812. doi:10.1016/j.envpol.2016.08.004
- Kissa, E. (2001). *Fluorinated Surfactants and Repellents, Second Edition*, : Marcell Dekker Inc., NY. .
- Kissa, E. (2005). *Fluorinated surfactants and repellents, 2nd ed.* (M. Dekker Ed.). New York.
- Kwan, W. C. (2001). *Physical property determination of perfluorinated surfactants*. (Masters of Science), University of Toronto,
- Larsen, P. B., & Giovalle, E. (2015). *Perfluoroalkylated substances: PFOA, PFOS and PFOSA*. Strandgade 29, 1401 Copenhagen K, Denmark: The Danish Environmental Protection Agency.
- Li, D. Y., Zhu, J. S., Wu, J. H., Yin, W. Z., Liang, H., & Lin, G. H. (2016). Development of an activated carbon-supported zero-valent iron catalyst (AC-Fe-0) for enhancing degradation of reactive brilliant orange and reducing iron sludge production. *Environmental Progress & Sustainable Energy*, *35*(4), 949-956. doi:10.1002/ep.12298
- Li, L., Fan, M. H., Brown, R. C., Van Leeuwen, J. H., Wang, J. J., Wang, W. H., . . . Zhang, P. Y. (2006). Synthesis, properties, and environmental applications of nanoscale iron-based materials: A review. *Critical Reviews in Environmental Science and Technology*, *36*(5), 405-431. doi:10.1080/10643380600620387
- Lide, D. R. (2005). Pentadecafluorooctanoic acid, nonadecafluorodecanoic acid, and heptafluorobutanoic acid. In Taylor & Francis (Eds.), *CRC handbook of chemistry and physics* (86th ed. ed., pp. 3-412, 413-372, 413-398). Boca Raton, FL.
- Lindstrom, A. B., Strynar, M. J., Delinsky, A. D., Nakayama, S. F., McMillan, L., Libelo, E. L., . . . Thomas, L. (2011). Application of WWTP Biosolids and Resulting Perfluorinated Compound Contamination of Surface and Well Water in Decatur, Alabama, USA. *Environmental science & technology*, *45*(19), 8015-8021. doi:10.1021/es1039425
- Liu, C. S., Higgins, C. P., Wang, F., & Shih, K. (2012). Effect of temperature on oxidative transformation of perfluorooctanoic acid (PFOA) by persulfate activation in water. *Separation and Purification Technology*, *91*, 46-51. doi:10.1016/j.seppur.2011.09.047
- Liu, J. X., & Avendano, S. M. (2013). Microbial degradation of polyfluoroalkyl chemicals in the environment: A review. *Environment International*, *61*, 98-114. doi:10.1016/j.envint.2013.08.022
- Liu, J. Y., Van Hoomissen, D. J., Liu, T. C., Maizel, A., Huo, X. C., Fernandez, S. R., . . . Strathmann, T. J. (2018). Reductive defluorination of branched per- and polyfluoroalkyl substances with cobalt complex catalysts. *Environmental Science & Technology Letters*, *5*(5), 289-294. doi:10.1021/acs.estlett.8b00122

- Liu, X. W., Zhang, T. Q., Wang, L. L., Shao, Y., & Fang, L. (2015). Hydrated electron-based degradation of atenolol in aqueous solution. *Chemical Engineering Journal*, 260, 740-748. doi:10.1016/j.cej.2014.08.109
- Liu, Z. Y., Lu, Y. L., Wang, T. Y., Wang, P., Li, Q. F., Johnson, A. C., . . . Sweetman, A. J. (2016). Risk assessment and source identification of perfluoroalkyl acids in surface and ground water: Spatial distribution around a mega-fluorochemical industrial park, China. *Environment International*, 91, 69-77. doi:10.1016/j.envint.2016.02.020
- Llorca, M., Farre, M., Tavano, M. S., Alonso, B., Koremblit, G., & Barcelo, D. (2012). Fate of a broad spectrum of perfluorinated compounds in soils and biota from Tierra del Fuego and Antarctica. *Environmental Pollution*, 163, 158-166. doi:10.1016/j.envpol.2011.10.027
- Lu, G. H., Jiao, X. C., Piao, H. T., Wang, X. C., Chen, S., Tan, K. Y., . . . Pan, J. (2018). The Extent of the Impact of a Fluorochemical Industrial Park in Eastern China on Adjacent Rural Areas. *Archives of Environmental Contamination and Toxicology*, 74(3), 484-491. doi:10.1007/s00244-017-0458-x
- Mansour, C., Berger, G., Fedoroff, M., Lefevre, G., Pages, A., Pavageau, E. M., . . . Zanna, S. (2010). Influence of temperature and reducing conditions on the sorption of sulfate on magnetite. *Journal of Colloid and Interface Science*, 352(2), 476-482. doi:10.1016/j.jcis.2010.08.014
- Marotta, E., Paradisi, C., & Scorrano, G. (2004). An atmospheric pressure chemical ionization study of the positive and negative ion chemistry of the hydrofluorocarbons 1,1-difluoroethane (HFC-152a) and 1,1,1,2-tetrafluoroethane (HFC-134a) and of perfluoro-n-hexane (FC-72) in air plasma at atmospheric pressure. *Journal of Mass Spectrometry*, 39(7), 791-801. doi:10.1002/jms.653
- Matheson, L. J., & Tratnyek, P. G. (1994). Reductive dehalogenation of chlorinated methanes by iron metal. *Environmental Science & Technology*, 28(12), 2045-2053. doi:10.1021/es00061a012
- Milonjic, S. K., Kopečni, M. M., & Ilic, Z. E. (1983). The point of zero charge and adsorption properties of natural magnetite. *J. Radioanal. Chem.*, 78(1), 15-24. doi:10.1007/bf02519745
- Moriwaki, H., Takagi, Y., Tanaka, M., Tsuruho, K., Okitsu, K., & Maeda, Y. (2005). Sonochemical decomposition of perfluorooctane sulfonate and perfluorooctanoic acid. *Environmental Science & Technology*, 39(9), 3388-3392. doi:10.1021/es040342v
- Myers, A. L., Jobst, K. J., Mabury, S. A., & Reiner, E. J. (2014). Using mass defect plots as a discovery tool to identify novel fluoropolymer thermal decomposition products. *Journal of Mass Spectrometry*, 49(4), 291-296. doi:10.1002/jms.3340
- Navarro, I., de la Torre, A., Sanz, P., Pro, J., Carbonell, G., & Martinez, M. D. (2016). Bioaccumulation of emerging organic compounds (perfluoroalkyl substances and halogenated flame retardants) by earthworm in biosolid amended soils. *Environmental Research*, 149, 32-39. doi:10.1016/j.envres.2016.05.004
- Ochoa-Herrera, V., Sierra-Alvarez, R., Somogyi, A., Jacobsen, N. E., Wysocki, V. H., & Field, J. A. (2008). Reductive defluorination of perfluorooctane sulfonate. *Environmental Science & Technology*, 42(9), 3260-3264. doi:10.1021/es702842q
- OECD. (2002). *Cooperation on existing chemicals, hazard assessment of perfluorooctane sulfonate (PFOS) and its salts report*. Paris, France: Organisation for Economic Cooperation and Development.

- Oliaei, F., Kriens, D., Weber, R., & Watson, A. (2013). PFOS and PFC releases and associated pollution from a PFC production plant in Minnesota (USA). *Environmental Science and Pollution Research*, 20(4), 1977-1992. doi:10.1007/s11356-012-1275-4
- Pandiyani, T., Martínez Rivas, O., Orozco Martínez, J., Burillo Amezcua, G., & Martínez-Carrillo, M. A. (2002). Comparison of methods for the photochemical degradation of chlorophenols. *Journal of photochemistry and photobiology.*, 146(3), 149-155. doi:10.1016/S1010-6030(01)00606-2
- Park, H., Vecitis, C. D., Cheng, J., Choi, W., Mader, B. T., & Hoffmann, M. R. (2009). Reductive Defluorination of Aqueous Perfluorinated Alkyl Surfactants: Effects of Ionic Headgroup and Chain Length. *Journal of Physical Chemistry A*, 113(4), 690-696. doi:10.1021/jp807116q
- Park, H., Vecitis, C. D., Cheng, J., Dalleska, N. F., Mader, B. T., & Hoffmann, M. R. (2011). Reductive degradation of perfluoroalkyl compounds with aquated electrons generated from iodide photolysis at 254 nm. *Photochem. Photobiol. Sci.*, 10(12), 1945-1953. doi:10.1039/c1pp05270e
- Park, S., de Perre, C., & Lee, L. S. (2017). Alternate reductants with VB12 to transform C8 and C6 perfluoroalkyl sulfonates: Limitations and insights into isomer specific transformation rates, products and pathways. *Environmental Science & Technology*, 51(23), 13869-13877. doi:10.1021/acs.est.7b03744
- Park, S., Lee, L. S., Medina, V. F., Zull, A., & Waisner, S. (2016). Heat-activated persulfate oxidation of PFOA, 6:2 fluorotelomer sulfonate, and PFOS under conditions suitable for in-situ groundwater remediation. *Chemosphere*, 145, 376-383. doi:10.1016/j.chemosphere.2015.11.097
- Park, S., Zenobio, J. E., & Lee, L. S. (2017). Perfluorooctane sulfonate (PFOS) loss with Pd0/nFe0 nanoparticles: Adsorption and aqueous Fe-complexation, not Transformation *Journal of hazardous materials*, 342, 20-28.
- Parks, G. A. (1965). Isoelectric points of solid oxides solid hydroxides and aqueous hydroxo complex systems. *Chem. Rev.*, 65(2), 177-&. doi:10.1021/cr60234a002
- Paul, A. G., Jones, K. C., & Sweetman, A. J. (2009). A First Global Production, Emission, And Environmental Inventory For Perfluorooctane Sulfonate. *Environmental Science & Technology*, 43(2), 386-392. doi:10.1021/es802216n
- Pereira, H. C., Ullberg, M., Kleja, D. B., Gustafsson, J. P., & Ahrens, L. (2018). Sorption of perfluoroalkyl substances (PFASs) to an organic soil horizon - Effect of cation composition and pH. *Chemosphere*, 207, 183-191. doi:10.1016/j.chemosphere.2018.05.012
- Pistocchi, A., & Loos, R. (2009). A map of European emissions and concentrations of PFOS and PFOA. *Environmental Science & Technology*, 43(24), 9237-9244. doi:10.1021/es901246d
- Rahman, M. F., Peldszus, S., & Anderson, W. B. (2014). Behaviour and fate of perfluoroalkyl and polyfluoroalkyl substances (PFASs) in drinking water treatment: A review. *Water Research*, 50, 318-340. doi:10.1016/j.watres.2013.10.045
- Ramirez, J. H., Maldonado-Hodar, F. J., Perez-Cadenas, A. F., Moreno-Castilla, C., Costa, C. A., & Madeira, L. M. (2007). Azo-dye Orange II degradation by heterogeneous Fenton-like reaction using carbon-Fe catalysts. *Applied Catalysis B-Environmental*, 75(3-4), 312-323. doi:10.1016/j.apcatb.2007.05.003

- Rayne, S., & Forest, K. (2009). Perfluoroalkyl sulfonic and carboxylic acids: A critical review of physicochemical properties, levels and patterns in waters and wastewaters, and treatment methods. *Journal of Environmental Science and Health Part a-Toxic/Hazardous Substances & Environmental Engineering*, 44(12), 1145-1199. doi:10.1080/10934520903139811
- Roberts, A. L., Totten, L. A., Arnold, W. A., Burris, D. R., & Campbell, T. J. (1996). Reductive elimination of chlorinated ethylenes by zero valent metals. *Environmental Science & Technology*, 30(8), 2654-2659. doi:10.1021/es9509644
- Royer, L. A., Lee, L. S., Russell, M. H., Nies, L. F., & Turco, R. F. (2015). Microbial transformation of 8:2 fluorotelomer acrylate and methacrylate in aerobic soils. *Chemosphere*, 129, 54-61. doi:10.1016/j.chemosphere.2014.09.077
- Schaefer, C. E., Andaya, C., Burant, A., Condee, C. W., Urtiaga, A., Strathmann, T. J., & Higgins, C. P. (2017). Electrochemical treatment of perfluorooctanoic acid and perfluorooctane sulfonate: Insights into mechanisms and application to groundwater treatment. *Chemical Engineering Journal*, 317, 424-432. doi:10.1016/j.cej.2017.02.107
- Schaefer, C. E., Choyke, S., Ferguson, P. L., Andaya, C., Burant, A., Maizel, A., . . . Higgins, C. P. (2018). Electrochemical Transformations of Perfluoroalkyl Acid (PFAA) Precursors and PFAAs in Groundwater Impacted with Aqueous Film Forming Foams. *Environmental Science & Technology*, 52(18), 10689-10697. doi:10.1021/acs.est.8b02726
- Schrick, B., Blough, J. L., Jones, A. D., & Mallouk, T. E. (2002). Hydrodechlorination of trichloroethylene to hydrocarbons using bimetallic nickel-iron nanoparticles. *Chemistry of Materials*, 14(12), 5140-5147. doi:10.1021/cm020737i
- Schroder, H. F., & Meesters, R. J. W. (2005). Stability of fluorinated surfactants in advanced oxidation processes - A follow up of degradation products using flow injection-mass spectrometry, liquid chromatography-mass spectrometry and liquid chromatography-multiple stage mass spectrometry. *Journal of Chromatography A*, 1082(1), 110-119. doi:10.1016/j.chroma.2005.02.070
- Schultz, M. M., Barofsky, D. F., & Field, J. A. (2004). Quantitative determination of fluorotelomer sulfonates in groundwater by LC MS/MS. *Environmental Science & Technology*, 38(6), 1828-1835. doi:10.1021/es035031j
- Schutz, A., Brandt, S., Liedtke, S., Foest, D., Marggraf, U., & Franzke, J. (2015). Dielectric barrier discharge ionization of perfluorinated compounds. *Anal. Chem.*, 87(22), 11415-11419. doi:10.1021/acs.analchem.5b03538
- Serp, P., & Machado, B. (2015). *Carbon (Nano)materials for Catalysis*. In: *Nanostructured Carbon Materials for Catalysis*: The Royal Society of Chemistry.
- Sharma, B. M., Bharat, G. K., Tayal, S., Larssen, T., Becanova, J., Karaskova, P., . . . Nizzetto, L. (2016). Perfluoroalkyl substances (PFAS) in river and ground/drinking water of the Ganges River basin: Emissions and implications for human exposure. *Environmental Pollution*, 208, 704-713. doi:10.1016/j.envpol.2015.10.050
- Shaw, D. M. J., Munoz, G., Bottos, E. M., Duy, S. V., Sauve, S., Liu, J. X., & Van Hamme, J. D. (2019). Degradation and defluorination of 6:2 fluorotelomer sulfonamidoalkyl betaine and 6:2 fluorotelomer sulfonate by *Gordonia* sp. strain NB4-1Y under sulfur-limiting conditions. *Science of the Total Environment*, 647, 690-698. doi:10.1016/j.scitotenv.2018.08.012

- Shih, Y. H., Chen, M. Y., & Su, Y. F. (2011). Pentachlorophenol reduction by Pd/Fe bimetallic nanoparticles: Effects of copper, nickel, and ferric cations. *Applied Catalysis B-Environmental*, 105(1-2), 24-29. doi:10.1016/j.apcatb.2011.03.024
- Shimakoshi, H., & Hisaeda, Y. (2017). A Hybrid Catalyst for Light-Driven Green Molecular Transformations. *Chempluschem*, 82(1), 18-29. doi:10.1002/cplu.201600303
- Song, Z., Tang, H. Q., Wang, N., & Zhu, L. H. (2013). Reductive defluorination of perfluorooctanoic acid by hydrated electrons in a sulfite-mediated UV photochemical system. *Journal of hazardous materials*, 262, 332-338. doi:10.1016/j.jhazmat.2013.08.059
- Sunderland, E. M., Hu, X. D. C., Dassuncao, C., Tokranov, A. K., Wagner, C. C., & Allen, J. G. (2019). A review of the pathways of human exposure to poly- and perfluoroalkyl substances (PFASs) and present understanding of health effects. *Journal of Exposure Science and Environmental Epidemiology*, 29(2), 131-147. doi:10.1038/s41370-018-0094-1
- Surma, M., & Zielinski, H. (2015). What do We Know about the Risk Arising from Perfluorinated Compounds. *Polish journal of environmental studies.*, 24. doi:10.15244/pjoes/30929
- Szabo, D., Coggan, T. L., Robson, T. C., Currell, M., & Clarke, B. O. (2018). Investigating recycled water use as a diffuse source of per- and polyfluoroalkyl substances (PFASs) to groundwater in Melbourne, Australia. *Science of the Total Environment*, 644, 1409-1417. doi:10.1016/j.scitotenv.2018.07.048
- Tachibana, K., Takeuchi, N., & Yasuoka, K. (2014). Reaction process of perfluorooctanesulfonic acid (PFOS) decomposed by DC plasma generated in argon gas bubbles. *Ieee Trans. Plasma Sci.*, 42(3), 786-793. doi:10.1109/tps.2014.2304520
- Tian, H. T., Gao, J., Li, H., Boyd, S. A., & Gu, C. (2016). Complete Defluorination of Perfluorinated Compounds by Hydrated Electrons Generated from 3-Indole-acetic-acid in Organomodified Montmorillonite. *Scientific Reports*, 6. doi:10.1038/srep32949
- Tian, H. T., & Gu, C. (2018). Effects of different factors on photodefluorination of perfluorinated compounds by hydrated electrons in organo-montmorillonite system. *Chemosphere*, 191, 280-287. doi:10.1016/j.chemosphere.2017.10.074
- Tokranov, A. K., Nishizawa, N., Amadei, C. A., Zenobio, J. E., Pickard, H. M., Allen, J. G., . . . Sunderland, E. M. (2019). How Do We Measure Poly- and Perfluoroalkyl Substances (PFASs) at the Surface of Consumer Products? *Environmental science & technology letters.*, 6(1), 38-43. doi:10.1021/acs.estlett.8b00600
- Torres, F. J., Ochoa-Herrera, V., Blowers, P., & Sierra-Alvarez, R. (2009). Ab initio study of the structural, electronic, and thermodynamic properties of linear perfluorooctane sulfonate (PFOS) and its branched isomers. *Chemosphere*, 76(8), 1143-1149. doi:10.1016/j.chemosphere.2009.04.009
- Tratnyek, P. G., Johnson, T. L., Scherer, M. M., & Eykholt, G. R. (1997). Remediating ground water with zero-valent metals: Chemical considerations in barrier design. *Ground Water Monitoring and Remediation*, 17(4), 108-114. doi:10.1111/j.1745-6592.1997.tb01270.x
- Trautmann, A. M., Schell, H., Schmidt, K. R., Mangold, K. M., & Tiehm, A. (2015). Electrochemical degradation of perfluoroalkyl and polyfluoroalkyl substances (PFASs) in groundwater. *Water Science and Technology*, 71(10), 1569-1575. doi:10.2166/wst.2015.143

- Tseng, N. S.-I. (2012). *Feasibility of Biodegradation of Polyfluoroalkyl and Perfluoroalkyl Substances*. (Master of Science), University of California, Los Angeles
- Uemichi, Y., Makino, Y., & Kanazuka, T. (1989). Degradation of polyethylene to aromatic-hydrocarbons over metal-supported activated carbon catalysts. *Journal of Analytical and Applied Pyrolysis*, 14(4), 331-344. doi:10.1016/0165-2370(89)80008-7
- Ullah, S., Alsberg, T., & Berger, U. (2011). Simultaneous determination of perfluoroalkyl phosphonates, carboxylates, and sulfonates in drinking water. *Journal of Chromatography A*, 1218(37), 6388-6395. doi:10.1016/j.chroma.2011.07.005
- Urriaga, A., Soriano, A., & Carrillo-Abad, J. (2018). BDD anodic treatment of 6:2 fluorotelomer sulfonate (6:2 FTSA). Evaluation of operating variables and by-product formation. *Chemosphere*, 201, 571-577. doi:10.1016/j.chemosphere.2018.03.027
- Van der Zee, F. P., Bisschops, I. A. E., Lettinga, G., & Field, J. A. (2003). Activated carbon as an electron acceptor and redox mediator during the anaerobic biotransformation of azo dyes. *Environmental Science & Technology*, 37(2), 402-408. doi:10.1021/es025885o
- Vecitis, C. D. (2009). *Chemical reactions at aqueous interfaces* (Doctor of Philosophy), California Institute of Technology,
- Vecitis, C. D., Park, H., Cheng, J., Mader, B. T., & Hoffmann, M. R. (2009). Treatment technologies for aqueous perfluorooctanesulfonate (PFOS) and perfluorooctanoate (PFOA). *Frontiers of Environmental Science & Engineering in China*, 3(2), 129-151. doi:10.1007/s11783-009-0022-7
- Wang, C. B., & Zhang, W. X. (1997). Synthesizing nanoscale iron particles for rapid and complete dechlorination of TCE and PCBs. *Environmental Science & Technology*, 31(7), 2154-2156. doi:10.1021/es970039c
- Wang, P., Lu, Y. L., Wang, T. Y., Zhu, Z. Y., Li, Q. F., Meng, J., . . . Sweetman, A. J. (2016). Coupled production and emission of short chain perfluoroalkyl acids from a fast developing fluorochemical industry: Evidence from yearly and seasonal monitoring in Daling River Basin, China. *Environmental Pollution*, 218, 1234-1244. doi:10.1016/j.envpol.2016.08.079
- Wang, T., Su, J., Jin, X. Y., Chen, Z. L., Megharaj, M., & Naidu, R. (2013). Functional clay supported bimetallic nZVI/Pd nanoparticles used for removal of methyl orange from aqueous solution. *Journal of hazardous materials*, 262, 819-825. doi:10.1016/j.jhazmat.2013.09.028
- Wang, Y. W., Fu, J. J., Wang, T., Liang, Y., Pan, Y. Y., Cai, Y. Q., & Jiang, G. B. (2010). Distribution of perfluorooctane sulfonate and other perfluorochemicals in the ambient environment around a manufacturing facility in China. *Environmental Science & Technology*, 44(21), 8062-8067. doi:10.1021/es101810h
- Wang, Z. Y., DeWitt, J. C., Higgins, C. P., & Cousins, I. T. (2017). A Never-Ending Story of Per- and Polyfluoroalkyl Substances (PFASs)? *Environmental Science & Technology*, 51(5), 2508-2518. doi:10.1021/acs.est.6b04806
- Wang, Z. Y., MacLeod, M., Cousins, I. T., Scheringer, M., & Hungerbühler, K. (2011). Using COSMOtherm to predict physicochemical properties of poly- and perfluorinated alkyl substances (PFASs). *Environmental Chemistry*, 8(4), 389-398. doi:10.1071/en10143
- Weber, A. K., Barber, L. B., LeBlanc, D. R., Sunderland, E. M., & Vecitis, C. D. (2017). Geochemical and Hydrologic Factors Controlling Subsurface Transport of Poly- and Perfluoroalkyl Substances, Cape Cod, Massachusetts. *Environmental Science & Technology*, 51(8), 4269-4279. doi:10.1021/acs.est.6b05573

- Xiao, F., Simcik, M. F., Halbach, T. R., & Gulliver, J. S. (2015). Perfluorooctane sulfonate (PFOS) and perfluorooctanoate (PFOA) in soils and groundwater of a U.S. metropolitan area: migration and implications for human exposure. *Water Res*, 72, 64-74. doi:10.1016/j.watres.2014.09.052
- Xiao, X., Ulrich, B. A., Chen, B. L., & Higgins, C. P. (2017). Sorption of Poly- and Perfluoroalkyl Substances (PFASs) Relevant to Aqueous Film-Forming Foam (AFFF)-Impacted Groundwater by Biochars and Activated Carbon. *Environmental Science & Technology*, 51(11), 6342-6351. doi:10.1021/acs.est.7b00970
- Xu, T. (2005). *Effect of zero valent metals and water miscible solvents on reductive dechlorination of polychlorinated biphenyls*. (Ph.D.), Purdue University,
- Yamamoto, T., Noma, Y., Sakai, S.-I., & Shibata, Y. (2007). Photodegradation of perfluorooctane sulfonate by UV irradiation in water and alkaline 2-propanol. *Environmental Science & Technology*, 41(16), 5660-5665. doi:10.1021/es0706504
- Yang, S., Cheng, J., Sun, J., Hu, Y., & Liang, X. (2013). Defluorination of Aqueous Perfluorooctanesulfonate by Activated Persulfate Oxidation. *Plos One*, 8(10). doi:10.1371/journal.pone.0074877
- Yasuoka, K., Sasaki, K., & Hayashi, R. (2011). An energy-efficient process for decomposing perfluorooctanoic and perfluorooctane sulfonic acids using dc plasmas generated within gas bubbles. *Plasma Sources Science & Technology*, 20(3). doi:10.1088/0963-0252/20/3/034009
- Zhang, G., Qu, J., Liu, H., Cooper, A. T., & Wu, R. (2007). CuFe₂O₄/activated carbon composite: A novel magnetic adsorbent for the removal of acid orange II and catalytic regeneration. *Chemosphere*, 68(6), 1058-1066. doi:10.1016/j.chemosphere.2007.01.081
- Zhang, L. L., Niu, J. F., Li, Y., Wang, Y. J., & Sun, D. (2013). Evaluating the sub-lethal toxicity of PFOS and PFOA using rotifer *Brachionus calyciflorus*. *Environmental Pollution*, 180, 34-40. doi:10.1016/j.envpol.2013.04.031
- Zhang, W. (2014). *Nanoparticle Aggregation: Principles and modeling*. (Vol. 811).
- Zhao, D. M., Cheng, J., Vecitis, C. D., & Hoffmann, M. R. (2011). Sorption of Perfluorochemicals to Granular Activated Carbon in the Presence of Ultrasound. *Journal of Physical Chemistry A*, 115(11), 2250-2257. doi:10.1021/jp111784k
- Zhuo, Q., Deng, S., Yang, B., Huang, J., & Yu, G. (2011). Efficient Electrochemical Oxidation of Perfluorooctanoate Using a Ti/SnO₂-Sb-Bi Anode. *Environmental Science & Technology*, 45(7), 2973-2979. doi:10.1021/es1024542
- Zhuo, Q. F., Deng, S. B., Yang, B., Huang, J., Wang, B., Zhang, T. T., & Yu, G. (2012). Degradation of perfluorinated compounds on a boron-doped diamond electrode. *Electrochimica Acta*, 77, 17-22. doi:10.1016/j.electacta.2012.04.145